NASA/TM-20205002936

Experimental Investigation of Drag Modulation Aerocapture: Drag-Skirt Separation in Hypersonic Free Flight

Michael C. Wilder
Ames Research Center, Moffett Field, California

Marcus A. Lobbia
Jet Propulsion Laboratory, California Institute of Technology, Pasadena, California

Adam P. Nelessen
Jet Propulsion Laboratory, California Institute of Technology, Pasadena, California

Alex Austin
Jet Propulsion Laboratory, California Institute of Technology, Pasadena, California

Joshua A. Ravich
Jet Propulsion Laboratory, California Institute of Technology, Pasadena, California

David W. Bogdanoff
Analytical Mechanics Associates, Inc.
Ames Research Center, Moffett Field, California

Paul F. Wercinski
Ames Research Center, Moffett Field, California

Ethiraj Venkatapathy
Ames Research Center, Moffett Field, California

July 2020

NASA STI Program ... in Profile

Since its founding, NASA has been dedicated to the advancement of aeronautics and space science. The NASA scientific and technical information (STI) program plays a key part in helping NASA maintain this important role.

The NASA STI program operates under the auspices of the Agency Chief Information Officer. It collects, organizes, provides for archiving, and disseminates NASA's STI. The NASA STI program provides access to the NTRS Registered and its public interface, the NASA Technical Reports Server, thus providing one of the largest collections of aeronautical and space science STI in the world. Results are published in both non-NASA channels and by NASA in the NASA STI Report Series, which includes the following report types:

- TECHNICAL PUBLICATION. Reports of completed research or a major significant phase of research that present the results of NASA Programs and include extensive data or theoretical analysis. Includes compilations of significant scientific and technical data and information deemed to be of continuing reference value. NASA counterpart of peer-reviewed formal professional papers but has less stringent limitations on manuscript length and extent of graphic presentations.

- TECHNICAL MEMORANDUM. Scientific and technical findings that are preliminary or of specialized interest, e.g., quick release reports, working papers, and bibliographies that contain minimal annotation. Does not contain extensive analysis.

- CONTRACTOR REPORT. Scientific and technical findings by NASA-sponsored contractors and grantees.

- CONFERENCE PUBLICATION. Collected papers from scientific and technical conferences, symposia, seminars, or other meetings sponsored or co-sponsored by NASA.

- SPECIAL PUBLICATION. Scientific, technical, or historical information from NASA programs, projects, and missions, often concerned with subjects having substantial public interest.

- TECHNICAL TRANSLATION. English-language translations of foreign scientific and technical material pertinent to NASA's mission.

Specialized services also include organizing and publishing research results, distributing specialized research announcements and feeds, providing information desk and personal search support, and enabling data exchange services.

For more information about the NASA STI program, see the following:

- Access the NASA STI program home page at http://www.sti.nasa.gov

- E-mail your question to help@sti.nasa.gov

- Phone the NASA STI Information Desk at 757-864-9658

- Write to:
  NASA STI Information Desk
  Mail Stop 148
  NASA Langley Research Center
  Hampton, VA 23681-2199

NASA/TM-20205002936

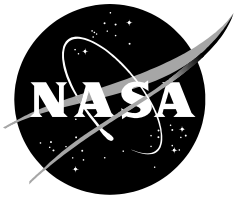

Experimental Investigation of Drag Modulation Aerocapture: Drag-Skirt Separation in Hypersonic Free Flight

Michael C. Wilder
Ames Research Center, Moffett Field, California

Marcus A. Lobbia
Jet Propulsion Laboratory, California Institute of Technology, Pasadena, California

Adam P. Nelessen
Jet Propulsion Laboratory, California Institute of Technology, Pasadena, California

Alex Austin
Jet Propulsion Laboratory, California Institute of Technology, Pasadena, California

Joshua A. Ravich
Jet Propulsion Laboratory, California Institute of Technology, Pasadena, California

David W. Bogdanoff
Analytical Mechanics Associates, Inc.
Ames Research Center, Moffett Field, California

Paul F. Wercinski
Ames Research Center, Moffett Field, California

Ethiraj Venkatapathy
Ames Research Center, Moffett Field, California

National Aeronautics and
Space Administration

Ames Research Center
Moffett Field, CA 94035-1000

July 2020

Acknowledgments

This work was supported by the Jet Propulsion Laboratory, California Institute of Technology, through Research and Technology Development (R&TD) Tasks #R.18.023.044 and R.18.023.044.2.RSA, and Ames Research Center, through the Center Innovation Fund (CIF) award “Single-event drag modulated aerocapture at Venus for a small satellite science mission”. The authors wish to thank the ballistic-range crew, Charles Cornelison, Donald Bowling, Alfredo Perez, Jon-Pierre (JP) Wiens, and Richard Ryzinga for their support in conducting the experiments and developing innovative tools and approaches to enable new testing methods.

NASA STI Support Services
Mail Stop 148
NASA Langley Research Center
Hampton, VA 23681-2199
757-864-9658

National Technical Information Service
5301 Shawnee Rd.
Alexandria, VA 22312
webmail@ntis.gov
703-605-6000

This report is also available in electronic form at http://www.sti.nasa.gov/ and http://ntrs.nasa.gov

Table of Contents

List of Figures

List of Tables

Abstract

Free flight tests were conducted in carbon dioxide at Mach 12 of notional drag modulation aerocapture configurations for a small satellite mission to Venus. The configurations were based on research conducted at the Georgia Institute of Technology, University of Colorado Boulder, Jet Propulsion Laboratory, and Ames Research Center. The drag modulation aerocapture approach being studied involves an atmospheric entry vehicle that employs an attached drag device, a drag skirt, that is jettisoned at the appropriate time to allow the payload-portion of the vehicle to exit the atmosphere, slowed enough to be captured into orbit. A total of eight tests were performed. Reynolds numbers, based on the pre-separation base diameter, ranged from 0.82×10^6 to 2.96×10^6. The tests demonstrated the feasibility of a clean drag skirt separation at hypersonic speeds and, for the conditions of the tests, the stability of the central flight system body during and after separation from the drag skirt. Two drag skirt geometries were tested: an axisymmetric conical frustum, and a faceted frustum representative of a mechanically-deployable device. Drag skirts of various masses were tested to examine the effect of pre- and post-separation ballistic coefficient ratio on the separation dynamics. A new test capability for multi-body interactions in hypersonic free flight was developed for these tests, and is described.

Nomenclature

A = Model, or vehicle, frontal area

a = Speed of sound, $a = (\gamma RT)^{1/2}$.

C_D = Drag coefficient

C_m = Pitching moment coefficient

C_{m_q} = Pitch damping coefficient

C_{m_α} = Moment curve slope, $\partial C_m / \partial \alpha$

D = Model diameter at the maximum diameter.

I_{xx} = Axial, or rolling, moment of inertia.

I_{yy} = Transverse, or pitching/yawing, moment of inertia. $I_{yy} = I_{zz}$.

L = Model length.

M = Mach number, V/a.

P_∞ = Free stream pressure.

R = Universal gas constant, R = 188.92 J/kg-K for CO_2.

Re_D = Freestream Reynolds number, $\rho_\infty V(x) D / \mu_\infty$.

T_∞ = Free stream gas temperature.

t = Time at which video or shadowgraph images were acquired.

V(x) = Velocity.

V_{av} = Average velocity on each measurement interval from eqn. (3).

x_{av} = Location where the velocity equals V_{av}, approximately half way between measurement stations (see section 7).

x_{CG} = Axial location of the center of gravity of the model component, measured from the geometric nose.

x, y, z = Location of the center of gravity of each model component in terms of the longitudinal, transverse, and vertical facility coordinates, respectively.

Δx = Axial separation distance between the center body and drag skirt model components, measured from the center of gravity of each component. The "Source" column indicates whether Δx was measured directly from an image (video or shadowgraph) capturing both components, or was inferred from a photobeam trace, as described in section 7.

γ = Ratio of specific heats, $\gamma = 1.2904$ for CO_2.

θ, ψ, ϕ = Pitch, yaw, and roll angles, respectively, measured relative to facility coordinate system.

μ_∞ = Test gas viscosity, calculated using Sutherland's law.

σ = Total angle of attack, $\sigma = (\theta^2 + \psi^2)^{1/2}$ (note: σ_{RMS}, the root-mean-square total angel of attack, is labeled α_{RMS} in the results discussion is section 8.

ρ_∞ = Test gas density, calculated for ideal gas, $\rho_\infty = P_\infty/RT_\infty$.

1. Introduction

In recent years, research conducted at the Georgia Institute of Technology, University of Colorado Boulder, Jet Propulsion Laboratory (JPL), and NASA Ames Research Center (ARC) has advanced the understanding of drag modulation (DM) methods (as opposed to the predominant bank-to-steer lifting methods) as a means to reduce aerocapture systems complexity. These techniques simplify the required avionics algorithms, sensors, and actuators, and eliminate the need for a center-of-gravity offset and an onboard propulsive reaction control system. Aerocapture coupled with drag modulation shows great promise for enabling small and large spacecraft to capture into orbit at lower cost and reduced risk compared to propulsive and traditional aero-assist techniques. In drag modulation aerocapture the spacecraft and drag skirt together make up the "pre-jettison" configuration, which is what enters the atmosphere and has a low ballistic coefficient to decrease the velocity sufficiently for the spacecraft to enter into orbit. During the aerocapture maneuver, the timing of drag skirt jettison is modulated based on sensed decelerations in order to target the desired orbit. The high ballistic coefficient spacecraft becomes the "post-jettison" configuration. The ratio of the ballistic coefficients between these two configurations determines how flexible the timing of the jettison event can be, with a higher value corresponding to more control authority. Studies of discrete single-event drag modulation aerocapture have shown these systems to be feasible at a variety of planetary destinations for a wide range of payloads. The current Research and Technology Development (R&TD) study results suggest that these systems can be robust to navigation errors and uncertainties in atmospheric density conditions.

While drag modulation shows promise for reducing the complexity of aerocapture systems, there are technical challenges that need to be addressed through engineering analysis and test. A limited number of ballistic range tests have been conducted to address some of these technical challenges. The test models were based on a notional flight system design presented in Ref. 1, and shown in Figure 1. The studies in Ref. 1 also considered the option of a deployable drag skirt, such as the Adaptable, Deployable Entry and Placement Technology (ADEPT) concept [2], also shown in Figure 1. ADEPT employs an umbrella-like deployable structure with a "skin" that is a 3-D woven carbon fabric to serve as the thermal protection system (TPS). The ADEPT structure is folded during launch and then deployed prior to atmospheric entry, which could enable the entire flight system to be packaged into a smaller volume to make it easier to launch as a secondary payload.

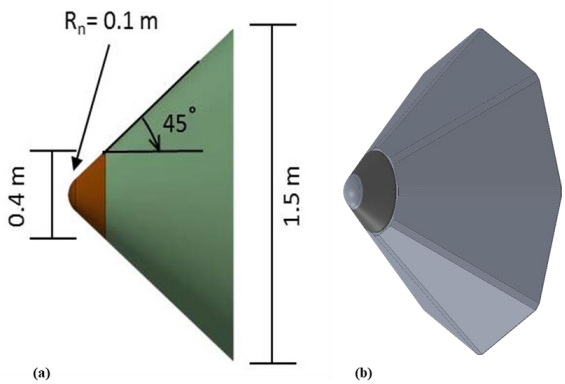

Figure 1: (a) Notional aerocapture flight system with the spacecraft central body (orange) and the drag skirt (green) (from Ref. 1); (b) concept with ADEPT drag skirt.

2. Test Objectives

A set of test objectives was developed based on the drag modulation aerocapture (DMA) mission scenarios being studied and primary areas of concern for DMA concepts. A total of eight were performed.

Primary Test Objectives:

1. Demonstrate the feasibility of a clean drag skirt separation
    a. Test at relevant hypersonic conditions to characterize flow-body interactions during the DM skirt separation event
    b. Verify the stability of the central flight system body during and after separation from the drag skirt
    c. Verify the stability (or lack thereof) of the skirt in the central body wake
2. Obtain experimental data of relevant configurations in hypersonic flow to benchmark CFD codes for future DM development work

Secondary Test Objectives:

3. Experimentally characterize the aerodynamic/stability coefficients of the vehicle, including the force, moment, and moment damping coefficients
4. Characterize any differences in flight/separation for an axisymmetric vs. faceted drag skirt configuration
5. Characterize changes in DM separation dynamics due to different flow conditions (e.g., Mach and Reynolds numbers)

Note that due to the limited number of test shots available, the secondary objectives are addressed to the extent possible. It is expected that future test campaigns (including tests at different types of facilities such as wind tunnels) will be required to further fulfill these secondary objectives.

Additionally, again due to the limited number of tests, the focus will be on the axisymmetric ("rigid") drag skirt configuration, as this removes the dependence of any test results on vehicle roll attitude and initial clock angle. While much of the current R&TD study effort is directed towards the ADEPT-derived faceted configuration, future testing can be used to further elucidate the effects of the faceted shape. This type of study might be better suited to a wind tunnel test entry, where (depending on the specific facility and test setup) a comprehensive test matrix can be executed to measure aerodynamic coefficients at different attitudes and flow conditions for both faceted and axisymmetric configurations.

3. Facility Overview

This test campaign was conducted in the NASA Ames ballistic range, the Hypervelocity Free-Flight Aerodynamics Facility (HFFAF) [3]. The facility consists of a model-launching gun, a section referred to as the sabot separation chamber, a 23 m long test section, and an impact chamber to stop the model. Photographs of the sabot separation chamber and the test section are shown in Figure 2. The facility can be pumped down to pressures below one atmosphere, or can be evacuated and backfilled with various gases to simulate flight through non-Terrestrial atmospheres. The current tests were conducted in CO_2 gas in order to simulate the DM configurations in a Venus-like atmosphere.

A variety of model-launching guns are available, including light-gas guns (7.1 to 38.1 mm bore) for hypersonic testing, and powder guns (20 to 61 mm) for supersonic and subsonic testing. The 38.1 mm light-gas gun was used for these tests. While velocities as high as 9 km/s have been achieved with this gun, structural limitations on the DM configuration launch package led to a maximum launch velocity of ~3.5 km/s in the current campaign. Ballistic-range models are packaged for launch in a segmented cylindrical carrier structure called a sabot, which is aerodynamically separated from the model while in the separation chamber. Although test-section pressures as low as 0.03 Torr (4 Pa) can be achieved, a relatively high pressure (~30 to 50 Torr) is required to achieve aerodynamic

sabot separation. Since drag-skirt separation also occurred in the separation chamber, this requirement placed a lower limit on the freestream gas pressure for these tests.

The separation chamber is equipped with four high-speed video cameras (30-80 kHz), as shown in Figure 2(a). Typically used for confirming the quality of sabot separation, these cameras were used here to image the drag-skirt separation process in the first 5 m of flight from the gun muzzle. The optical arrangements of these cameras are sketched in Figure 3. The main test section is equipped with 16 shadowgraph stations, evenly spaced every 1.524 m (5 feet), with the first station located 10 m from the gun, as sketched in Figure 3. Each station provides orthogonal side- and top-view shadowgraphs, from which the instantaneous position and orientation of the model can be measured relative to reference wires mounted outside the test section. The shadowgraph cameras are spark-illuminated, and Kerr-cell shuttered, to produce an exposure time of 40 ns. Elapsed-time data are provided by 16 high-speed digital counters, synchronized by the gun-fire signal, and each stopped by that station's shadowgraph shutter. The video cameras are also triggered by the gun-fire signal, thereby providing a common time base for all images. Further details about the imaging systems will be given in section 6.

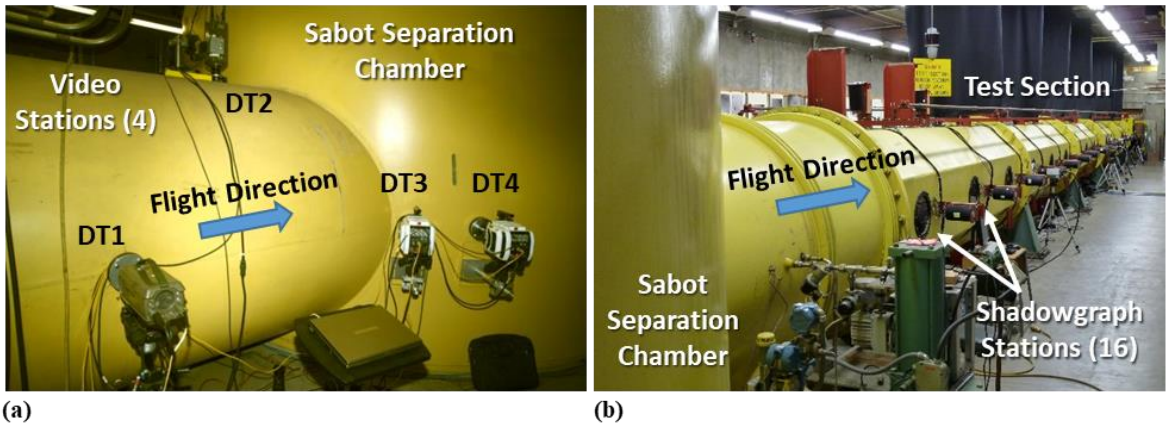

Figure 2: The Hypervelocity Free Flight Aerodynamic Facility: (a) four high-speed video stations on the separation chamber; (b) the main test section with 16 shadowgraph stations.

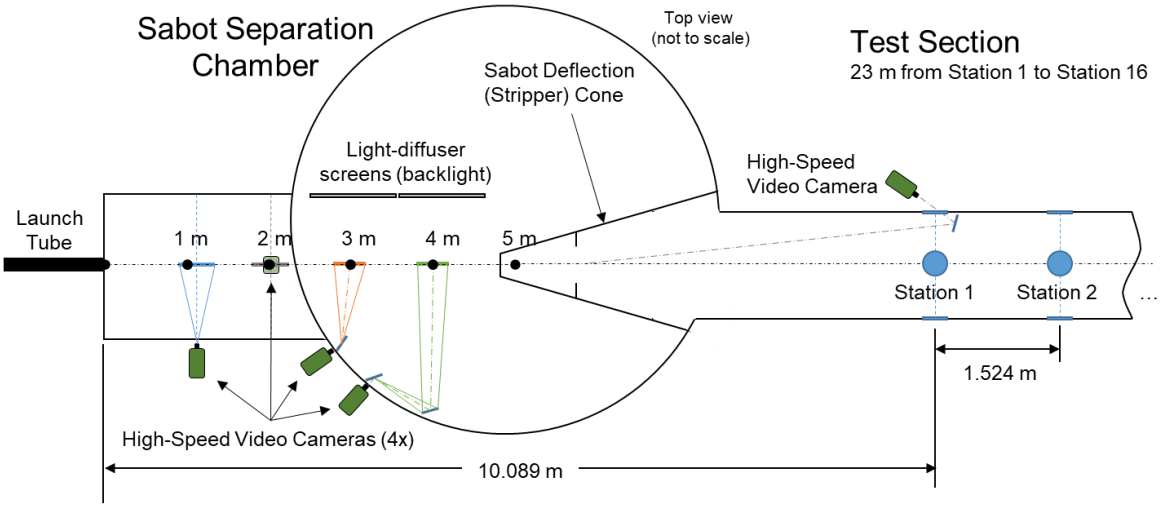

Figure 3: Sketch of sabot separation chamber showing the high-speed video camera setup and approximate fields of view.

4. Model Configurations

Designing a ballistic-range model that could jettison the drag skirt at a specific time in the flight was outside the budget and schedule scopes of this project. The simplest approach was to hold the un-connected components in their pre-separation configuration in the launch sabot, and allow the drag skirt separation to begin as soon as released by the sabot. With this approach, the drag skirt separation must be imaged in the sabot-separation chamber of the ballistic range, and the possibility of unwanted interactions with the sabot segments arises. A pathfinder test, briefly described in Refs. 1 and 4, was performed in 2018 to develop the necessary instrumentation setup (shown in Figure 3 and described in section 6), and to evaluate the degree of sabot interference. Based of those results, it was decided to proceed with the same approach for the current test campaign.

The drag skirt of the notional flight system shown in Figure 1 is an open-back shell, as shown in cross-section in *Figure 4*(a). The ballistic range model experiences extreme acceleration loads during a hypersonic gun launch (greater than 100,000 g), and an un-supported shell could not withstand such high loads. The ballistic-range model drag skirt, shown in Figure 4(b), was a nearly-solid frustum with a cylindrical hole through the center. The hole diameter was scaled to the diameter of the forward opening in the flight-system drag skirt. This allowed for flow through the drag skirt, although the expansion of flow through the skirt model was expected to differ from the flight system. During launch, the center body model component sat on the leading edge of the drag skirt, and was held in place by the sabot, as shown in Figure 4(b) and Figure 5. The base of the sabot was sealed with a thin base plate, referred to as an obturator disk, which also served as a gas seal to prevent penetration of the hot propellant gas into and around the sabot. To facilitate aerodynamic separation of the base plate from the drag skirt, the plate was made as thin as structurally possible. Figure 5 shows a photograph of an assembled model in the sabot with two sabot segments removed to show interior detail. Looking ahead, Figure 12 in section 6 shows stages of a sabot separation.

The center body model had a forebody geometry equivalent to that of the Pioneer-Venus probes: a 45° half-angle cone with a spherical nose radius equal to half the base radius. Unlike Pioneer-Venus, which had a spherical afterbody, the afterbody of the notional aerocapture flight system center body has a faceted shape. The faceted afterbody of the ballistic-range model is shown in Figure 6. The center body model nose radius was 0.203 cm (0.08 in). The base diameter, had there been no shoulder radius, was 0.813 cm (0.320 in). However, a shoulder radius of 0.015 cm (0.006 in) was added, resulting in an as-built base diameter of 0.767 cm (0.302 in), and an actual nose-to-base radius ratio of 0.53, rather than the 0.5 of Pioneer-Venus. The center body model was of bimetallic construction in order to achieve the desired axial center of gravity location. The model was fabricated from a tungsten alloy in order to provide the highest ballistic coefficient possible, with an aluminum nose piece for CG placement. Detailed drawings with dimensions are provided in Appendix A.

Two drag-skirt geometries were tested: a 45° axisymmetric cone, and a faceted cone representing an ADEPT deployable system [1, 2] with a 45° half angle along the largest diameter, representing the structural ribs of the ADEPT. The base diameter of the drag skirts, prior to adding a radius at the shoulder, was 3.048 cm (1.2 in). A 0.007 cm (0.003 in) radius was then applied to the shoulder. The drag skirts were made of various metal alloys (magnesium, aluminum, titanium, and stainless steel) to provide a range of ballistic coefficients. Examples of both drag skirt geometries are shown in Figure 6, and detailed drawings with dimensions are provided in Appendix A. Note that the titanium drag skirts were added to the test matrix in the course of testing. Fabrication of these parts was outsourced to a commercial rapid-prototyping shop in order to meet the on-going testing schedule. Due to tooling limitations of the fabricator the undercut area of the base, and the center-hole diameter, were slightly different. An as-built drawing of the titanium drag skirt is also provided in Appendix A.

The ballistic-range models are single-use, therefore multiple copies of each component were fabricated to execute the test program. Table 1 lists the number of each type of model component fabricated, as well as key characteristics for each relevant to the test.

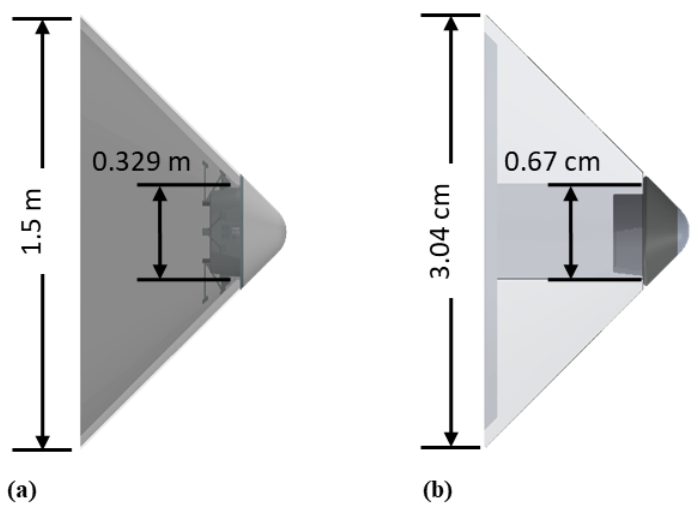

Figure 4: Notional aerocapture flight system (a), and ballistic range model (b), with the drag skirts shown in cross section.

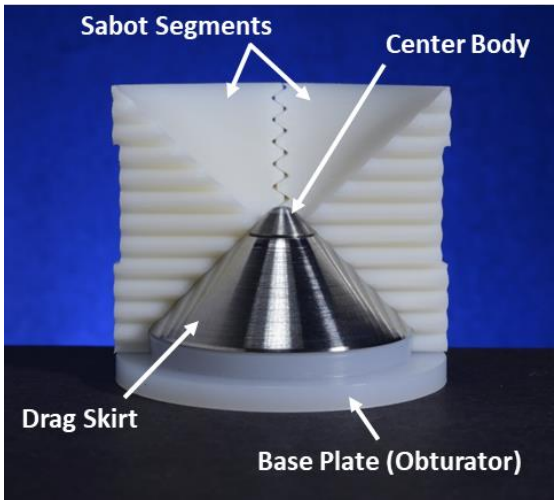

Figure 5: Ballistic range model in launch sabot with two segments removed.

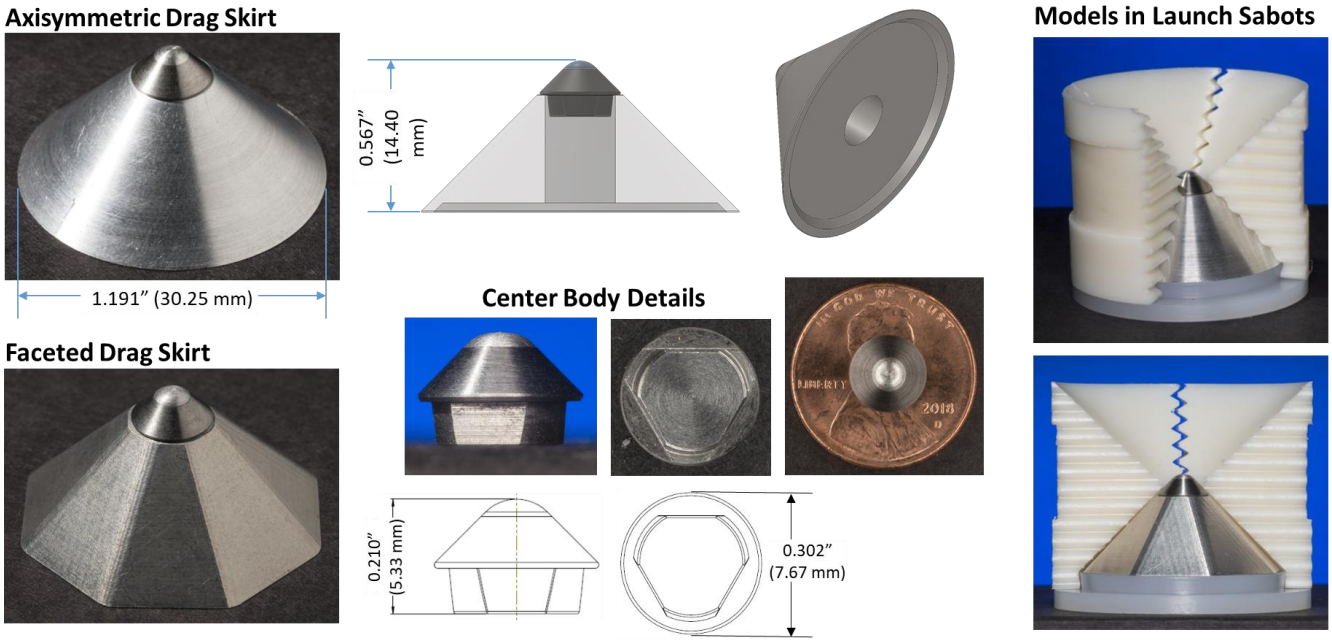

Figure 6: Pictures of as-fabricated test model components.

Table 1: Fabricated model parts, with characteristics based on nominal design.

	Material	Qty Fabricated	BR[1]
Center Body	Tungsten w/ Aluminum tip	10	-
Drag Skirt (Axisymmetric), Low-BR	Steel	2	1.3
Drag Skirt (Axisymmetric), Low/Mid-BR	Titanium	2	2.2
Drag Skirt (Axisymmetric), Mid-BR	Aluminum	2	3.1
Drag Skirt (Axisymmetric), High-BR	Magnesium	2	4.3
Drag Skirt (Faceted), Low-BR	Steel	2	1.4
Drag Skirt (Faceted), Mid-BR	Aluminum	1	3.4
Drag Skirt (Faceted), High-BR	Magnesium	1	4.7

[1]BR is calculated as the center body divided by the integrated vehicle ballistic coefficients, assuming $C_d = 1$

Measurements were made of each as-fabricated model component and the results are listed in Table 2 along with the as-designed values. The length, diameter, and mass were measured for all components. The axial center of gravity (CG) location and the principal moments of inertia were measured for each center body model. The axial center of gravity (CG) location of the drag skirts was measured only for the last three models tested, and only the roll-axis moment of inertia was measured for any of the drag skirts. Since the drag skirts were of a simple geometry and single-material construction, and it was anticipated that the drag skirt separation from the center body would place it out of the view of most of the shadowgraph stations, which would preclude aerodynamic coefficient determinations, it was decided to rely on the mass properties computed from the CAD models. The axial, or roll-axis, moment of inertia, which did not require fabricating a new mounting fixture, was measured as a cross check of the CAD model values. After several drag skirts were observed to tumble after separation, a CG instrument fixture was modified to allow measurement of the drag-skirt CG location for the final three models tested.

The coordinate systems for model measurements are shown in Figure 7. Moments of inertia were measured about the center of gravity for all models, and the values of the axial CG, x_{CG}, given in Table 2, are relative to the geometric nose of each part. For the center body models the orientation of the y and z axes was selected so that a flat segment of the afterbody was down, as shown in Figure 7. Similarly, the ADEPT drag skirts were oriented with a flat segment down, as also shown in Figure 7. All models were loaded with the z axis nominally oriented up, aligned with the test facility vertical axis, although precise orientation cannot be achieved during loading of the gun.

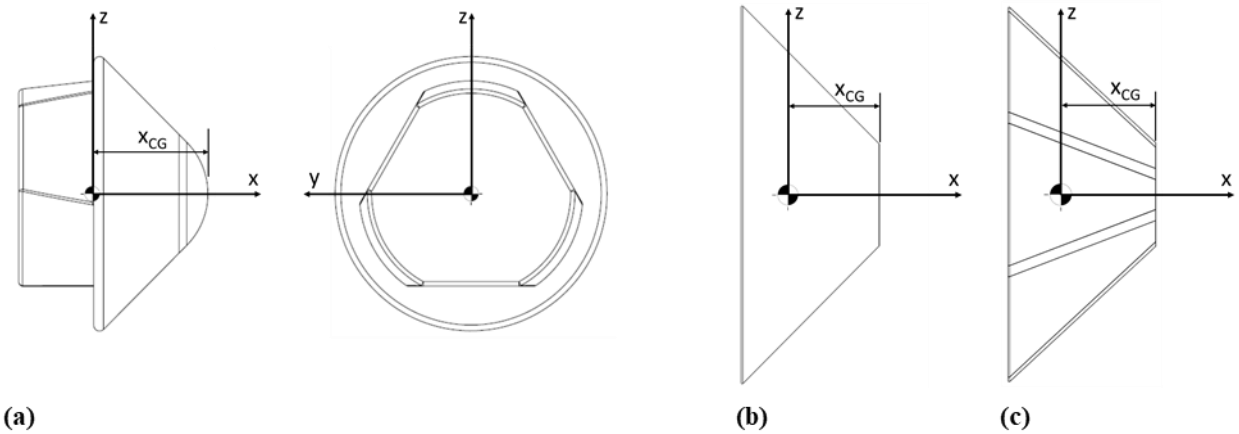

Figure 7: Coordinate system orientation for the model mass properties (a) Center body; (b) Axisymmetric drag skirt; (c) ADEPT drag skirt.

Table 2: Geometric and mass properties of tested configurations.

		Baseline Test Series					Bonus Tests		
Test #		1	2	3	4	5	6	7	8
Shot #		2815	2816	2817	2818	2819	2820	2821	2822
Skirt Shape		Axisymmetric	Axisymmetric	Faceted	Axisymmetric	Axisymmetric	Axisymmetric	Axisymmetric	Faceted
Skirt Material		Steel	Aluminum	Steel	Steel	Titanium	Titanium	Aluminum	Aluminum
Center Body									
Model ID	-	FS-01	FS-02	FS-03	FS-04	FS-05	FS-06	FS-08	FS-09
As-Measured									
Length	*cm*	0.531	0.536	0.538	0.536	0.536	0.535	0.527	0.534
Diameter	*cm*	0.767	0.767	0.766	0.766	0.768	0.769	0.769	0.767
Mass	*g*	1.98	1.96	1.97	2.00	1.97	2.02	1.97	1.98
x_{CG} from Nose	*cm*	0.325	0.329	0.331	0.326	0.327	0.323	0.320	0.325
x_{CG}/Diameter	*%*	42.4%	42.9%	43.2%	42.6%	42.6%	42.1%	41.6%	42.3%
I_{xx} (axial moment)	*g-cm^2*	0.08	0.08	0.09	0.09	0.09	0.10	0.11	0.10
I_{yy}, I_{zz} (transverse)	*g-cm^2*	0.07	0.07	0.09	0.07	0.07	0.10	0.08	0.08
As-Designed									
Length	*cm*	0.533	(same)	(same)	(same)	(same)	(same)	(same)	(same)
Diameter	*cm*	0.767	(same)	(same)	(same)	(same)	(same)	(same)	(same)
Mass	*g*	1.96	(same)	(same)	(same)	(same)	(same)	(same)	(same)
Nose Radius	*cm*	0.203	(same)	(same)	(same)	(same)	(same)	(same)	(same)
x_{CG} from Nose	*cm*	0.326	(same)	(same)	(same)	(same)	(same)	(same)	(same)
x_{CG}/Diameter	*%*	42.5%	(same)	(same)	(same)	(same)	(same)	(same)	(same)
I_{xx} (axial moment)	*g-cm^2*	0.095	(same)	(same)	(same)	(same)	(same)	(same)	(same)
I_{yy}, I_{zz} (transverse)	*g-cm^2*	0.073	(same)	(same)	(same)	(same)	(same)	(same)	(same)
Drag Skirt									
Model ID	-	DS-SS01	DS-AL01	DS-ADEPT-SS01	DS-SS02	DS-Ti01	DS-Ti02	DS-AL02	DS-ADEPT-Al01
As-Measured									
Length	*cm*	1.113	1.129	1.123	1.118	1.118	1.120	1.127	1.119
Diameter	*cm*	3.025	3.034	3.040	3.033	3.020	3.018	3.032	3.035
Mass	*g*	21.27	7.75	19.74	21.37	11.98	11.91	7.69	7.08
x_{CG} from Nose	*cm*	-	-	-	-	-	0.706	0.734	0.719
x_{CG}/Diameter	*%*	-	-	-	-	-	23.4%	24.2%	23.7%
I_{xx} (axial moment)	*g-cm^2*	-	5.86	13.68	16.26	9.37	9.29	5.83	4.94
As-Designed									
Length	*cm*	1.118	1.118	1.118	1.118	1.118	1.118	1.118	1.118
Diameter[1]	*cm*	3.025	3.025	3.025	3.025	3.025	3.025	3.025	3.025
Mass	*g*	22.09	7.76	19.98	22.09	12.11	12.11	7.76	7.02
x_{CG} from Front Face	*cm*	0.725	0.725	0.719	0.725	0.720	0.720	0.725	0.719
x_{CG}/Diameter	-	24.0%	24.0%	23.8%	24.0%	23.8%	23.8%	24.0%	23.8%
I_{xx} (axial moment)	*g-cm^2*	16.709	5.869	13.760	16.709	9.326	9.326	5.869	4.833
I_{yy}, I_{zz} (transverse)	*g-cm^2*	9.666	3.395	8.044	9.666	5.388	5.388	3.395	2.826

[1] *Diameter for faceted configurations defined as rib-to-rib at rib center; faceted shapes have face-to-face diameter of 2.830 cm.*

Lengths and diameters were measured using a calibrated digital micrometer. A minimum of four measurements were made of each dimension, and averaged. Repeatability was to within ±0.0013 cm (±0.0005 in). Mass was measured on a Mettler Toledo model MS304S digital balance. The instrument repeatability is 0.0001 g standard deviation. For each model a minimum of four readings were averaged and the standard deviation was less than 0.0002 g.

Center of gravity location was measured using a Space Electronics, Inc. model SE300 single axis CG instrument. The instrument is designed to precisely locate the CG of small test objects along a single axis. Off-axis CG displacement can be determined by differencing measurements made with the model rotated 180° about the primary measurement axis. Based on the standard deviation of repeated measurements, the CG position along the primary measurement axis was determined to within ± 0.005 cm (± 0.002 in). While not reported in Table 2 the transverse (off-axis) CG position was zero (to within the measurement uncertainty) for all parts measured. All parts were measured at least four times, with the part rotated 90° about the measurement axis for each measurement, and the results averaged. In some cases additional measurements were made as a check on repeatability. In addition, before and after each measurement session, measurements were made of a precision right cylinder with known CG location to calibrate the location of the model mounting fixture relative to the instrument axes. The standard deviation of all right cylinder measurements was 0.0005 cm (0.0002 in). All measurements were made relative to

the flat base of the model and translated to the leading edge (the geometric nose tip of the center body models, and the top of the frustum of the drag skirts, where the skirt contacts the center body before separation) by subtracting from the measured lengths. The measured CG location of the center body models differed no more than 0.006 cm (0.0024 in) from the as-designed position, with only two models differing by more than 0.003 cm (0.001 in).

Moments of inertia were measured using a Space Electronics, Inc. model XKR1A4 moment of inertia instrument. The instrument operates on the principle of the inverted torsion pendulum. The test object rests on a table attached to precision low friction bearings which constrain the motion of this torsion member to pure rotation. A sensing device produces timing pulses which start and stop a digital period counter to determine the period of the oscillating system. The moment of inertia about the axis of the torsion rod is proportional to the square of the period of oscillation. The proportionality constant is determined by measuring the oscillation period of a precision sphere of known mass and diameter. The instrument specifications quotes an accuracy of 0.5% for moment of inertia greater than 1.5 g-cm^2. This value, however, is nearly two orders of magnitude larger than the expected moment of inertia of the center body models. In order to assess the measurement accuracy for small moments of inertia, a series of measurements were made of several precision spheres. Results are shown in Figure 8, which compares the mean measured moments of inertia against the expected values for each sphere. The error bars are ± 3 standard deviations from the mean, and the data labels give the percent difference of the mean value form the expected value. In the range of values expected for the center body moment of inertia, the sphere measurements differed from 12% to 34% from the expected values. The transverse moment of inertia (I_{yy}) measurement results for the center body models shown in Table 2 differ no more than 33% from the as-designed value, with only two models differing more than 11%.

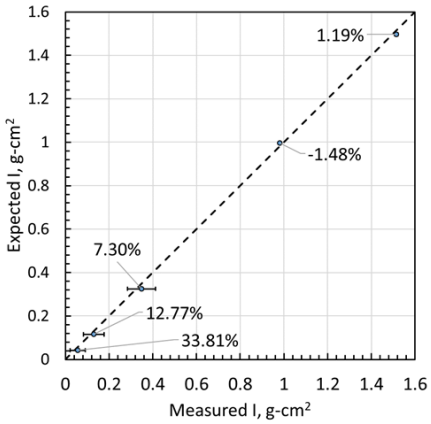

Figure 8: Moment of inertia measurement accuracy for small values as determined from measurements of precision spheres.

5. Test Matrix

When designing a ballistic-range test, the choice of test conditions (velocity, pressure, and test gas) and the model design (size and materials) are driven by the test objectives, and by physical constraints such as the launch stresses and launcher diameter. Ordinarily, the design goal for a ballistic-range aerodynamics test is to achieve, if possible, both aerodynamic and dynamic similarity with full-scale flight, and if not possible, to prioritize the various similarity parameters based on the test objectives. These parameters are typically the Mach and Reynolds numbers, and the scaled mass properties, represented as $I/\rho_\infty D^5$ and $m/\rho_\infty D^3$ [5, 6].

Flight conditions at the time of drag-skirt jettison for two notional entry trajectories studied under the Aerocapture R&TD project [1, 10] are given in Table 3. The trajectory designations refer to whether the DM flight system is delivered to the vicinity of Venus on a flyby mission, using Venus as a gravity assist, or a mission entering orbit around Venus [1]. In either case, the DM flight system is released on approach to the planet, while still at super-orbital speed. The ballistic-range tests were conducted in CO_2 in order to simulate the DM configurations in

a Venus-like atmosphere. Although flight Mach numbers could not be achieved in the ballistic range, it was expected that the drag, pitching moment, and pitch damping coefficients would be nearly constant for Mach numbers greater than ~8, based on the aerodynamics of the Pioneer-Venus entry vehicle [18-20]. References 19 and 20 also showed that there was only a weak Reynolds number dependence on the hypersonic drag coefficient for 45° sphere-cones for $Re > 10^4$. For average model velocities ~3 km/s in CO_2 the freestream Mach number was ~11 and the center body Reynolds number based of diameter was ~4×10^5, therefore, the test Mach and Reynolds numbers were considered acceptable.

The aerocapture trajectories traverse the upper levels of the atmosphere with the drag skirt jettison event occurring around 100 km altitude, at atmospheric densities on the order of 10^{-4} kg/m^3. At the model scale a test section pressure lower than 1 Torr would be required to achieve mass and moment of inertia similarity with the flight system center body, even when using a dense material like tungsten for the model. As discussed in section 3, this is about two orders of magnitude lower than the minimum pressure required for aerodynamic sabot separation. Therefore, short of developing a new launch technique, these tests could not achieve mass or moment of inertia similarity. However, since the primary objective of this test campaign was to study the drag-skirt separation event, the relative separation rate of the components was proposed as a more relevant scaling parameter. This could be matched by decreasing the ballistic coefficient ratio for the model, thereby slowing the separation rate relative to the velocity in compensation for the higher freestream density. It should be noted that this parameter was expected to apply only in the initial stages of the separation, since the interactions of the drag skirt with the wake and free shear layers of the center body at larger separation distances would be influenced by the mass and moment of inertia scaling.

Table 3: Notional Venus drag-modulation aerocapture flight parameters at drag skirt separation.

Trajectory	**V_∞ km/s**	**M_∞**	**Re_{D_2}**	**T_∞, K**	**ρ_∞, kg/m^3**	**P_∞, N/m^2**
flyby	10.0	38	6.9×10^4	171.5	1.48×10^{-4}	4.87
orbiter	9.3	35	3.4×10^4	174.1	7.98×10^{-5}	2.67

A simplistic estimate of drag-skirt separation was made by calculating trajectories under the influence of drag at the conditions given in Table 3 for the drag skirt, and for the center body, separately, and subtracting their positions as a function of time. The same drag coefficient was used for each component, making the assumption that this is approximately true while the components are in close proximity. This approach gave reasonable estimates of the separation distances measured during the pathfinder ballistic-range tests for separation distances up to ~2 diameters of the center body, as shown in Figure 9, which plots the separation distance in center-body diameters ($\Delta x/D_2$) as a function of a dimensionless time (tV/D_2) - the time for the center body to travel a diameter, D_2. Similar calculations were performed for a full-scale vehicle with a ballistic coefficient ratio of 7.58 at the two conditions given in Table 3. Results are plotted in Figure 10 along with results for ballistic range models with various ballistic coefficient ratios, and at several free stream pressures. It can be seen that by decreasing the model-scale ballistic coefficient ratio, the initial separation rate approaches that of flight at a higher ballistic coefficient ratio and lower atmospheric pressure.

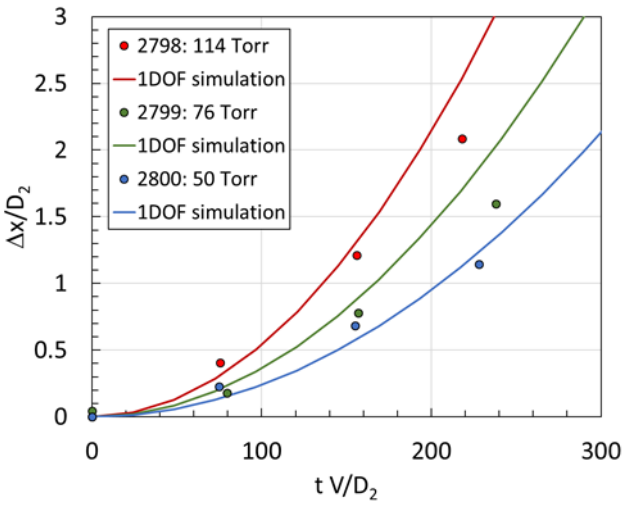

Figure 9: Non-dimensional drag-skirt separation distance as a function of non-dimensional flight distance for the pathfinder ballistic range test: Simple drag simulation (solid lines), and test results (symbols).

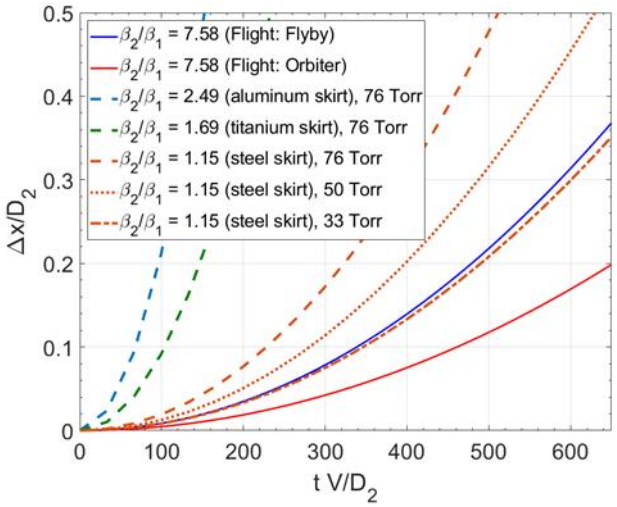

Figure 10: Non-dimensional drag-skirt separation distance as a function of non-dimensional flight distance for two flight trajectories (solid lines) and ballistic-range tests (broken lines) having various ballistic-coefficient ratios and freestream pressures.

In order to assess the effect of ballistic coefficient ratio on drag skirt separation, skirts were made from various materials, giving ballistic coefficient ratios from 1.3 to 4.3 for the axisymmetric drag skirt; however, the largest ballistic-coefficient-ratio configuration has not been tested. An initial prioritized test matrix was developed for six shots addressing the test objectives discussed above. However, it was expected that the results from each test would be used to inform whether to continue with the initial plan, or potentially change the priority of the matrix and/or look at alternative tests not initially planned. As the tests proceeded, this approach led to many incremental changes, including the fabrication of the titanium drag skirts to provide a set of low/mid-BR test shots. Additionally, the facility was able to execute additional tests beyond the initial six planned, and therefore additional "bonus" tests were also added to the test matrix.

The final test matrix (with 8 shots in total) is shown in Table 4. The primary investigations included looking at variations in ballistic coefficient ratio (low, low/mid, and mid), axisymmetric vs. faceted drag skirts, and effects of freestream pressure on the skirt separation and flight dynamics of both center body and skirt. A repeat shot of the baseline test was also performed to gage the repeatability of the ballistic range shots for this test application.

Table 4: As-planned and executed test matrix, where primary delta from baseline test (shot 2815) is shown in red.

		Baseline Test Series					Bonus Tests		
Test #		1	2	3	4	5	6	7	8
Shot #		2815	2816	2817	2818	2819	2820	2821	2822
Name		Baseline	Mid-BR	ADEPT	Repeat Baseline	Low/Mid-BR	High Pressure	Low Pressure	Mid-BR ADEPT
Skirt Shape		Axisymmetric	Axisymmetric	Faceted	Axisymmetric	Axisymmetric	Axisymmetric	Axisymmetric	Faceted
Skirt Material		Steel	Aluminum	Steel	Steel	Titanium	Titanium	Aluminum	Aluminum
Ballistic Coeff. Ratio		1.3	3.2	1.4	1.3	2.2	2.2	3.2	3.5
Planned Test Conditions									
Velocity	*m/s*	3298	3298	3298	3298	3298	3298	3298	3298
Pressure	*atm*	0.150	0.150	0.150	0.150	0.150	0.250	0.066	0.150
Temperature	*K*	293	293	293	293	293	293	293	293
Mach	-	12.3	12.3	12.3	12.3	12.3	12.3	12.3	12.3
Actual Test Conditions									
At Launch									
Velocity	*m/s*	3279	3023	3233	3217	3305	3247	3390	3287
Mach	-	12.19	11.26	12.04	11.97	12.32	12.07	12.61	12.25
Re_D (Center Body)	-	4.56E+05	4.23E+05	4.51E+05	4.48E+05	4.64E+05	7.54E+05	2.08E+05	4.60E+05
Re_D (Drag Skirt)	-	1.80E+06	1.67E+06	1.79E+06	1.77E+06	1.83E+06	2.96E+06	8.22E+05	1.82E+06
Dynamic Pressure	*Pa*	1.46E+06	1.24E+06	1.42E+06	1.41E+06	1.49E+06	2.38E+06	6.87E+05	1.47E+06
At Mid-Range									
Velocity	*m/s*	3083	2826	3054	3040	3100	2930	3291	3085
Mach	-	11.46	10.53	11.37	11.32	11.56	10.90	12.24	11.49
Re_D (Center Body)	-	4.56E+05	4.23E+05	4.51E+05	4.48E+05	4.64E+05	7.54E+05	2.08E+05	4.60E+05
Re_D (Drag Skirt)	-	1.80E+06	1.67E+06	1.79E+06	1.77E+06	1.83E+06	2.96E+06	8.22E+05	1.82E+06
Dynamic Pressure	*Pa*	1.29E+06	1.09E+06	1.27E+06	1.26E+06	1.31E+06	1.94E+06	6.47E+05	1.30E+06
Test Section									
Pressure	*atm*	0.150	0.150	0.150	0.150	0.150	0.250	0.066	0.150
Pressure	*Pa*	15199	15199	15199	15199	15199	25331	6687.5	15199
Temperature	*K*	296.66	295.66	295.96	296.06	295.26	296.66	296.26	295.46
Viscosity	*kg/m-s*	1.50E-05	1.49E-05	1.49E-05	1.49E-05	1.49E-05	1.50E-05	1.49E-05	1.49E-05
Density	kg/m^3	0.2712	0.2721	0.2719	0.2718	0.2725	0.4520	0.1195	0.2723
Test Gas	-	CO_2	CO_2	CO_2	CO_2	CO_2	CO_2	CO_2	CO_2
Relative Humidity	*%*	3.1	0.08	3.2	3.2	4.1	2.2	2.9	2.9
Speed of Sound	*m/s*	268.9	268.5	268.6	268.6	268.3	268.9	268.7	268.4

6. Measurement Setup

6.1. Sabot Separation Chamber Setup

As discussed above in the test facility description, a series of high-speed video cameras and shadowgraph stations were used to record the model as it traveled through the separation chamber and test section. In a typical ballistic range aerodynamics test all data are obtained in the test section, beginning approximately 10 m downrange of the launcher muzzle. Since the drag skirt separation begins shortly after launch in the current tests, an approach was developed for obtaining quantitative measurements in the separation chamber during the first 5 m of flight. There is no optical access to the region between 5 m (the start of the sabot deflection cone) and 10 m (the first test section optical station).

The separation chamber data acquisition system consists of four Vison Research Phantom high-speed digital video cameras arranged on the exterior of the separation chamber as sketched in Figure 3, and shown in Figure 2(a). All four stations have a 3 in diameter (2.5 in clear view) window port. Video stations 1, 3 and 4 provide a horizontal view of the projectile, while the station 2 port is located on the top of the facility, giving a vertical view. The cameras are triggered by the facility signal that initiates firing the gun, and the cameras record frame time stamps relative to this gun-fire signal. The same signal initializes the shadowgraph camera timers, giving all imaging systems the same relative time base. Video stations 1 and 2 were equipped with Model v12.1 monochrome cameras, and model v2512 color cameras were at the video stations 3 and 4. The v12.1 cameras were configured to record at a resolution of 1024 x 184 pixels, or 2.69 pixels/mm, at 32,000 frames per second, giving 3 to 4 frames across the field of view. Both cameras used a Nikon 50 mm imaging lens. The v2512 cameras were configured to record at a resolution of 1024 x 352 pixels at 68,000 frames per second. The camera at video station 3 used a Nikon 135 mm imaging lens,

giving a resolution of 4.15 pixels/mm, and 4 to 6 frames in the field of view (depending on the rate of drag-skirt separation). The camera at video station 4 used a Nikon 80-200 mm zoom lens at 200 mm, giving a resolution of 2.91 pixels/mm, and 6 to 8 frames in the field of view. Due to the longer object distance at this station (see Figure 3), a 300 mm lens was required to achieve the same resolution as the station 3 camera, however, a 300 mm lens with a sufficiently large aperture for the lighting conditions had an objective too large for the 2.5 in window port. All four cameras were operated at the minimum exposure times of 285 ns for the v12.1 cameras, and 276 ns for the v2512 cameras. The model moved about 1 mm in the exposure time, resulting in about 3 pixels of motion blur.

All four video stations imaged the model against a backlighting system consisting of two 1000 W halogen lamps and a Polypropylene diffuser, some of which can be seen in Figure 11. An example set of video frames from each camera, taken from shot 2819, is shown in Figure 12. The frames in this figure have been aligned horizontally to the drag skirt in order to illustrate the development of the sabot and drag skirt separation. The flight distances from the gun muzzle are, from top to bottom, 1.1 m, 2.0 m, 3.0 m, and 4.0 m. The frames have been cropped horizontally, but show the full-frame vertical field of view of each camera.

The position and attitude of the field of view of each camera, relative to the gun muzzle and the facility axes, was determined before each test using a taut catenary line and a plumb line, both visible in Figure 11. The catenary line was run along the tunnel centerline from a plug inside the sabot defection cone to a pulley mounted at the gun muzzle. The line was run over the pulley and held taut by a weight at the pulley end. The plumb line was mounted on a tripod and moved to each successive camera station where an alignment image was captured. The resolution and image distortions of each camera was determined from images of a checkerboard pattern, aligned with the reference lines, captured at each station (seen Figure 11). The catenary line initially had spherical beads attached at known locations to provide a distance scale, however, several of the beads were dislodged in the process of installing, and removing, the line before each shot. Beginning with the third test, shot 2817, a steel surveying tape measure was added to the alignment system. The tape was attached at the sabot defection cone plug next to the catenary line, and could be lowered while imaging the reference lines, then pulled taut to provide a distance measure.

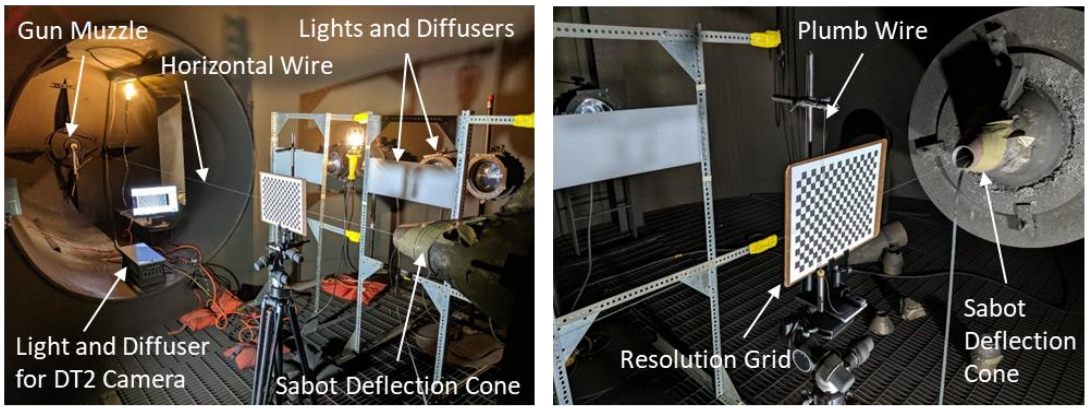

Figure 11: Interior of the sabot separation chamber showing the backlighting system and the video camera alignment and calibration approach: (a) looking uprange towards the gun; (b) looking downrange towards the test section.

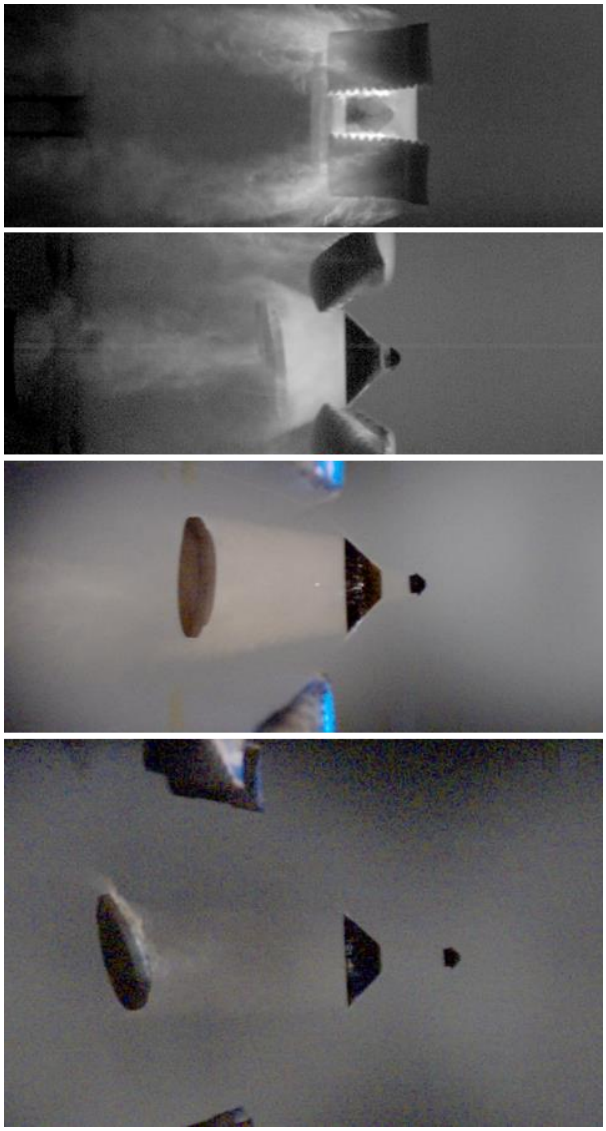

Figure 12: Example set of video frames (shot 2819), aligned vertically at the drag-skirt base, to illustrate sabot and drag skirt separation. Distance from muzzle, top to bottom: 1.1 m, 2.0 m, 3.0 m, 4.0 m.

6.2. Test Section Setup

The main test section, as described in section 3, has 16 spark-illuminated focused shadowgraph stations evenly spaced every 1.524 m (5 feet). The first station is 10 m from the gun muzzle. Each station has two, orthogonal, optical paths through the test section for shadowgraph imaging. The field of view at the first nine stations is 0.3 m (12 in) in diameter, and at the remaining stations is 0.38 m (15 in) in diameter. All stations utilize digital imaging sensors, which are described in detail in Ref. 4. All the horizontal stations, and 10 of the vertical stations, are equipped with Nikon D3200 digital SLR cameras and use Kerr-cell electro-optical shutters [7] to provide a 40 ns exposure. The Nikon cameras use a 6000 x 4000 pixels CMOS sensor. The imaging optics were chosen to fill (approximately) the smaller sensor dimension with shadowgraph window diameter, resulting in an image resolution of about 13 pixels/mm (330 pixels/in) for the smaller windows at the first nine stations, and 10 pixels/mm (260 pixels/in) at the remaining stations. The remaining six vertical stations (4, 6, 8, 10, 11, and 13) use Princeton Instruments PI-MAX 1024 gated intensified CCD (ICCD) cameras. These cameras are operated at a shutter (gate) speed of 5 ns and do not require a Kerr-cell shutter. The sensor size is 1024 x 1024 pixels. Because of the lower pixel count of these sensors, imaging optics with a higher magnification are used to slightly improve the resolution.

Only the central region 10 inches (approximately) of the window diameter is imaged, giving a resolution of about 4 pixels/mm (100 pixels/in) for both window sizes. For typical model sizes this is an acceptable resolution, but is lower than desired for the small diameter of the center body model used in this test, and resulted in a higher than usual uncertainty in the yaw angle determination at these stations. Figure 13 shows an example image from each camera system taken at station 4 for shot 2815.

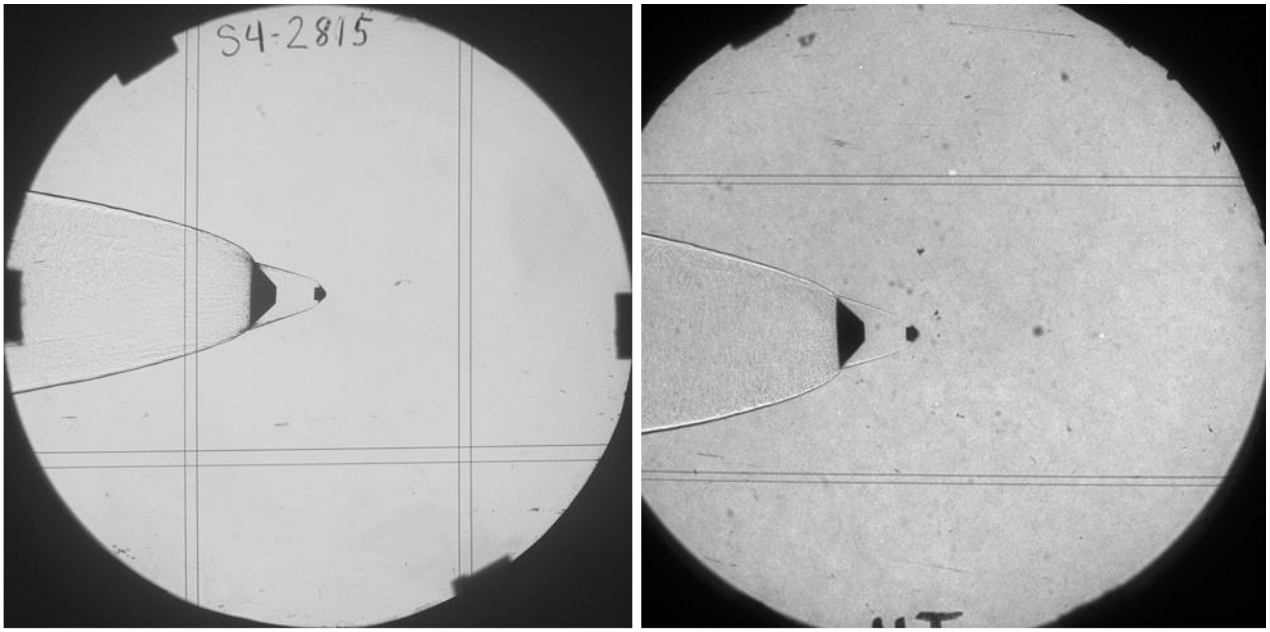

Figure 13: Example shadowgraph images at test section station 4, shot 2815: (a) Nikon D3200 image, horizontal view; (b) PI-MAX 1024 image, vertical view.

While the stations are typically setup and used in shadowgraph configuration, the first station was reconfigured to produce Schlieren images in an attempt to provide further insight into the flowfield and any flow interactions between the center body and drag skirt models. In both the side and top views a knife edge was added at the image of the light source, which happened to be at the back face of the Kerr cell. The knife edge was oriented in the vertical direction, relative to the image coordinates, for both.

Unlike the video cameras on the separation chamber, the shadowgraph cameras acquire a single image each per shot. Acquisition is initiated by a model detection system at each station, which is fully described in Ref. 4. The heritage model detection system was designed and built in the 1960s and employs vacuum-tube-based electronics for signal detection and conditioning. Three stations (6, 10, and 12) have been equipped with a commercially-available IR diode-based detection system, but still require the heritage signal-conditioning electronics to supply the high-voltage output required by the spark-gap light sources and the Kerr-cell shutters. Both approaches detect the model by passing a light sheet (also referred to as a photobeam) through the test section, collecting the light on a photo-detection device (photomultiplier tubes for the heritage systems, and solid-state photodetectors for the diode systems), and then analyzing the detector signal in real time for a change in the light level produced by the passage of the model. When the model is detected a signal is sent to fire the light sources, which then trigger the camera shutters (Kerr cell, or ICCD gate), which, in turn, stop the high-speed timer (HP 53131A Universal Counter) associated with that station. The timers for all 16 stations are synchronized by the gun-fire signal that also triggers the video cameras. For this test campaign the signal output by the photobeam photomultiplier tube for half the stations (1, 3, 5, 7, 9, 11, 13, and 16) were recorded on oscilloscopes in order to determine the temporal separation between the center body and drag skirt in cases where both components were not within the field of view of the shadowgraph image. An example photobeam trace is shown in Figure 14. Analysis of these data will be discussed

in the next section. The diode light screen at station 6 tends to trigger late, with the detected model past the downrange plumb lines. Fortuitously, this allowed capturing an image of both model components at this station for all tests, with the exception of shot 2822, in which the separation was too great even with the delay. Finally, the diode light screen at station 12 proved insensitive to the center body model alone, and in all tests with large separation triggered on the passage of the drag skirt.

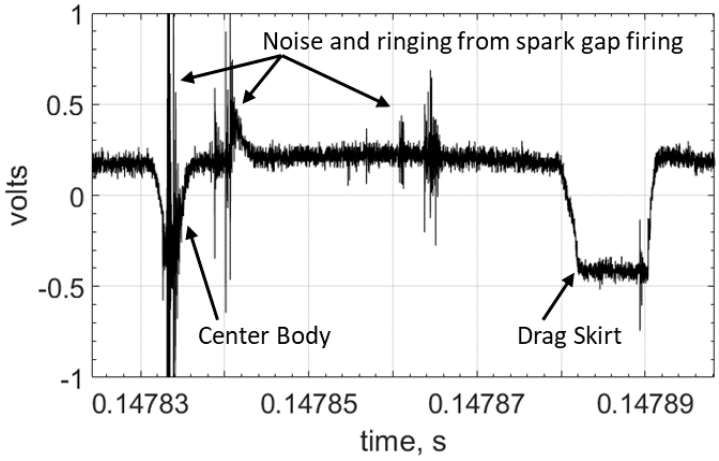

Figure 14: Example signal trace from model-detection photobeam from station 1, shot 2816.

Two additional Phantom video cameras (model v12.1 color cameras) were used for diagnostic visualizations. One was located at shadowgraph station 1 and viewed the model as it exited the sabot separation chamber, as sketched in Figure 3, and was used to verify that the sabot segments were fully deflected by the cone. The second was placed at shadowgraph station 16 and viewed the full length of the test section. These cameras rely on available light for illumination, which is usually supplied by the gun muzzle flash as the hot hydrogen propellant gas contacts the air in the facility. Since the current tests were conducted in a CO_2 atmosphere, there was very little muzzle flash illumination. Even so, the videos did confirm that sabot separation was good for all shots, that the sabot base plate struck the deflection-cone wall on shot 2820, and it was possible to identify whether the drag skirt tumbled, which occurred for shots 2816 and 2820.

The main test section has a fixed fiducial system against which the position and attitude of the model is measured. The system consists of six taut wires that run the full length of the test section: two above the top windows, two below the bottom windows, and two catenary wires, one on either side of the tunnel outside the side windows. In addition, there are four plumb lines at each station, two on either side. These wires can be seen in the shadowgraph images in Figure 13, and the system is described in detail in Ref. 13.

7. Data Reduction Approach

The primary data acquired in each ballistic-range test were four video sequences, 32 shadowgraph images, the time of acquisition of each image, and the test gas pressure, temperature, and relative humidity. In addition, the raw output of the model-detection system was recorded for half the stations to allow determining of the drag-skirt separation in cases where the separation distance from the center body model was too large to capture both components in the shadowgraph images. As discussed in the following sections, the images were measured to determine the position and orientation of each component imaged, from which the separation as a function of flight time, or distance, was determined. The trajectories thus obtained were analyzed to give, where possible, aerodynamic coefficients. At a minimum, a mean drag coefficient was obtained.

7.1. Image Reading

The location and orientation of the model components were identified from the shadowgraph and video images by performing cross-correlation pattern matching using templates generated from the CAD models of each component as described in Ref. 4. Example results are shown in Figure 15 for the two shadowgraph images shown

in Figure 13, and in Figure 16 for the video frames shown in Figure 12. The CAD model center of gravity of each part is marked with the "⊕" symbol in each figure, and the red line marks the projection of the model axis, connecting the geometric nose and tail through the CG. Due to the non-axisymmetric, faceted, profile of the afterbody of the center body model and of the ADEPT drag skirt, it was also possible to estimate the roll angle from the template matches. Figure 17 shows the trajectory of a center body model read from the set of shadowgraph images for shot 2819. To more-clearly see the effect of drag, the down-range position (Figure 17(a)) is plotted as a distance decrement relative to a zero-drag trajectory at the launch velocity. The time and down-range distance are relative to the gun muzzle, that is t = 0 is the time when the model was at the muzzle, x = 0. The cross-range distances, y and z, are relative to the facility centerline. Pitch (θ) and yaw (ψ) angles are relative to the facility axes, so are not exactly the wind-relative pitch and yaw angles α and β. The model was packaged for launch with a roll angle of zero, however, it was not possible to precisely control the roll position during loading. The model does not appear to be rolling for this shot, and the scatter in data may be a reasonable indication of roll angle measurement uncertainty for this approach. For a model the size of the drag skirt, measurement uncertainty for shadowgraph images was estimated in Ref. 4 to be ±3 pixels (±0.3 mm for the Nikon images) for position, and ±0.6° for pitch and yaw angles. Roll angle uncertainty is several degrees. These uncertainty estimates were based on images acquired in transonic testing where the bow shock standoff distance was large enough that there were no density-gradient-induced distortions to the image of the model leading-edge profile, as were present in the current tests. In addition, angle uncertainties are expected to be higher for center body model due to its small size: approximately 20 to 100 pixels in diameter, depending on the imaging system. Further analysis is required to fully estimate measurement uncertainty for images acquired under hypersonic conditions, and to assess any impact of motion blur on the video-image measurements.

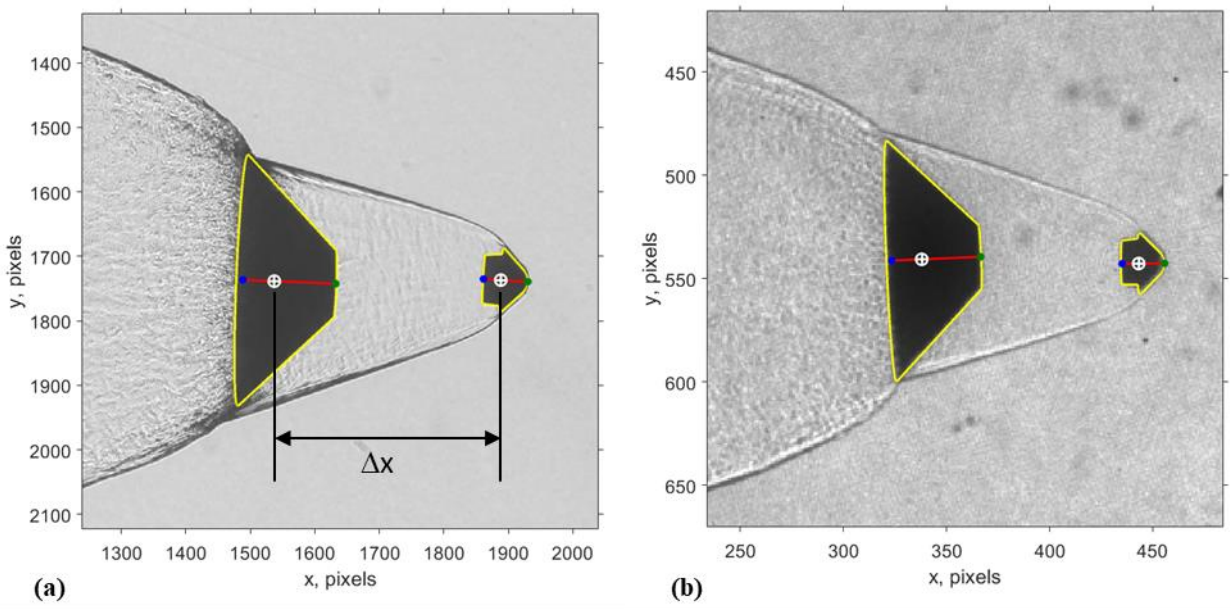

Figure 15: Example of pattern-matching results for images shown in Figure 13.

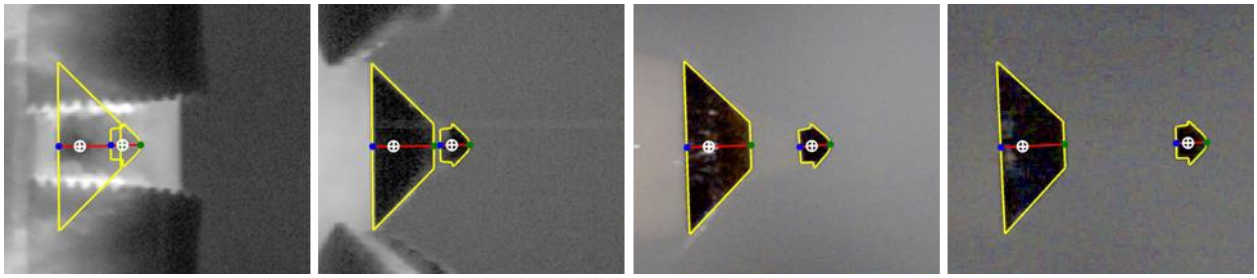

Figure 16: Example of pattern-matching results for the video frames shown in Figure 12. Distance from muzzle left to right: 1.1 m, 2.0 m, 3.0 m, 4.0 m.

The drag-skirt separation distance from the center body is defined here as the distance between the center of gravity of each model component along the test-section x axis (as shown in Figure 15), and was determined by simply subtracting the measured x-position of each component for each image. In cases where the drag-skirt separation was too great to capture both components in the shadowgraph images, the temporal separation determined from the photobeam traces (Figure 14) was used. The position of the drag skirt at the time of passage through the photobeam was assumed to be equal to the measured position of the center body when it passed through the photobeam. The velocity of the drag skirt could then be determined from the x-t data acquired this way, and the local velocity then used, along with the measured temporal separation, to determine the spatial separation of the two components.

The launch velocity and the mean drag coefficient was found for each shot using methods described in Ref. 14 (equations 7.109b and 7.118, respectively). These equations can be derived by integrating the equations of motion in cases when the density, reference area, mass, and drag coefficient are all constants.

$$V(x) = V_0 e^{-KC_D(x-x_0)} \tag{1}$$

$$t(x) = t_0 + \frac{1}{V_0}x + \frac{KC_D}{2V_0}x^2 \tag{2}$$

where $K = \rho_\infty A/2m$, ρ_∞ is the freestream density, A is the reference area, and m is the model mass. The initial conditions are $t = t_0$, $V = V_0$, at $x = x_0$. Least-squares fits are made to the data, using the average velocity on each interval between image stations defined as

$$V(x_{av}) = V_{av} = \frac{x_i - x_{i-1}}{t_i - t_{i-1}} \tag{3}$$

where the indices represent the station number. For small deceleration the average velocity occurs approximately at the mid-point between stations. An iterative refinement process described in Ref. 14 identifies more precisely where on each interval the average velocity occurred, which was typically within the measurement uncertainty (0.3 mm) of the center of the interval for these tests. These curve fits were performed on the center-body data acquired in the test section from the standard shadowgraph stations. Setting x_0 to be the gun muzzle yields the launch time, t_0, and velocity, V_0, assuming that the effects of the sabot separation and propellant gases can be ignored. Example fits are shown in Figure 18 for shot 2821. The center-body velocity fit was made on the shadowgraph data and extrapolated back to the muzzle. For the drag skirt, two velocity fits are shown, one using the photobeam data acquired in the test section, and the other using the video data acquired in the separation chamber.

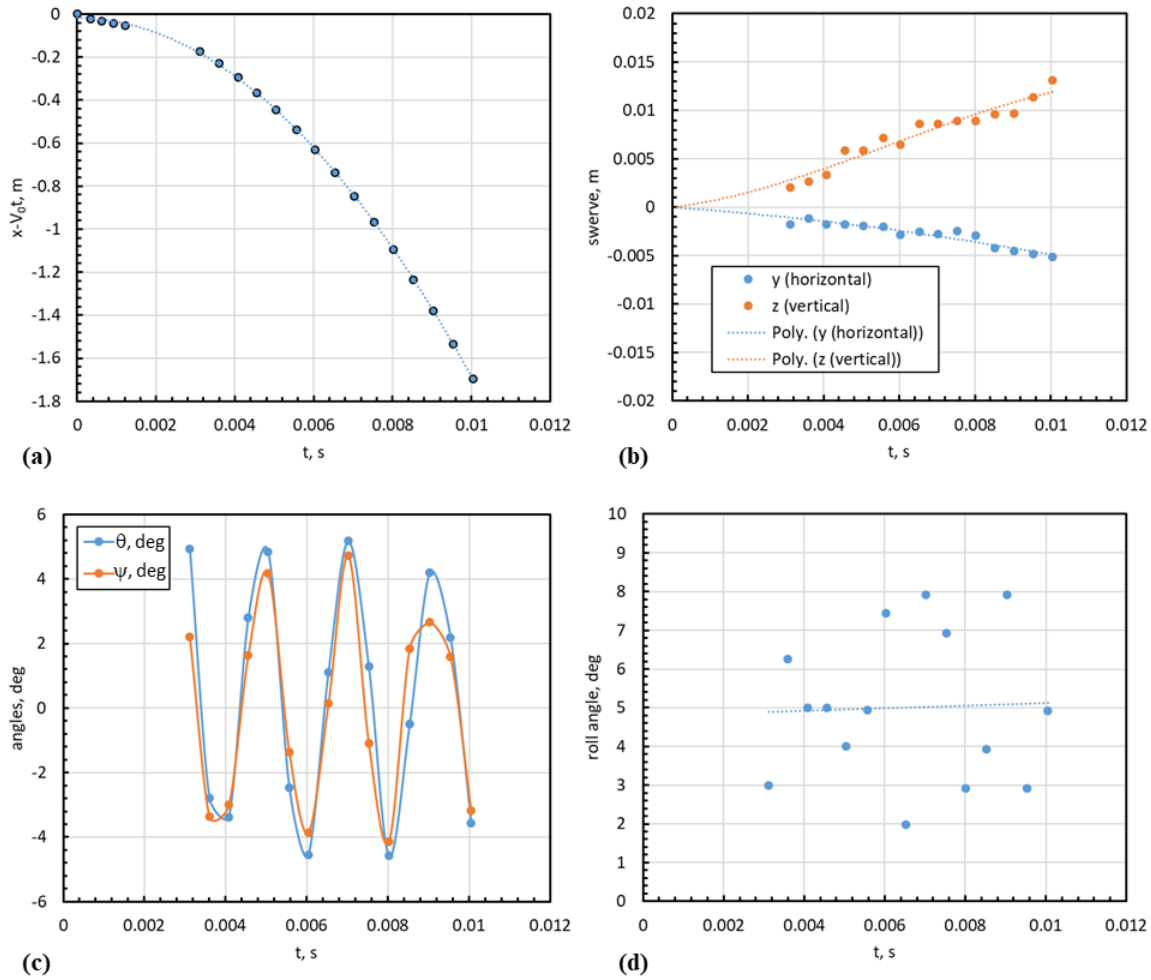

Figure 17: Example trajectory measurements of the center body model from the test-section shadowgraph images, shot 2819: (a) down-range position plotted as a distance decrement (position relative to a zero-drag trajectory), (b) the horizontal and vertical swerve, (c) the pitch and yaw angles relative to the facility axes, (d) roll angle.

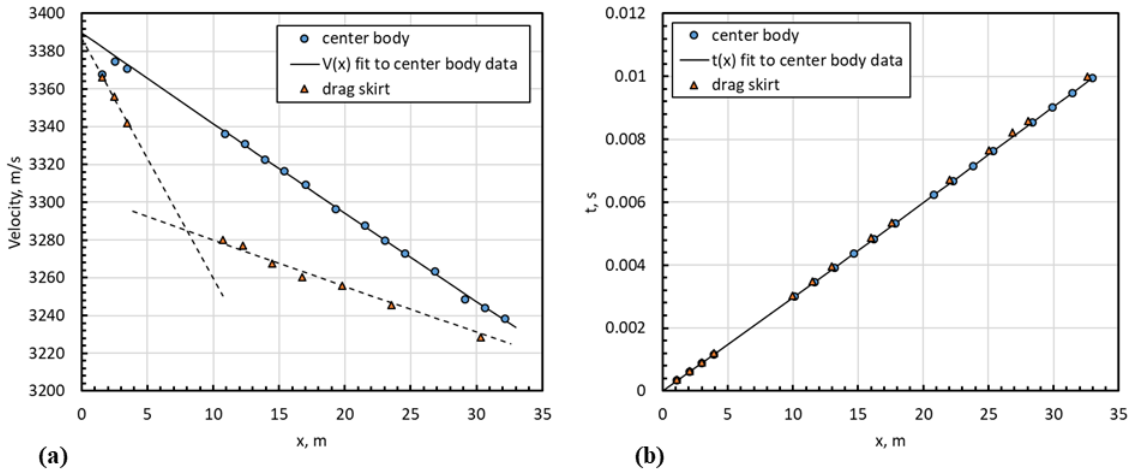

Figure 18: Examples of fits to data for initial drag estimates (shot 2821): (a) velocity vs. flight distance; (b) time vs. distance.

7.2. Aerodynamic Analysis

The aerodynamics of the ballistic-range model in flight can be deduced from angular and linear position data measured from the shadowgraphs. With sufficient data of high precision it would be possible to curve-fit the position and angular orientation data and differentiate the fitted curves twice to obtain the accelerations that are directly related to the aerodynamic forces and moments acting on the body. Instead, an inverse approach is followed here. Given the equations for the motion, the aerodynamic coefficients which best describe that motion are determined using a least-squares, differential correction procedure, which adjusts the aerodynamic parameters and initial conditions until a best least-squares fit of the trajectory measurements is obtained. Since it is not known a priori what the functional relationships will be, it is necessary to assume either that the aerodynamics are linear or nonlinear, and if nonlinear, the form they take. Where possible, the data were analyzed in this way using the Comprehensive Aerodynamic Data Reduction System for Aeroballistic Ranges software component CADRA2-J [15, 16] ("2" refers to the component of the CADRA system that determine aerodynamic coefficients, and "J" identifies the version with a Java-based user interface).

Determining the pitch damping coefficients this way requires trajectories that undergo between ~1.5 and ~3.5 pitch oscillation cycles. The number and spacing of shadowgraph stations in the HFFAF is optimized for 2 cycles of motion, giving eight samples per cycle. With fewer cycles the damping cannot be determined, and with more cycles the data become too sparse to accurately determine the waveform due to the spacing of the shadowgraph stations. It was possible to analyze the center-body data for the five shots that did not experience re-contact with the drag skirt, although, for all but the low-pressure shot (2821), the model executed more oscillation cycles than optimal. The drag skirts could not be analyzed for aerodynamic coefficients, other than the average drag coefficient, because, either there were too few images of the skirt, or the skirt was in the wake of the center body. Average drag coefficients, while reported here, are likely influenced by interaction with the center body wake.

Because of the limited size of this data set (number of shots, range of Mach numbers and root-mean-square (RMS) angles of attack) the functional relationships for the aerodynamic parameters used in the analysis are

$$C_D = const. \tag{4}$$

$$C_L = C_{L_\sigma} sin\alpha \tag{5}$$

$$C_m = C_{m_\sigma} sin\alpha \tag{6}$$

$$C_{m_q} + C_{m_{\dot{\alpha}}} = const. \tag{7}$$

where σ represents the RMS total angle of attach for each shot. The coefficients derived this way for the center body will be discussed in the next section, and compared with values used for the Pioneer Venus entry vehicle.

8. Results

The 8 tests were conducted in the summer 2019 timeframe. All tests executed as expected, with relatively clean separation of the drag skirt from the center body. All tests included expected collection of data (high-speed video in the sabot separation chamber, and Schlieren/shadograph images in test section). There were a few instances where a given station did not fire as intended (mistimed, or triggered off the drag skirt rather than center body passage) – however, the test campaign exceeded expectations in providing a rich dataset to address the test objectives defined in Section 2.

In terms of test process, all shots were executed with the same team and procedure, and with the only variations being due to model configuration, ambient temperature and humidity, and test section pressure (for the specific tests targeting different pressures). The one exception to this is the second test (shot 2816), which utilized a reduced powder charge in the gun as an attempt to keep launch velocity approximately constant while compensating for the lower mass of the aluminum drag skirt. However, this resulted in a launch velocity almost 8% lower than the first test, and hence the decision was made to run the initial powder charge in all subsequent tests rather than attempt to tailor it on a per-shot basis. This led to a variability in launch velocity for the remaining shots that ranged from -3.4% (low) to +1.9% (high), which is near the generally observed variability of the ballistic range launch velocity of approximately ±3%.

8.1. Separation Event

In terms of meeting the first test objective, all tests demonstrated a clean separation in hypersonic flow of the center body from the drag skirt. As was expected, in all tests the center body separated quickly in the Sabot Separation Chamber. High-speed video indicated no unexpected behavior or interactions – rather, the separation event appeared to be minimally influenced by the actual separation of the sabot pieces.

After drag skirt separation, the center body flew in a stable manner down the tunnel (in cases where no re-contact with skirt occurred). Although some attitude oscillations were observed (see Aerodynamic Results section below for further details), no areas of concern were noted in the limited length of the tunnel test section.

While the center body exhibited stable flight characteristics post-separation, the drag skirt typically showed much larger attitude and positional variation, and in some cases tumbling-like flight dynamics. This is potentially caused by the non-aerodynamic shape of the drag skirts interacting with the wake flow of the center body. The drag skirts may also have seen a larger influence of potential sabot flow-interaction effects, due to the larger surface area (vs. the center body) and larger duration of exposure to flow affected by the sabot pieces. (See Figure 19 for an example image from the high-speed video recording of the sabot separation event. While shock waves from the sabot pieces are not visible, it can be argued that there is likely shock wave impingement on the aft portions of the drag skirt as the pieces peel off.)

Overall, these tests provide confidence in the DM approach using a separable drag skirt, as the ballistic range tests included various effects (e.g., sabot flow interactions, very small model sizes and masses) that will not be present at flight conditions/scale.

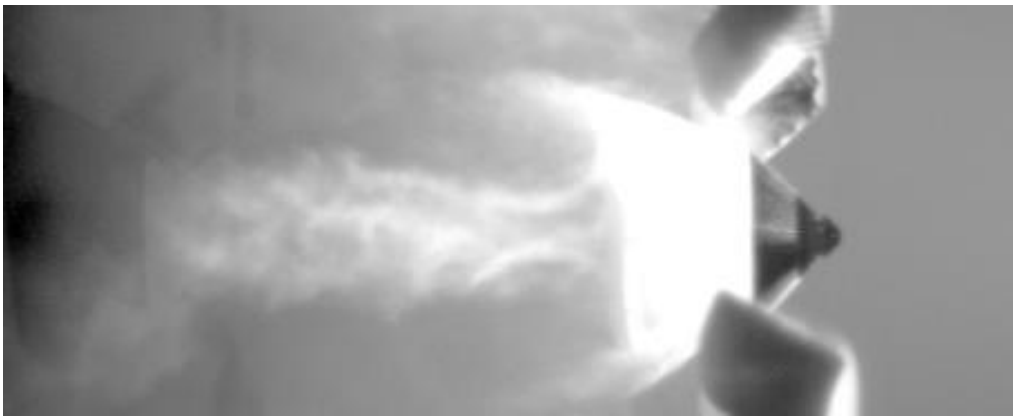

Figure 19: High-speed video frame capture of sabot separation in shot 2815 (axisymmetric steel drag skirt).

8.2. Close-Proximity Flight Visualization

The second primary test objective focused on obtaining experimental data of the relevant configurations in hypersonic flow to benchmark CFD and similar types of analysis in future DM development efforts. While this would be ideally satisfied by capturing Schlieren or shadowgraph images of the actual drag skirt separation event, the team recognized this would not be possible due to the passive separation design of the test models, as well as the fact that separation was always expected to occur in the Sabot Separation Chamber prior to the test section. As part of the initial test matrix development, the team discussed ideas about utilizing an adhesive that would delay separation until later in the test section – the adhesive would melt as the model temperature rapidly increased due to hypersonic flow heating, allowing the models to separate in the test section. While a potential "development" test was initially planned for late in the test campaign, there were concerns regarding the ability to accurately delay separation until the test section (e.g., in the presence of the shock loads from the gun launch, uncertainties in hypersonic heating and adhesive melt temperature, and uncertainty in obtaining a uniform break in the adhesive bond vs. partial break in the bond inducing attitude perturbations).

Ultimately, however, the test results provided several examples where the center body and drag skirt were captured in the test section in close proximity. This was due to the low ballistic coefficient ratio cases allowing the drag skirt to "catch up" to the center body (this will be discussed further below). Several examples of these images are show in Figure 20 and Figure 21, where the wake flow and shock wave characteristics are readily visible in the shadowgraph images. While it is recognized that these images do not correspond to the actual separation event (i.e., the drag skirt is approaching the center body rather than separating from it), the close proximity flow details and interactions are primarily dependent on the flow velocity (due to the orders-of-magnitude smaller delta-velocity between the center body and drag skirt), and hence these can be considered representative of the flowfield during the actual drag skirt separation.. These and similar images from the test campaign will be used as a set of validation data in benchmarking CFD codes in future DM-related analyses.

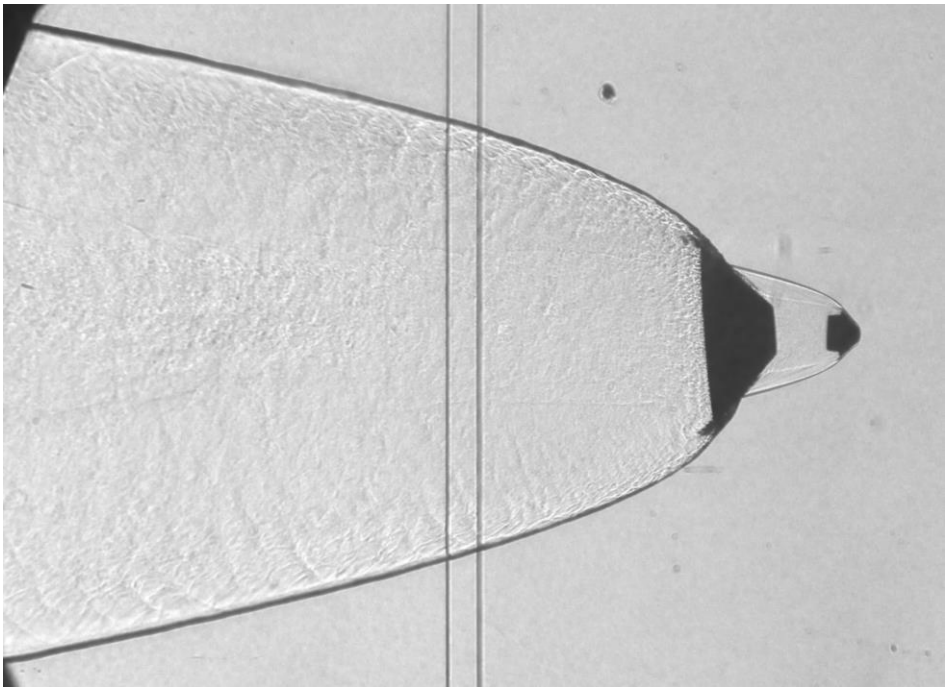

Figure 20: Station 5 (side) shadowgraph image from Shot 2815 (axisymmetric steel drag skirt).

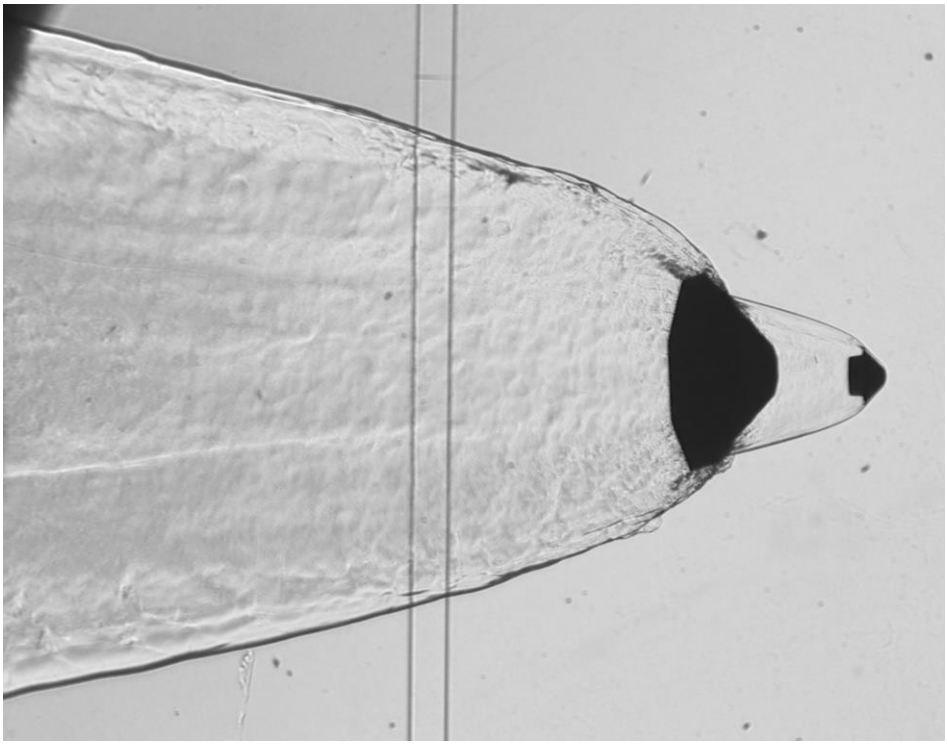

Figure 21: Station 9 (side) shadowgraph image from shot 2817 (faceted steel drag skirt).

8.3. Effect of Ballistic Coefficient Ratio

While not explicitly outlined in the test objectives, understanding any differences in the drag skirt separation event due to ballistic coefficient differences is a key part of demonstrating the feasibility of a DM architecture for aerocapture. In an actual flight mission, the drag skirt needs to separate quickly and avoid recontact with the center body to ensure mission success. It is expected that the larger the ballistic coefficient ratio between the drag skirt and center body, the more rapid this event will be. Therefore, an inherent part of the test campaign was to assess different ballistic coefficient ratios and their effects on drag skirt separation.

As was noted above, however, one of the limitations in the ballistic range test was that the center body and drag skirt were not attached to each other, and separation started as soon as the sabot detached from the test articles. Secondly, a rapid separation of the drag skirt was expected to lead to test results where the drag skirt quickly went out of view in the test section images, and the majority of the Schlieren/shadowgraph images would then be of the center body flying by itself. These considerations led to focusing the tests on several drag skirt options with a significantly lower ballistic coefficient ratio than would be present in an actual flight mission design. For example, the Venus DM mission being considered has a ballistic coefficient ratio (center body only / integrated vehicle) of approximately 7.6, whereas the test articles ranged from 1.3 (steel drag skirt) to 3.5 (aluminum faceted drag skirt).

The initial separation event, as discussed above, appeared to be nominal for all three ballistic coefficient ratios tested. Figure 22 shows data at 2, 3, and 4 m downrange from the gun exit. It can be seen that no significant attitude dynamics are induced on the center body or drag skirt during the separation event. The expected trend in separation rate is also observed, with the higher ballistic coefficient ratio case showing a more rapid increase in distance between the center body and drag skirt, and the lower ballistic coefficient ratio test showing the opposite.

As the ballistic coefficient ratio for all tests is greater than unity, the initial expectation was that the drag skirt would always fall back from the center body at an ever-increasing distance. However, it turns out that this is not always the case – Figure 23 shows plots of the drag skirt and center body separation distance vs. time, and it can be seen that the low and low/mid ballistic coefficient ratios (1.3 and 2.2, respectively) show the drag skirt initially

separating, but eventually catching back up to the center body. In retrospect, this should not be a surprise, as the center body wake results in a lower dynamic pressure on portions of the drag skirt post-separation, and this effectively reduces the drag force on the skirt.

While many of the tests utilized configurations with non-flight-like ballistic coefficient ratios, this approach did provide a set of useful data that met test objectives, allowing the collection of high-resolution shadowgraph imagery of the center body and drag skirt in close proximity. It also generated a set of data demonstrating that, within the constraints on scale and test conditions in the range, a ballistic coefficient ratio of 3.2 or higher ensured clean separation and no possibility of re-contact of the drag skirt with the center body. This provides evidence that the DM approach for a flight mission is feasible for the ballistic coefficient ratios (>4) being considered.

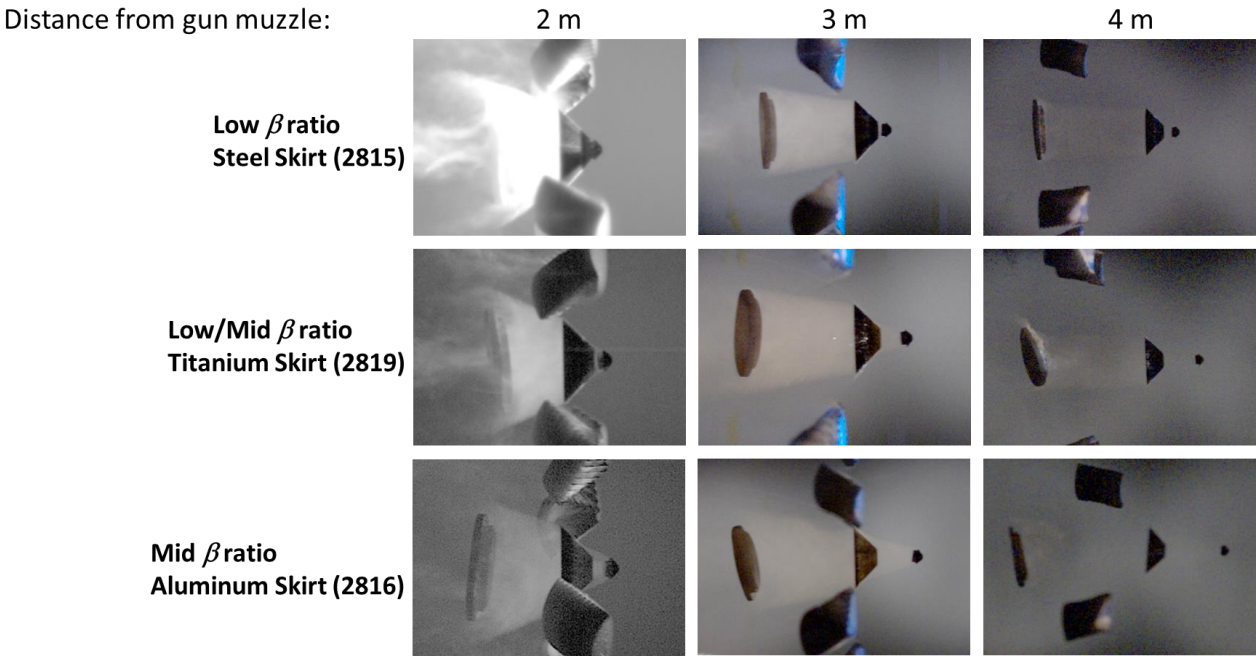

Figure 22: High-speed video frames showing effect of ballistic coefficient (beta) ratio on initial separation event.

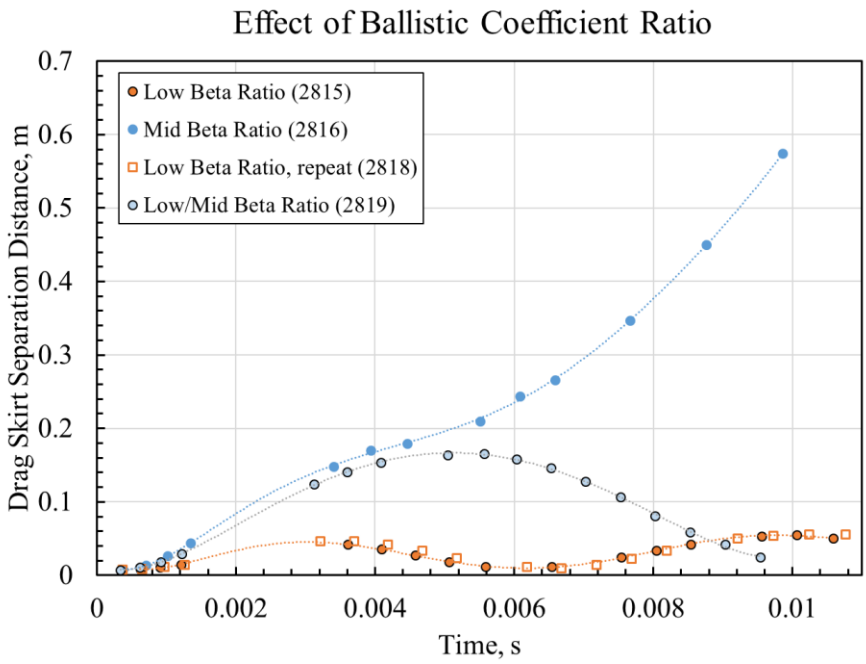

Figure 23: Effect of ballistic coefficient (beta) ratio on drag skirt separation distance vs. time for the steel (low beta ratio = 1.3), titanium (low/mid beta ratio = 2.2), and aluminum (mid beta ratio = 3.2) axisymmetric drag skirts.

8.4. Effect of Freestream Pressure

Understanding the effect of different flow conditions on the separation event was one of the secondary test objectives. In particular, two shots were executed at different gas pressures to determine the influence of this parameter on drag skirt separation and subsequent flight of the center body and skirt. The first of the tests targeted a 67% higher pressure (0.250 atm rather than the 0.150 atm run for most tests), whereas the second targeted a 56% lower pressure (0.066 atm vs. 0.150 atm). Due to the limited number of drag skirt test articles, the high-pressure test was performed with a titanium drag skirt, whereas the low-pressure test used an aluminum drag skirt.

Figure 26 compares the separation distance vs. time for each of these tests, relative to the appropriate baseline pressure shots using the same type of drag skirt. As can be seen in the plot, the initial separation rate (distance vs. time) increases for the high-pressure test of each drag skirt. This is also observed in the high-speed video data for the cases (Figure 24 for the low-pressure comparison, and Figure 25 for the high-pressure comparison). Interestingly, increasing the freestream pressure for the titanium drag skirt test attenuated the "catch up" phenomena discussed above, and eliminated the possibility of re-contact for that configuration.

This result should not be surprising, considering that increasing the freestream pressure (with temperature left constant) leads to an increase in density, and hence larger dynamic pressure acting on the vehicle. As is discussed further in Appendix B, a simplified linear model of the drag skirt separation can be reduced to:

$$t = \sqrt{\frac{2(ds)}{q_\infty \left(\frac{k}{\beta_S} - \frac{1}{\beta_C}\right)}} \tag{8}$$

where t is the time for separating the drag skirt and center body a distance ds, q_∞ is the dynamic pressure, β_S and β_C represent the ballistic coefficients of the drag skirt and center body, respectively, and k is a constant ≤ 1 that

accounts for the reduction in drag that would be seen by the drag skirt due to the center body wake effects. As is shown in Eq. (8), an increase in the dynamic pressure should result in a shorter time to separate the center body and drag skirt by a given distance.

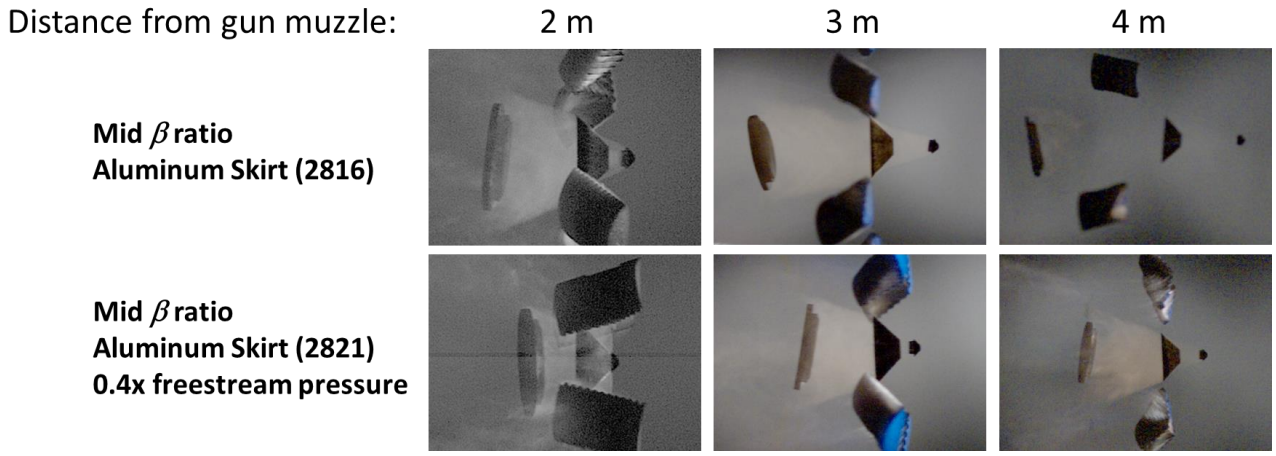

Figure 24: High-speed video frames showing effect of decreasing freestream pressure on initial separation event.

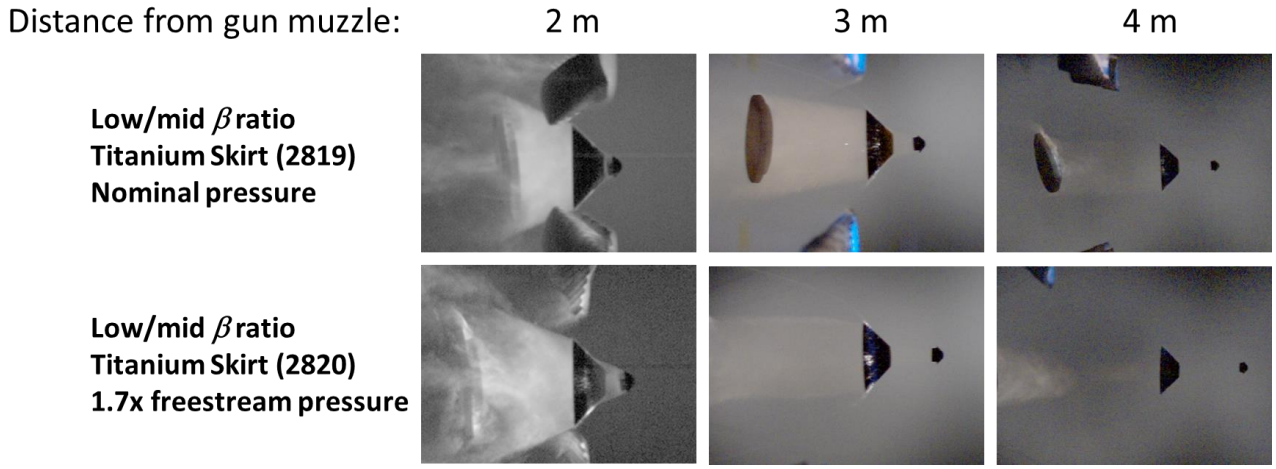

Figure 25: High-speed video frames showing effect of increasing freestream pressure on initial separation event.

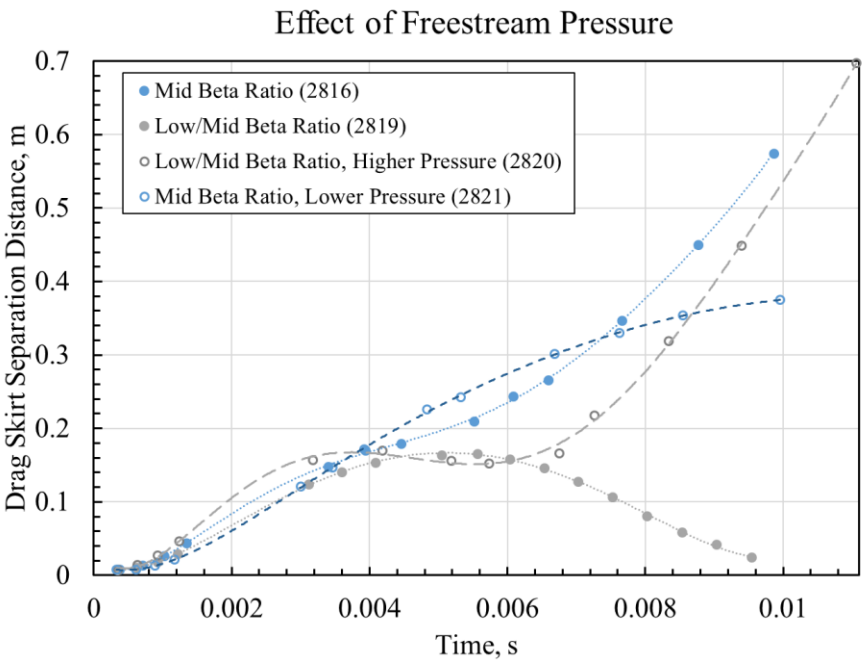

Figure 26: Effect of freestream pressure on drag skirt separation distance vs. time for the titanium (low/mid beta ratio = 2.2), and aluminum (mid beta ratio = 3.2) axisymmetric drag skirts.

8.5. Effect of Drag Skirt Shape

As was discussed in Section 2, the test focus was on using the axisymmetric drag skirts where possible to eliminate the variable of roll angle potentially affecting the separation and flight dynamics, due to the faceted shape of the ADEPT-derived drag skirt. However, as ADEPT is one of the options being considered for the DM aerocapture mission design, several tests were conducted to determine differences due to the drag skirt shape.

The results for comparisons of the axisymmetric and faceted shapes for the low and mid ballistic coefficient ratio drag skirts is shown in Figure 27. It can be observed that while the initial separation distance vs. time trend is similar for a given ballistic coefficient ratio, the faceted skirt tests exhibit a delay in the "catch up" phenomena versus the axisymmetric skirt tests. This can be partially explained by the overall smaller projected area (which would correlate with drag force, assuming the same drag coefficient) of the faceted skirt (672 mm^2, as compared with 719 mm^2 for the axisymmetric designs). It is also expected that the faceted nature of the ADEPT-derived skirt may lead to a different drag coefficient. Future computational fluid dynamics analysis are recommended to provide greater insight into this possible effect.

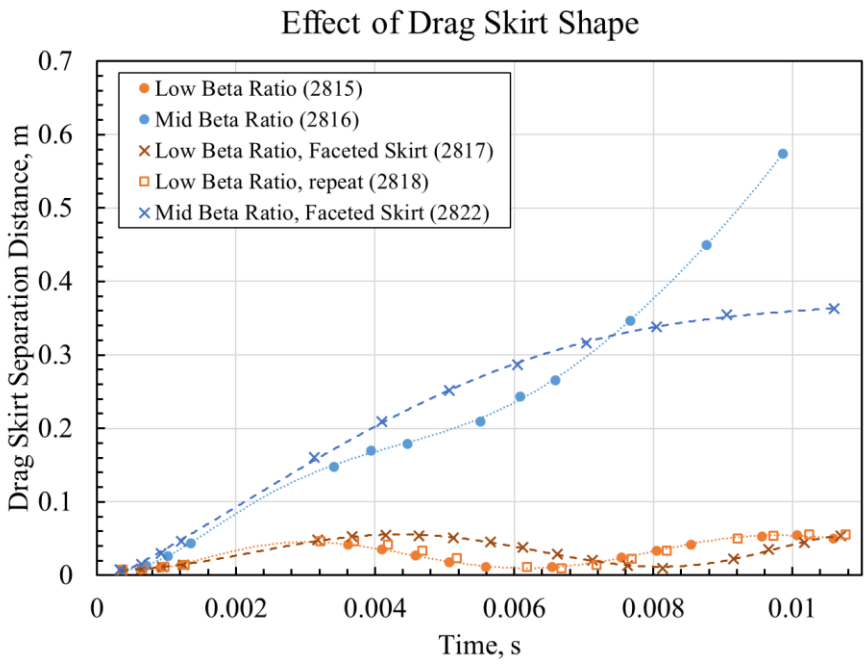

Figure 27: Effect of drag skirt shape on separation distance vs. time for the steel skirt (low beta ratio) and aluminum skirt (mid beta ratio) designs.

8.6. Aerodynamic Coefficients

The trajectory measurements obtained from the test-section shadowgraph images of the center body models were reduced to the final aerodynamic information by analyzing the individual runs with the CADRA2-J software using the linear aerodynamics models given in section 7. The resulting data points represent average values of the coefficients that are valid for the particular RMS angle of attack of the trajectory from which they were taken. The average coefficients are given in Table 5 for each shot that could be analyzed. Tables for each trajectory are given in Appendix D. Given data from a larger range of conditions (angle, Mach number, and/or Reynolds number) plots of these average linear coefficients could be used to determine the presence of any nonlinear trends in the aerodynamics, and the analysis would then be repeated with the appropriate nonlinear aerodynamics math modeling functions. Because of the limited test envelope in Mach number and RMS angle of attack space, only the linear aerodynamics analysis was performed. The five shots were also analyzed as a set (referred to as a "multifit"), and the results are given in Table 5 and Figure 29(b).

Table 5. Estimated aerodynamic coefficients for the center body model.

Measured Values						CADRA Analysis Results								
						Drag		Lift		Pitching Moment and Slope			Pitch Damping	
Shot #	RMS total angle, σ (deg)	Average Velocity (m/s)	Average Mach number	Average Re_D	C_D from V(x) fit	C_D	error	$C_L/\sin\sigma$	error	$C_m/\sin\sigma$	error	C_{m_σ} (avg)	$C_{m_q} + C_{m_{\dot\alpha}}$	error
2816	7.77	2,818	10.50	395,742	1.037	1.034	0.002	0.072	0.351	-0.140	0.001	-0.139	-0.095	0.099
2819	4.57	3,076	11.47	435,497	1.036	1.035	0.001	-0.091	0.544	-0.138	0.002	-0.137	-0.446	0.223
2820	5.41	2,930	10.90	680,051	1.037	1.037	0.001	0.032	0.307	-0.184	0.001	-0.183	-0.279	0.081
2821	1.46	3,287	12.23	201,493	1.017	1.016	0.003	-3.567	1.097	-0.150	0.003	-0.150	0.092	0.731
2822	3.46	3,060	11.40	433,482	1.034	1.034	0.001	0.105	0.388	-0.152	0.001	-0.152	-0.430	0.127
"Multifit" Results (simultaneous fit to all five shots)						1.035	0.001	0.109	0.154	-0.139	0.001		-0.219	0.130

The variation of drag coefficient with Mach number and Reynolds number is shown in Figure 28, and compared with the aerodynamic model [18] and data from previous ballistic-range tests [19] for Pioneer Venus. The average drag coefficients are relatively independent of Mach number and Reynolds number over the range of these tests, and compared well with the Pioneer Venus data. The results from shot 2821 (the low-pressure shot) deviated the most from Pioneer Venus (~3%), and from the other shots. Without additional data it cannot be concluded whether this is evidence of an actual trend, or simply due to measurement/analysis uncertainty. This shot also had the lowest angles of attack.

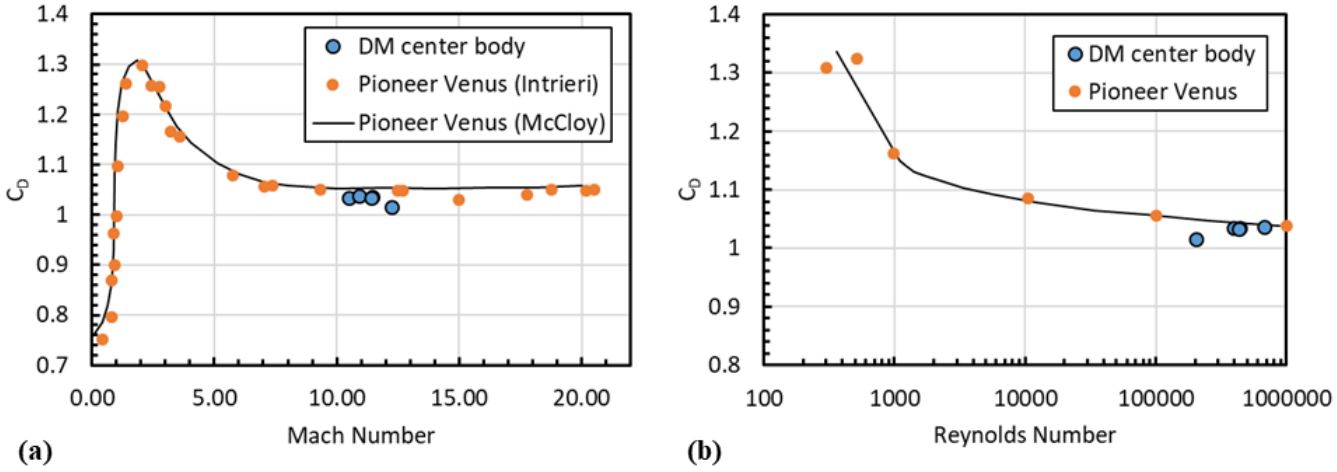

Figure 28: Variation of drag coefficient of the DM center body as compared with the Pioneer Venus aerodynamic model of Ref.18 and ballistic range data of Ref. 19: (a) vs. Mach number and (b) vs. Reynolds number.

Figure 29 shows the pitching moment slope variation, C_{m_σ}, with Mach number and RMS angle of attack. (Note: The symbol α was used to represent the total angle of attack in Refs. 18-20, and is used interchangeably with σ in this section.) The Mach number variation of C_{m_σ} is compared with the Pioneer Venus aerodynamics model [18]. As with Pioneer Venus, there was little variation with Mach number over the range of test conditions, however, with the exception of the high Reynolds number shot 2820, the magnitude of C_{m_σ} for the DM center body configuration was about 3% lower that Pioneer Venus. This difference may be due to the difference in center of gravity location: Ref. 18 gives the Pioneer Venus CG location as $x_{CG}/D = 0.396$, where D is defined as the first major diameter; the average CG location for the current test was $x_{CG}/D = 0.423$, where D is the actual base diameter of the models at the shoulder with radius. Variation of C_{m_σ} with angle of attack was not provided in Ref. 18, so these data are compared with ballistic range data acquired for two configurations of the Galileo entry vehicle [20]. Again, with the exception of the high Reynolds number shot, there was little variation with angle of attack. The values determined for the DM center body configuration fall between those of the two Galileo configurations, as does the CG location and the average Reynolds number. The Galileo ballistic range tests [20] were performed at 3.1 km/s average velocity.

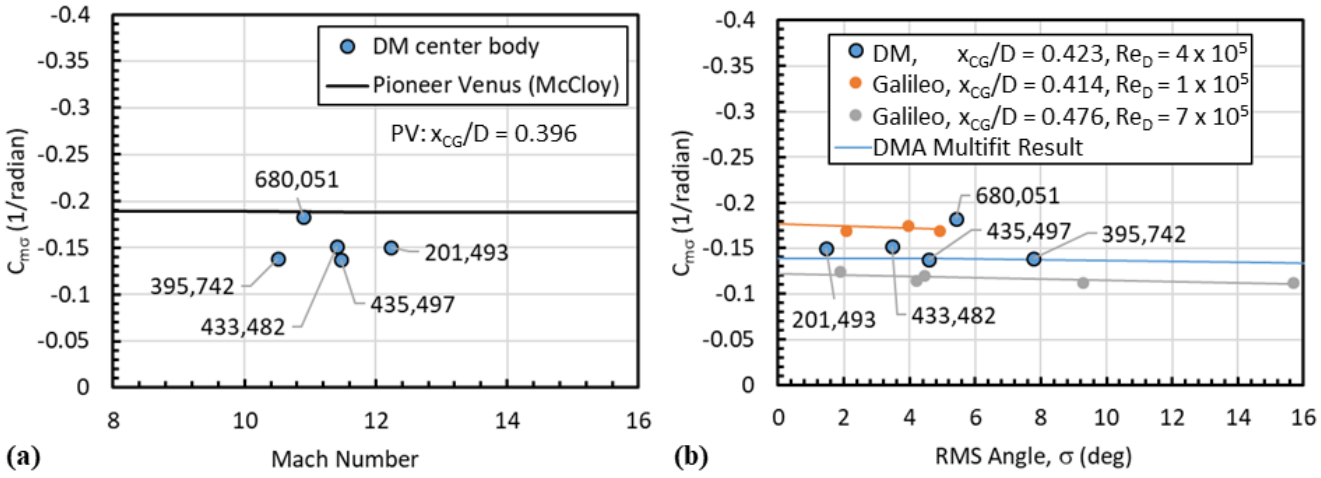

Figure 29: Variation of pitching moment coefficient slope with (a) Mach number, (b) RMS total angle of attack. (Note: Data point labels are average Reynolds number for each shot.)

Finally, the pitch-damping parameter $C_{m_q} + C_{m_{\dot{\alpha}}}$ is shown in Figure 30(a). The model appears to be dynamically stable for moderate pitch amplitudes, but dynamically unstable for low-amplitude oscillation. This is an expected result for supersonic and transonic flight of blunt bodies. For comparison, Figure 30(b) shows the pitch-damping parameter for Pioneer Venus from Ref. 18, which indicates dynamically stable behavior at hypersonic conditions. It is stated in Ref. 18 that the maximum entry angles of attack used to design the Pioneer Venus probes were 45 and 5 degrees for the small and large probes, respectively, and that the dynamic motion of both probe configurations throughout entry is "well behaved hypersonically." Also, Ref. 18 states that nonlinear aerodynamics were employed to analyze vehicle dynamics in six-degree-of-freedom simulations to account for the effects due to a large entry angle of attack and transonic and subsonic dynamic instability. Further tests are required before nonlinear aerodynamics analysis of the DM center body model can be performed, and before a strong conclusion regarding dynamic stability at hypersonic conditions can be reached.

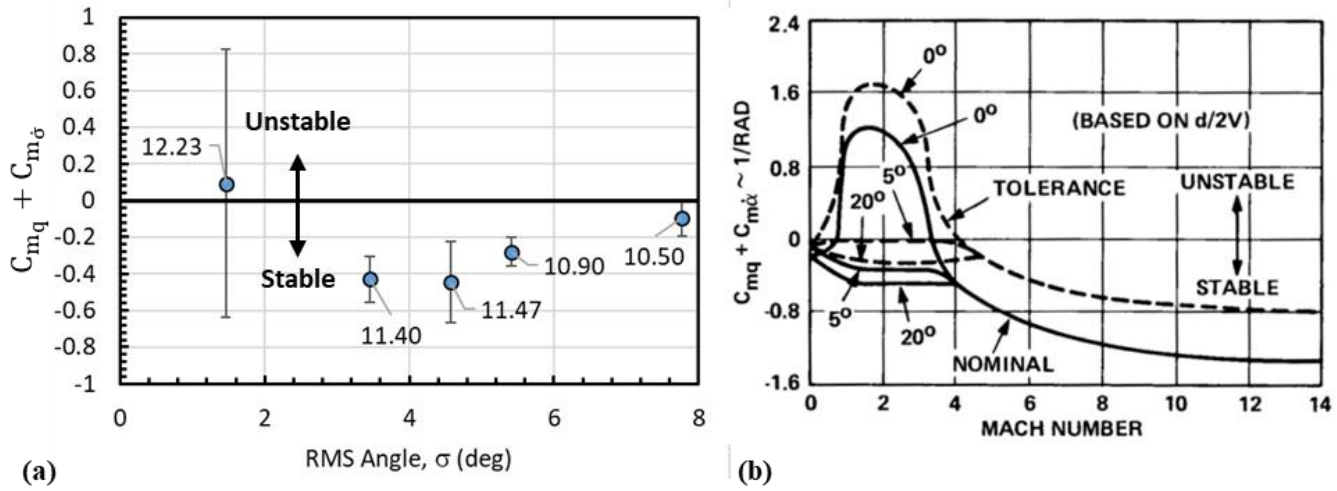

Figure 30: Dynamic stability (pitch damping) parameter: (a) test results for DM center body model, (b) Pioneer Venus data from Ref. 18, Fig. 5. Data point labels in (a) are average shot Mach number.

Several factors affect the accuracy of the estimated aerodynamic coefficients, including the math models used for the coefficients, the range of angles and Mach numbers covered by the tests, and the measurement accuracy.

The estimated 3-σ uncertainties were obtained from the least-squares method and are proportional to the covariance matrix and residual errors [15]. Any errors in modeling the aerodynamic coefficients are reflected in larger residual errors and, therefore, estimated uncertainties. Finally, as stated in Section 7, further analysis is required to fully estimate measurement uncertainty for the small model size of these tests.

9. Conclusions

9.1. Summary of Results

Overall, the test campaign met the objectives outlined in Section 2. All tests demonstrated clean separation of the drag skirt from the center body, and provided a plethora of data to use in benchmarking future simulations related to DMA development work. While not initially expected, the results where the low ballistic coefficient ratio drag skirt separated and eventually caught up to the center body allowed high-quality shadowgraph imaging of the bodies in close proximity, which will be useful in verifying simulations of these types of flow-body interaction effects. The results indicated stable flight of the center body down the range, and provided characterization in many cases of how the drag skirt reacted to the center body wake flow.

In terms of secondary test objectives, static and dynamic aerodynamic coefficients were derived for the center body based on the test results, and compared relatively well to historical data on 45-deg sphere-cone shapes. However, as was expected, the limited quantity of test shots, along with a focus on obtaining data on flow-body interaction effects, led to a sparsity of data that could be used to address these objectives.

Finally, effects on separation and flight dynamics due to several parameters were ascertained from the data. For example, for the baseline test conditions it was found that the mid ballistic coefficient ratio configuration (titanium drag skirt) resulted in continuing separation of the drag skirt from the center body, whereas lower ballistic coefficients indicated an eventual "catch up" of the skirt due to the lower drag experienced in the center body wake. Effects of freestream pressure were also determined, and indicated (as expected) that increasing freestream and dynamic pressure leads to a more effective (i.e., mitigated "catch up" effect) drag skirt separation. Lastly, the drag skirt shape was shown to have a relatively minor effect, with the faceted shape appearing to experience less drag force in the center body wake (not unexpected due to the lower projected area of the faceted skirt).

9.2. Future Test Recommendations

Based on the execution of 8 shots in this test campaign, model parts remain to allow a further two tests should the opportunity arise in the future. Based on the test objectives discussed in this report, the team recommends the following shots (listed in priority order):

- Repeat of low ballistic coefficient ratio (steel) ADEPT drag skirt configuration at baseline test conditions. This will provide additional confidence in the repeatability of the ballistic range results, as well as another data point on the faceted drag skirt shape. The low ballistic coefficient ratio will likely result in additional shadowgraph images of the skirt and center body in close proximity (due to the expected "catch up" effect of the skirt), which will provide further data to meet the primary test objectives.
- Low-pressure test of the high ballistic coefficient ratio (magnesium) axisymmetric drag skirt. This will provide data on a fourth ballistic coefficient ratio configuration closer to that expected on a flight vehicle, as well as provide insight into whether the higher beta ratio will ensure continuing separation of the drag skirt from the center body. Due to the expected rapid separation and increasing distance between skirt and center body, a lower-pressure test condition is recommended to provide a higher chance of obtaining data on the separation event as well as any flow-body interactions between the two models.

References

1. Austin, A., *et al.*, "SmallSat Aerocapture to Enable a New Paradigm of Planetary Missions," 2019 IEEE Aerospace Conference, Big Sky, MT, 2-9 March 2019.
2. Smith et al., "Nano-ADEPT: An Entry System for Secondary Payloads," IEEE Aerospace Conference, Big Sky, MT, March 2015.

3. Wilder, M.C., Bogdanoff, D. W., and Cornelison, C. J., "Hypersonic Testing Capabilities at the NASA Ames Ballistic Ranges," AIAA 2015-3339, 53rd AIAA Aerospace Sciences Meeting, Kissimmee, Florida, 5-9 January 2015.
4. Beck, R., et al., "Studies in Support of Venus Aerocapture Utilizing Drag Modulation," 15th International Planetary Probe Workshop, Boulder, CO, 11-15 Jun. 2018.
5. Cruz, J. R., "Nondimensional Scaling of Aerodynamic Decelerator Tests," 20th AIAA Aerodynamic Decelerator Systems Technology Conference and Seminar, Parachute Systems Tests and Evaluation: Processes and Technology, May 4, 2009.
6. Bogdanoff, D. W. and Wilder, M. C., "Upgrades and Modifications of the NASA Ames HFFAF Ballistic Range," 68th Meeting of the Aeroballistic Range Association, Monterey, CA, September 17-23, 2017.
7. Canning, T. N., Seiff, A., and James, C. S. (Ed.), "Ballistic Range Technology," AGARDograph No. 138, 1970, pp. 323-325.
8. Ibid, p. 103.
9. Gupta, A., Ruffin, S. M., Newfield, M. E., and Yates, L., "Aerothermodynamic performance enhancement and design of sphere-cones using the artificially blunted leading edge concept," AIAA Paper 1999-897.
10. Strauss, B., and Austin, A., "DSENDS Trajectory Results," JPL RT&D *Small Satellite Aerocapture for Increased Mass Delivered to Venus and Beyond* internal project document, January 9, 2017.
11. Bogdanoff, D. W. and Wilder, M. C., "Upgrades and Modifications of the NASA Ames HFFAF Ballistic Range," 68th Meeting of the Aeroballistic Range Association, Monterey, CA, September 17-23, 2017.
12. Canning, T. N., Seiff, A., and James, C. S. (Ed.), "Ballistic Range Technology," AGARDograph No. 138, 1970, pp. 205-206.
13. *Ibid*, pp. 207-210.
14. *Ibid*, pp. 290-291.
15. Yates, L. A. and Chapman, G. T., "Aerodynamic Ballistic Range Analysis using Generalized Math Models," AIAA 1996-3360, AIAA Atmospheric Flight Mechanics Conference, San Diego, CA, July 29-31, 1996.
16. Yates, L. A., "A Comprehensive Automated Aerodynamic Reduction System for Ballistic Ranges," Wright Laboratory, Armament Directorate, WL-TR-95-7059, Oct. 1996.
17. Brown, J., Yates, L., Bogdanoff, D., Chapman, G., Loomis, M., and Tam, T., "Free Flight Testing in Support of the Mars Science Laboratory Aerodynamics Database," *Journal of Spacecraft and Rockets*, Vol. 43, No. 2, pp. 293-302, 2006.
18. R. McCloy, "Entry dynamics performance predictions for Pioneer Venus probes", AIAA 1978-1370, 4th Atmospheric Flight Mechanics Conference, https://doi.org/10.2514/6.1978-1370.
19. Intrieri, P. F. and Kirk, D. B., "High-Speed Aerodynamics of Several Blunt-Cone Configurations," *Journal of Spacecraft*, Vol. 24, No. 2, March-April 1987, pp. 127 – 132.
20. Intrieri, P. F., "Experimental Investigation of Hypersonic Aerodynamics," Research Report, Cooperative Agreement No.: NCC2-475, June 1988.

Appendix A: Test Model Drawings

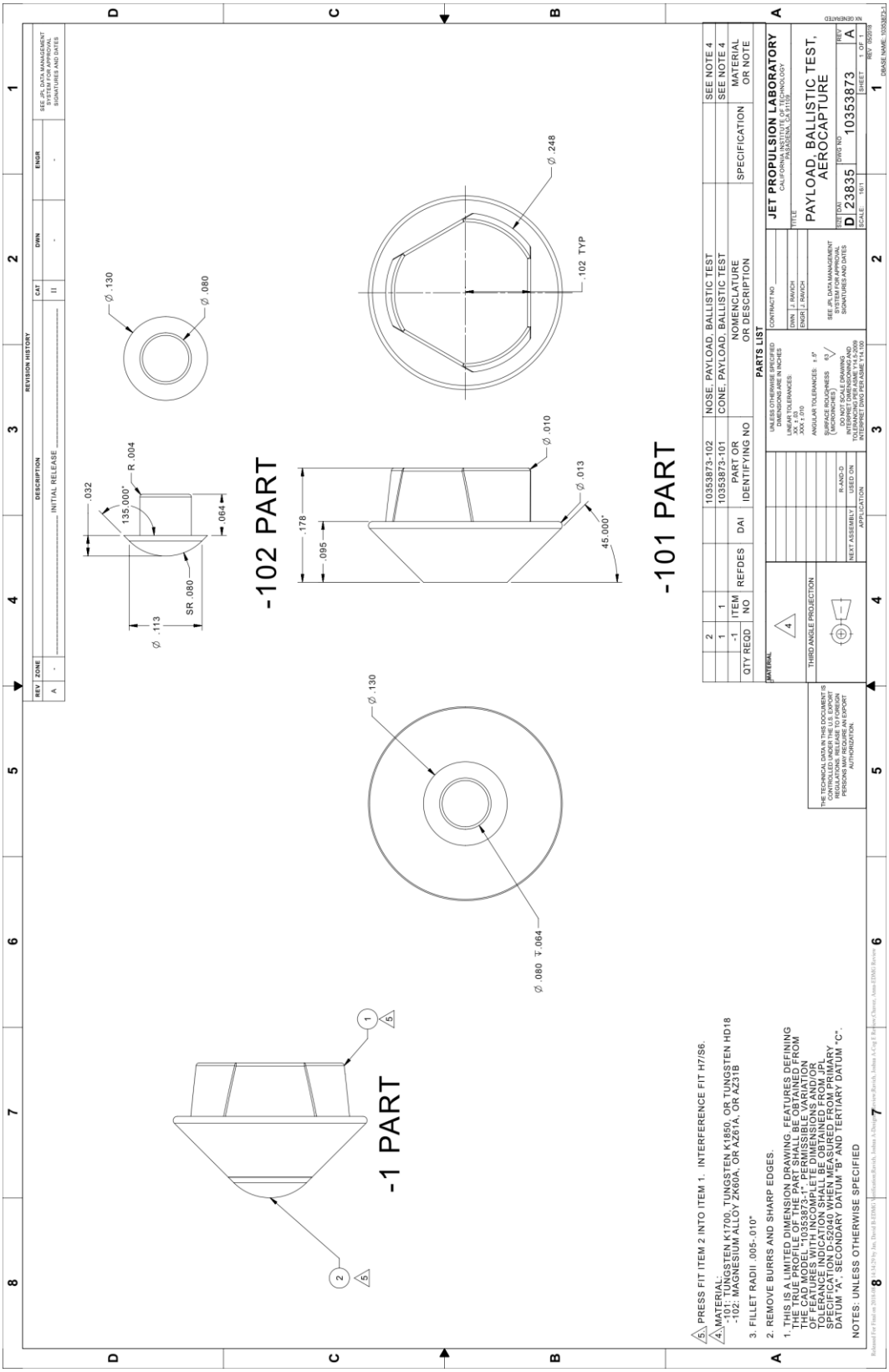

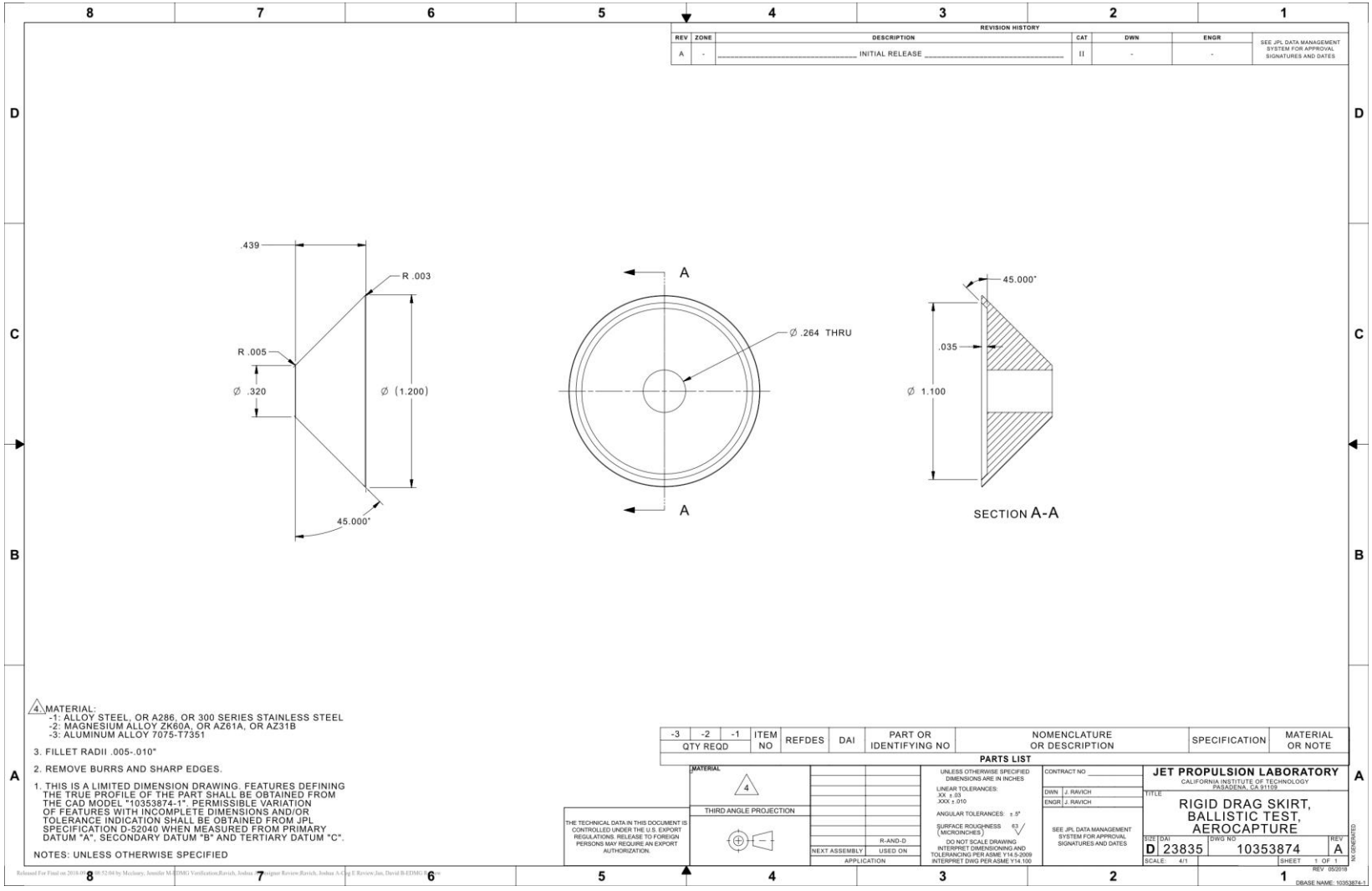
REVISION HISTORY
REV ZONE DESCRIPTION CAT DWN ENGR
A - INITIAL RELEASE II - -
SEE JPL DATA MANAGEMENT SYSTEM FOR APPROVAL SIGNATURES AND DATES
.439
R .003
R .005
Ø .320
Ø (1.200)
45.000°
A
Ø .264 THRU
A
45.000°
.035
Ø 1.100
SECTION A-A
4 MATERIAL:
-1: ALLOY STEEL, OR A286, OR 300 SERIES STAINLESS STEEL
-2: MAGNESIUM ALLOY ZK60A, OR AZ61A, OR AZ31B
-3: ALUMINUM ALLOY 7075-T7351
3. FILLET RADII .005-.010"
2. REMOVE BURRS AND SHARP EDGES.
1. THIS IS A LIMITED DIMENSION DRAWING. FEATURES DEFINING THE TRUE PROFILE OF THE PART SHALL BE OBTAINED FROM THE CAD MODEL "10353874-1". PERMISSIBLE VARIATION OF FEATURES WITH INCOMPLETE DIMENSIONS AND/OR TOLERANCE INDICATION SHALL BE OBTAINED FROM JPL SPECIFICATION D-52040 WHEN MEASURED FROM PRIMARY DATUM "A", SECONDARY DATUM "B" AND TERTIARY DATUM "C".
NOTES: UNLESS OTHERWISE SPECIFIED
-3 -2 -1 QTY REQD
ITEM NO
REFDES
DAI
PART OR IDENTIFYING NO
NOMENCLATURE OR DESCRIPTION
SPECIFICATION
MATERIAL OR NOTE
PARTS LIST
MATERIAL
4
THIRD ANGLE PROJECTION
THE TECHNICAL DATA IN THIS DOCUMENT IS CONTROLLED UNDER THE U.S. EXPORT REGULATIONS. RELEASE TO FOREIGN PERSONS MAY REQUIRE AN EXPORT AUTHORIZATION.
R-AND-D
NEXT ASSEMBLY USED ON
APPLICATION
UNLESS OTHERWISE SPECIFIED DIMENSIONS ARE IN INCHES
LINEAR TOLERANCES: .XX ± .03 .XXX ± .010
ANGULAR TOLERANCES: ± 5°
SURFACE ROUGHNESS (MICROINCHES) 63
DO NOT SCALE DRAWING. INTERPRET DIMENSIONING AND TOLERANCING PER ASME Y14.5-2009 INTERPRET DWG PER ASME Y14.100
CONTRACT NO
DWN J. RAVICH
ENGR J. RAVICH
SEE JPL DATA MANAGEMENT SYSTEM FOR APPROVAL SIGNATURES AND DATES
JET PROPULSION LABORATORY
CALIFORNIA INSTITUTE OF TECHNOLOGY
PASADENA, CA 91109
TITLE
RIGID DRAG SKIRT, BALLISTIC TEST, AEROCAPTURE
SIZE D DAI 23835 DWG NO 10353874 REV A
SCALE: 4/1
SHEET 1 OF 1
REV 05/2018
DBASE NAME: 10353874-1
Released For Final on 2018/05/09 09:52:06 by Mezhoury, Jennifer M.-EDMG Verification,Ravich, Joshua A.-Originator Review,Ravich, Joshua A.-Org E Review,Jun, David B-EDMG-Chk

REVISION HISTORY						
REV	ZONE	DESCRIPTION	CAT	DWN	ENGR	SEE JPL DATA MANAGEMENT SYSTEM FOR APPROVAL SIGNATURES AND DATES
A	-	INITIAL RELEASE	II	-	-	

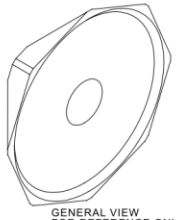

GENERAL VIEW
FOR REFERENCE ONLY

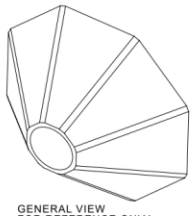

GENERAL VIEW
FOR REFERENCE ONLY

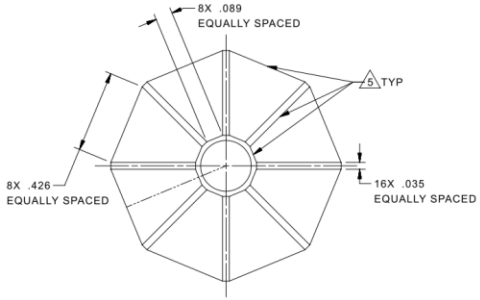

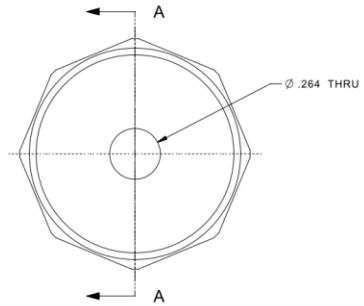

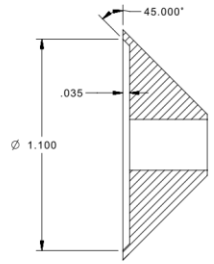

SECTION A-A

5 RADIUS EXTERNAL EDGES .003"

4 MATERIAL:
-1: ALLOY STEEL, OR A286, OR 300 SERIES STAINLESS STEEL
-2: MAGNESIUM ALLOY ZK60A, OR AZ61A, OR AZ31B
-3: ALUMINUM ALLOY 7075-T7351

3. FILLET RADII .005-.010"

2. REMOVE BURRS AND SHARP EDGES.

1. THIS IS A LIMITED DIMENSION DRAWING. FEATURES DEFINING THE TRUE PROFILE OF THE PART SHALL BE OBTAINED FROM THE CAD MODEL "10353875-1". PERMISSIBLE VARIATION OF FEATURES WITH INCOMPLETE DIMENSIONS AND/OR TOLERANCE INDICATION SHALL BE OBTAINED FROM JPL SPECIFICATION D-52040 WHEN MEASURED FROM PRIMARY DATUM "A", SECONDARY DATUM "B" AND TERTIARY DATUM "C".

NOTES: UNLESS OTHERWISE SPECIFIED

-3	-2	-1	ITEM NO	REFDES	DAI	PART OR IDENTIFYING NO	NOMENCLATURE OR DESCRIPTION	SPECIFICATION	MATERIAL OR NOTE
QTY REQD									

PARTS LIST

MATERIAL 4

THIRD ANGLE PROJECTION

THE TECHNICAL DATA IN THIS DOCUMENT IS CONTROLLED UNDER THE U.S. EXPORT REGULATIONS. RELEASE TO FOREIGN PERSONS MAY REQUIRE AN EXPORT AUTHORIZATION.

R-AND-D

NEXT ASSEMBLY | USED ON

APPLICATION

UNLESS OTHERWISE SPECIFIED DIMENSIONS ARE IN INCHES
LINEAR TOLERANCES:
.XX ± .03
.XXX ± .010
ANGULAR TOLERANCES: ± .5°
SURFACE ROUGHNESS 63 (MICROINCHES)
DO NOT SCALE DRAWING
INTERPRET DIMENSIONING AND TOLERANCING PER ASME Y14.5-2009
INTERPRET DWG PER ASME Y14.100

CONTRACT NO

DWN J. RAVICH
ENGR J. RAVICH

SEE JPL DATA MANAGEMENT SYSTEM FOR APPROVAL SIGNATURES AND DATES

JET PROPULSION LABORATORY
CALIFORNIA INSTITUTE OF TECHNOLOGY
PASADENA, CA 91109

TITLE
ADEPT DRAG SKIRT, BALLISTIC TEST, AEROCAPTURE

SIZE	DAI	DWG NO	REV
D	23835	10353875	A

SCALE: 4/1 SHEET 1 OF 1

REV 05/2018

DBASE NAME: 10353875-1

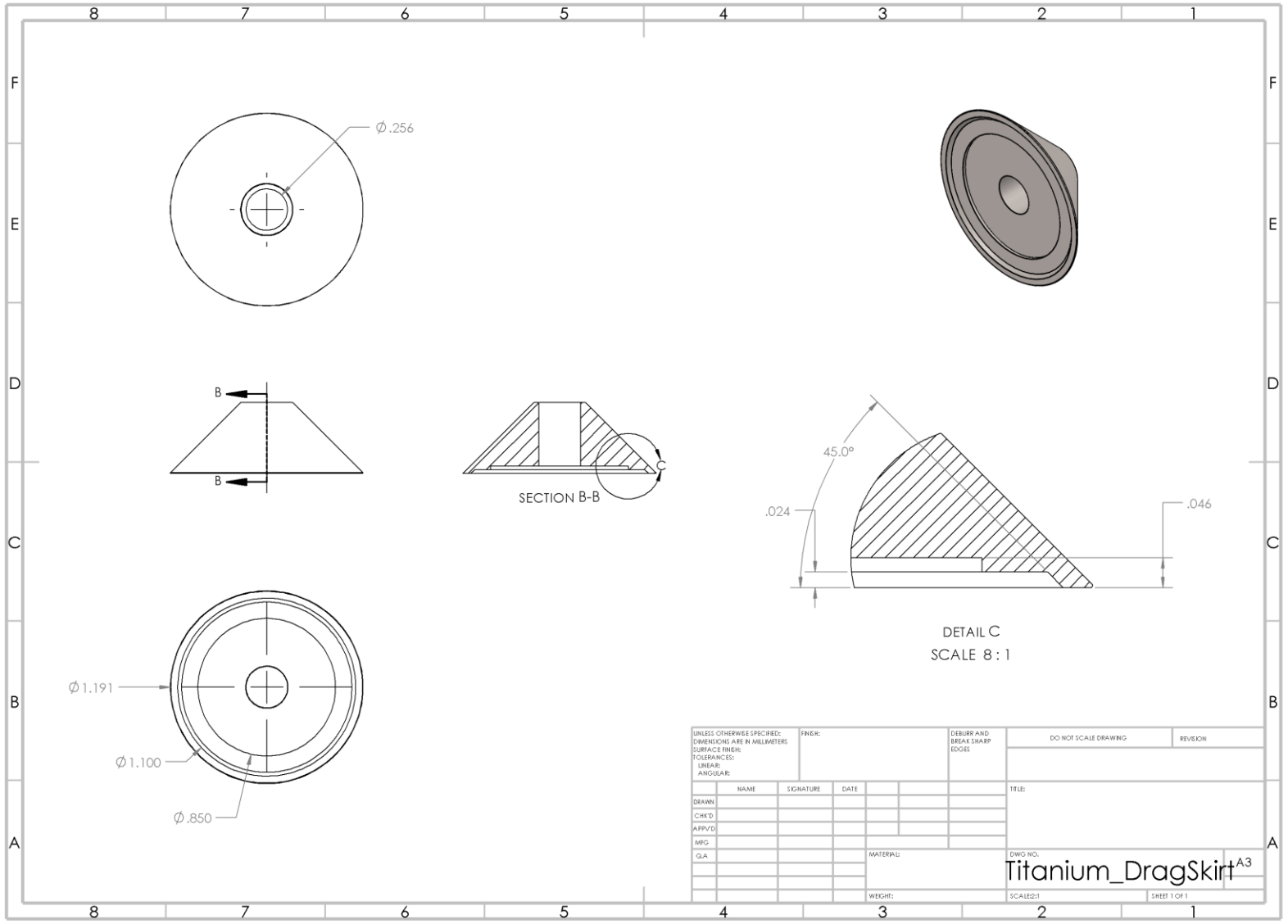
Ø.256
B
B
SECTION B-B
45.0°
.024
.046
DETAIL C
SCALE 8 : 1
Ø1.191
Ø1.100
Ø.850
UNLESS OTHERWISE SPECIFIED:
DIMENSIONS ARE IN MILLIMETERS
SURFACE FINISH:
TOLERANCES:
LINEAR:
ANGULAR:
FINISH:
DEBURR AND BREAK SHARP EDGES
DO NOT SCALE DRAWING
REVISION
NAME
SIGNATURE
DATE
DRAWN
CHK'D
APPV'D
MFG
QA
TITLE:
MATERIAL:
DWG NO.
Titanium_DragSkirt
A3
WEIGHT:
SCALE:2:1
SHEET 1 OF 1

Appendix B: Analytical Linear Model for Drag Skirt Separation

The simplified spacecraft bodies are shown below in Figure B1, in an initial state just after mechanical jettison, but before aerodynamic forces have started separating the two bodies. In the figure, the blue body denotes the delivered flight system (FS) capsule (denoted *C* in equations to follow), and the grey 45 degree cone frustum represents the separating drag skirt (DS) body (denoted *S* in equations to follow).

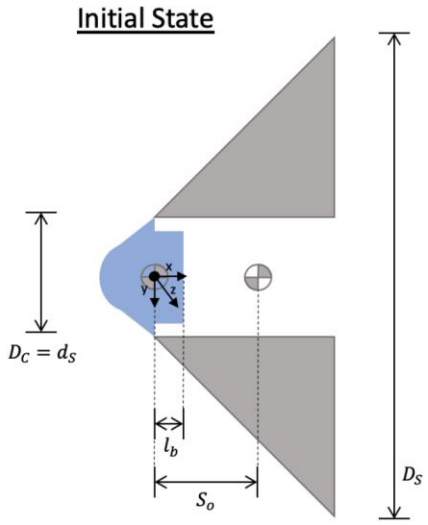

Figure B1: Definition of initial state.

A three-axis body-fixed coordinate system is placed at the FS center of gravity, with its *x*-axis oriented positive along the freestream flow velocity direction. This coordinate system was chosen in order that the drag skirt motions can be computed relative to the motions of the FS capsule. D_C and D_S denote the outer diameters of the FS capsule and DS, respectively. *dS* represents the inner diameter of the D_S. L_b is the length of the backshell, and S_o is the initial separation distance between the FS and the DS centers of gravity (CG).

In the Backshell Clearance State depicted in Figure B2, the two bodies are shown after a separation time t_b has elapsed, at which point they are separated by a backshell clearance distance S_b. While the drag skirt is in close proximity to the backshell, the allowable relative rotational motions between the two bodies is significantly smaller than after S_b has been reached. Considering that the FS CG (and our coordinate system) is located at the max diameter *x*-position of the FS at this state, we can define the backshell clearance distance S_b that must be travelled as the backshell length plus the initial separation distance, as pictured.

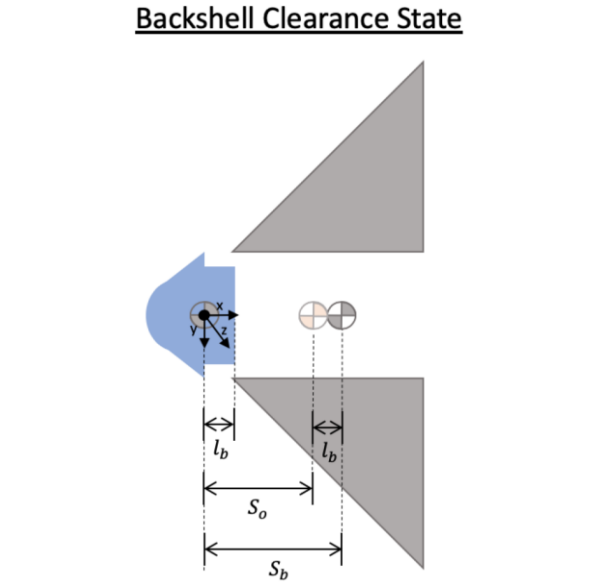

Figure B2: Definition of backshell clearance state.

In the Safe Separation State depicted in Figure B3, the two bodies are shown after a separation time t_{sep} has elapsed, at which point they are separated by a safe separation distance S_{sep}. Although we will assume no rotational motion for this linear translation analysis, the bounding separation distance is governed by the largest dimension of the two bodies, which is the max diameter point for each. Therefore, we define the safe separation distance S_{sep} that must be travelled as the FS capsule radius plus the DS radius, as pictured.

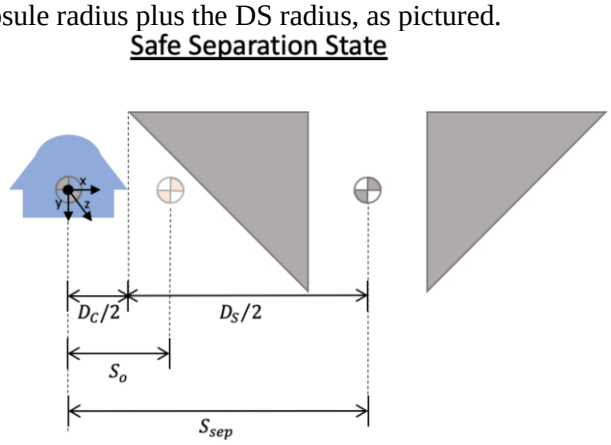

Figure B3: Definition of safe separation state.

In order to compute the time required to reach a given final state, we begin by assuming linear translational motion and constant acceleration for both bodies. Thus, we start with the following equations:

$$F = ma \tag{B1}$$

$$S = S_o + v_o t + \frac{1}{2} a t^2 \tag{B2}$$

Recognizing that $a = F/m$, we note the following:

$$a_S - a_C = \frac{F_S}{m_S} - \frac{F_C}{m_C} \tag{B3}$$

We solve for a_S and a_C through the use of Eq. (B2), as follows:

$$a_S = \frac{2}{t^2}\left(S_S - S_{o,S} - v_{o,S}t\right) \tag{B4}$$

$$a_C = \frac{2}{t^2}\left(S_C - S_{o,C} - v_{o,C}t\right) \tag{B5}$$

However, note in Eq. (B4) that the initial relative velocity between the DS and the FS (and therefore to the body-fixed coordinate system) is zero if no springs or other push-off mechanisms are used ($v_{o,S} = 0$). The initial position of the drag skirt is equivalent to S_o. Also, noting that the CG of the FS is attached to the coordinate system, we can reduce the terms inside the parentheses of Eq. (B5) to zero, leaving:

$$a_S = \frac{2}{t^2}(S_S - S_o) \tag{B6}$$

$$a_C = 0 \tag{B7}$$

Now, substituting Eq. (B6) and (B7) into Equation (B3), we see that:

$$\frac{2}{t^2}(S_S - S_o) = \frac{F_S}{m_S} - \frac{F_C}{m_C} \tag{B8}$$

Then, we substitute the equation for the force due to drag,

$$\frac{2}{t^2}(S_S - S_o) = \frac{1}{2}\rho_\infty v_\infty^2\left(\frac{C_{D,S}A_S}{m_S} - \frac{C_{D,C}A_C}{m_C}\right) \tag{B9}$$

Now, note the presence of ballistic coefficient and dynamic pressure within the right side of Eq. (B9) due to $\beta = m/C_DA$ and $q_\infty = (1/2)\rho_\infty v_\infty^2$.

$$\frac{2}{t^2}(S_S - S_o) = q_\infty\left(\frac{1}{\beta_S} - \frac{1}{\beta_C}\right) \tag{B10}$$

However, recognizing that the drag skirt will travel in the wake of the FS capsule, and thus will not experience the full freestream dynamic pressure, we add in a conservative k factor of 0.5 as a multiplier on the dynamic pressure seen by the skirt.

$$\frac{2}{t^2}(S_S - S_o) = q_\infty\left(\frac{k}{\beta_S} - \frac{1}{\beta_C}\right) \tag{B11}$$

Now we can solve for t to yield the following expression for the time to reach a given separation distance S:

$$t = \sqrt{\frac{2(ds)}{q_\infty\left(\frac{k}{\beta_S} - \frac{1}{\beta_C}\right)}} \tag{B12}$$

We can substitute S_b and S_{sep} into Eq. (B12) to solve for $t_b = 34.5$ msec and $t_{sep} = 87.3$ msec, respectively. These points are annotated on a plot of separation distance versus time below in Figure B4. The results and full set of inputs are displayed in Table B1.

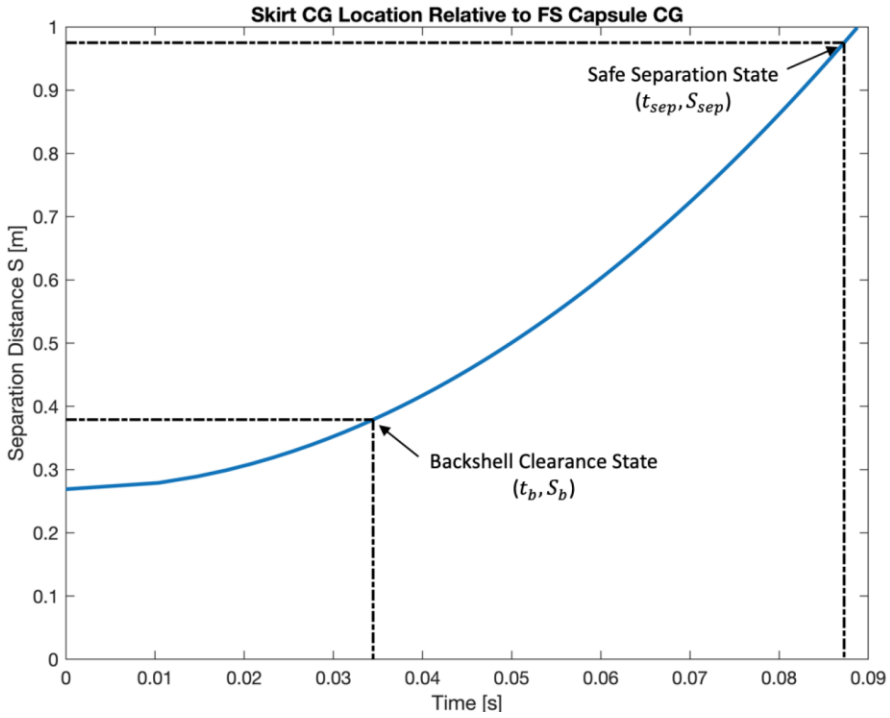

Figure B4: Example drag skirt separation distance vs. time.

Table B1: Variables and inputs for example analysis shown in Figure B4.

Variable	Value	Units
S_o	0.269	m
S_b	0.379	m
S_{sep}	0.975	m
k	0.5	–
q_∞	8,800	Pa
β_S	21	kg/m^2
β_C	224	kg/m^2
v_o	0	m/s
ρ_∞	2.59E-04	kg/m^3
v_∞	8250	m/s
m_C	36.7	kg
m_S	42	kg
A_C	0.159	m^2
A_S	1.634	m^2
$C_{D,C}$	1.03	–
$C_{D,S}$	1.25	–
D_C	0.45	m
D_S	1.5	m
l_b	0.11	m

Appendix C: Data Tables

The following tables provide the free stream test conditions, the measured model properties, and the measured and calculated trajectory for each component, for each shot.

Free Stream Conditions: Measured quantities are pressure, P_∞ (Torr), T_∞ (K), and Relative Humidity. Other values were calculated.

Model Properties: Empty cells indicate values that were not measured. See Table 2 for a list of the as-designed values, and section 4 for a description of the measurement methods.

Trajectory Tables:

- a -Speed of sound, $a = (\gamma RT)^{1/2}$.
- D -Model diameter at the maximum diameter.
- I_{xx} -Axial, or rolling, moment of inertia.
- I_{yy} -Transverse, or pitching/yawing, moment of inertia. $I_{yy} = I_{zz}$.
- L -Model length.
- M -Mach number, V/a.
- P_∞ -Free stream pressure.
- R -Universal gas constant, $R = 188.92$ J/kg-K for CO_2.
- Re_D -Freestream Reynolds number, $\rho_\infty V(x) D/\mu_\infty$.
- T_∞ -Free stream gas temperature.
- t -Time at which video or shadowgraph images were acquired. Note: The measured time is arbitrarily initialized by the gun-fire sequence. The launch time, $t(x = 0)$, was determined with eqn. (2) by fitting the measurements made of the center body model in the main test section from stations 1 to 16, and subtracted from the measured times in order to give $t(x = 0) = 0$, as reported in the following tables.
- $V(x)$ -Velocity as determined with eqn. (1) using measurements made in the main test section from stations 1 to 16.
- V_{av} -Average velocity on each measurement interval from eqn. (3).
- x_{av} -Location where the velocity equals V_{av}, approximately half way between measurement stations (see section 7).
- x_{CG} -Axial location of the center of gravity of the model component, measured from the geometric nose.
- x, y, z -Location of the center of gravity of each model component in terms of the longitudinal, transverse, and vertical facility coordinates, respectively.
- Δx -Axial separation distance between the center body and drag skirt model components, measured from the center of gravity of each component. The "Source" column indicates whether Δx was measured directly from an image (video or shadowgraph) capturing both components, or was inferred from a photobeam trace, as described in section 7.
- γ -Ratio of specific heats, $\gamma = 1.2904$ for CO_2.
- θ, ψ, ϕ -Pitch, yaw, and roll angles, respectively, measured relative to facility coordinate system.
- μ_∞ -Test gas viscosity, calculated using Sutherland's law.
- σ -Total angle of attack, $\sigma = (\theta^2 + \psi^2)^{1/2}$ (note: σ_{RMS}, the root-mean-square total angel of attack, is labeled α_{RMS} in the results discussion is section 8.
- ρ_∞ -Test gas density, calculated for ideal gas, $\rho_\infty = P_\infty/RT_\infty$.

Free Stream Conditions:

Shot #	P_∞ (atm)	P_∞ (Torr)	P_∞ (N/m^2)	T_∞ (K)	ρ_∞ (kg/m^3)	μ_∞ (kg/m-s)	Sound speed (m/s)	Relative humidity (%)	Test Gas
2815	0.150	114.00	15198.75	296.66	2.712E-01	1.50E-05	268.92	3.10	CO_2

Model Properties:

Component	Model ID	L (cm)	D (cm)	Mass (g)	%diff as designed	x_{CG} from nose (cm)	st dev (cm)	%diff as designed	I_{yy} (g-cm^2)	st dev	%diff as designed	I_{xx} (g-cm^2)	st dev	%diff as designed
Center Body	FS-01	0.531	0.767	1.9843	1.02%	0.325		-0.30%	0.07		1.02%	0.08		-12.90%
Drag Skirt	DS-SS01	1.113	3.025	21.2691										

Center Body

Station #	Time, t (s)	x (m)	y (m)	z (m)	θ (deg)	ψ (deg)	ϕ (deg)	total angle σ (deg)	V(x) from eqn. 1 (m/s)	M	Re_D	Measured velocity x_{av} (m)	Measured velocity V_{av} (m/s)
muzzle	0	0							3273.2	12.17	4.55E+05		
DT1	0.000314	1.0576		0.0103	−0.22				3262.8	12.13	4.53E+05		
DT2	0.000624	2.0530	-0.0044			−0.22			3253.0	12.10	4.52E+05	1.5552	3209.9
DT3	0.000909	2.9671		0.0092	−1.52				3244.0	12.06	4.51E+05	2.5100	3215.5
DT4	0.001207	3.9291		0.0064	0.46				3234.6	12.03	4.50E+05	3.4480	3222.6
2	0.003609	11.6281	-0.0023	0.0068	4.85	0.12	15.88	4.86	3160.2	11.75	4.39E+05		
3	0.004089	13.1423	-0.0030	0.0082	2.09	−2.11	23.88	2.97	3145.8	11.70	4.37E+05	12.3855	3151.0
4	0.004573	14.6591	-0.0033	0.0113	−3.34	0.88	27.88	3.45	3131.4	11.64	4.35E+05	13.9010	3136.7
5	0.005062	16.1866	-0.0039	0.0118	−1.76	3.19	19.88	3.64	3117.0	11.59	4.33E+05	15.4231	3124.5
6	0.005589	17.8276	-0.0043	0.0136	3.58	0.56	20.88	3.63	3101.5	11.53	4.31E+05	17.0074	3109.9
8	0.00654	20.7625	-0.0049	0.0131	−12.04	−9.22	29.91	15.16	3074.2	11.43	4.27E+05	19.2961	3088.3
10	0.007535	23.8122	-0.0048	0.0107	10.39	9.30	50.91	13.94	3046.0	11.33	4.23E+05	22.2885	3062.9
11	0.008044	25.3598	-0.0052	0.0091	2.71	−1.82	54.03	3.26	3031.8	11.27	4.21E+05	24.5863	3043.9
12	0.008539	26.8557	-0.0064	0.0086	−5.81	−14.59	69.22	15.70	3018.1	11.22	4.19E+05	26.1080	3022.5
14	0.009554	29.9048	-0.0070	0.0079	0.98	16.06	98.97	16.09	2990.4	11.12	4.16E+05	28.3814	3004.0
15	0.010063	31.4234	-0.0072	0.0078	3.15	3.45	129.97	4.67	2976.7	11.07	4.14E+05	30.6644	2981.9
16	0.010583	32.9674	-0.0068	0.0048	3.04	−15.08	119.97	15.38	2962.9	11.02	4.12E+05	32.1957	2968.4

Drag Skirt

Station #	Time, t (s)	x (m)	y (m)	z (m)	θ (deg)	ψ (deg)	ϕ (deg)	total angle σ (deg)	V(x) from eqn. 1 (m/s)	Drag Skirt Separation Δx, m	Source	Measured velocity x_{av} (m)	Measured velocity V_{av} (m/s)
muzzle	0	0							3301.6				
DT1	0.000314	1.0504		0.0103	−0.23				3289.8	0.0072	image		
DT2	0.000624	2.0446	-0.0045			1.33			3278.7	0.0084	image	1.5552	3209.9
DT3	0.000909	2.9560		0.0094	0.91				3268.5	0.0111	image	2.5100	3215.5
DT4	0.001207	3.9148		0.0067	1.44				3257.8	0.0143	image	3.4480	3222.6
2	0.003609	11.5862	-0.0019	0.0066	3.21	4.45		5.49	3173.7	0.0419	image		
3	0.004089	13.1061	-0.0025	0.0082	3.32	−0.35		3.33	3157.3	0.0362	image	12.3855	3151.0
4	0.004573	14.6319	-0.0033	0.0112	−2.31	2.82		3.65	3140.9	0.0272	image	13.9010	3136.7
5	0.005062	16.1683	-0.0039	0.0118	4.23	−1.89		4.64	3124.4	0.0182	image	15.4231	3124.5
6	0.005589	17.8157	-0.0042	0.0127	3.46	−5.67		6.64	3106.9	0.0119	image	17.0074	3109.9
8	0.00654	20.7509	-0.0050	0.0151	−2.62	5.02		5.66	3076.0	0.0116	image	19.2961	3088.3
10	0.007535	23.7878	-0.0051	0.0158	1.68	−4.04		4.37	3044.3	0.0244	image	22.2885	3062.9
11	0.008044	25.3258	-0.0060	0.0134	14.47	2.63		14.71	3028.3	0.0340	image	24.5863	3043.9
12	0.008539	26.8137	-0.0070	0.0102	29.09	−0.57		29.10	3013.0	0.0420	image	26.1080	3022.5
14	0.009554	29.8512	-0.0054	0.0040	−39.97	7.94		40.75	2981.9	0.0536	image	28.3814	3004.0
15	0.010063	31.3684	-0.0058	0.0022	−40.14	83.98		93.08	2966.5	0.0550	image	30.6644	2981.9
16	0.010583	32.9169	-0.0054	0.0000	−11.32	120.20		120.73	2950.9	0.0505	image	32.1957	2968.4

Free Stream Conditions:

Shot #	P_∞ (atm)	P_∞ (Torr)	P_∞ (N/m^2)	T_∞ (K)	ρ_∞ (kg/m^3)	μ_∞ (kg/m-s)	Sound speed (m/s)	Relative humidity (%)	Test Gas
2816	0.150	114.10	15212.08	295.66	2.724E-01	1.49E-05	268.47	0.08	CO_2

Model Properties:

Component	Model ID	L (cm)	D (cm)	Mass (g)	%diff as designed	x_{CG} from nose (cm)	st dev (cm)	%diff as designed	I_{yy} (g-cm^2)	st dev	%diff as drawn	I_{xx} (g-cm^2)	st dev	%diff as designed
Center Body	FS-02	0.536	0.767	1.9589	-0.27%	0.329		0.92%	0.07	0.01	0.64%	0.08		-14.72%
Drag Skirt	DS-AL01	1.129	3.034	7.7516	-0.09%				5.86		-0.18%			

Center Body

Station #	Time, t (s)	x (m)	y (m)	z (m)	θ (deg)	ψ (deg)	ϕ (deg)	total angle σ (deg)	V(x) from eqn. 1 (m/s)	M	Re_D	**Measured velocity** x_{av} (m)	V_{av} (m/s)
muzzle	0	0							3019.7	11.25	4.23E+05		
DT1	0.000377	1.1272		0.0056	−0.86				3008.4	11.21	4.21E+05		
DT2	0.000701	2.0943	-0.0040			0.24			2998.7	11.17	4.20E+05	1.6109	2987.1
DT3	0.001016	3.0262		0.0071	−6.44				2989.4	11.14	4.19E+05	2.5605	2956.8
DT4	0.001343	3.9942		0.0034	−1.58				2979.8	11.10	4.17E+05	3.5104	2959.8
1	0.003404	10.1016	-0.0010	0.0028	−5.33	−1.87	96.62	5.65	2919.8	10.88	4.09E+05		
2	0.003933	11.6414	-0.0006	0.0035	8.46	3.43	141.88	9.12	2904.9	10.82	4.07E+05	10.8719	2911.1
3	0.004461	13.1733	-0.0009	0.0043	6.05	2.09	82.39	6.41	2890.1	10.77	4.05E+05	12.4077	2898.0
4	0.004977	14.6590	-0.0009	0.0069	−7.49	−1.13	98.50	7.57	2875.8	10.71	4.03E+05	13.9164	2882.8
5	0.005511	16.1915	-0.0013	0.0070	−7.70	−1.77	80.00	7.90	2861.2	10.66	4.01E+05	15.4255	2869.2
6	0.00608	17.8147	-0.0012	0.0084	6.53	1.33	95.75	6.67	2845.8	10.60	3.98E+05	17.0034	2854.0
7	0.006587	19.2542	-0.0020	0.0079	8.17	3.23	75.75	8.79	2832.1	10.55	3.97E+05	18.5347	2837.6
8	0.007131	20.7921	-0.0017	0.0102	−5.10	−1.79	78.25	5.41	2817.7	10.50	3.95E+05	20.0235	2825.1
9	0.007662	22.2846	-0.0018	0.0101	−8.78	−2.49	77.00	9.13	2803.7	10.44	3.93E+05	21.5387	2811.5
10	0.008216	23.8339	-0.0015	0.0107	3.55	0.16	76.50	3.55	2789.3	10.39	3.91E+05	23.0596	2796.6
11	0.008765	25.3609	-0.0022	0.0108	9.51	2.55	74.50	9.84	2775.1	10.34	3.89E+05	24.5977	2782.5
13	0.009858	28.3807	-0.0038	0.0120	−10.54	−2.55	71.63	10.84	2747.4	10.23	3.85E+05	26.8720	2762.6
14	0.010415	29.9055	-0.0042	0.0147	−0.05	0.38	65.13	0.39	2733.4	10.18	3.83E+05	29.1434	2738.2
15	0.010971	31.4231	-0.0045	0.0161	8.85	5.47	67.13	10.41	2719.7	10.13	3.81E+05	30.6646	2726.7

Drag Skirt

Station #	Time, t (s)	x (m)	y (m)	z (m)	θ (deg)	ψ (deg)	ϕ (deg)	total angle σ (deg)	V(x) from eqn. 1 (m/s)	Drag Skirt Separation Δx, m	Source	**Measured velocity** x_{av} (m)	V_{av} (m/s)
muzzle	0	0							3074.8				
DT1	0.000377	1.1189		0.0065	1.50				3055.8	0.0083	image		
DT2	0.000701	2.0805	-0.0039			0.30			3039.5	0.0138	image	1.6001	2970.2
DT3	0.001016	2.9997		0.0072	0.18				3024.1	0.0265	image	2.5405	2916.5
DT4	0.001343	3.9502		0.0038	−5.23				3008.1	0.0440	image	3.4754	2906.4
1	0.003404	9.9535	-0.0013	0.0025	−32.33	−11.77		34.41	2909.6	0.1481	image		
2	0.003933	11.4708	-0.0006	0.0035	−49.94	199.22		205.39	2885.1	0.1706	image	10.7127	2868.5
3	0.004461	12.9941							2860.7	0.1791	photobeam	12.2367	2895.7
5	0.005511	15.9816							2813.7	0.2099	photobeam	14.4972	2846.5
6	0.00608	17.5704		0.0162	182.60	3.08		182.62	2789.1	0.2442	image	16.7802	2780.9
7	0.006587	18.9880							2767.1	0.2662	photobeam	18.2833	2808.6
9	0.007662	21.9380							2722.2	0.3466	photobeam	20.4722	2743.6
11	0.008765	24.9103							2677.6	0.4506	photobeam	23.4335	2695.3
12	0.009476	26.8014	0.0160	0.0281	211.68	15.00		212.21	2649.8			25.8603	2648.9
13	0.009858	27.8061							2634.9	0.5746	photobeam	27.3076	2649.6

Free Stream Conditions:

Shot #	P_∞ (atm)	P_∞ (Torr)	P_∞ (N/m^2)	T_∞ (K)	ρ_∞ (kg/m^3)	μ_∞ (kg/m-s)	Sound speed (m/s)	Relative humidity (%)	Test Gas
2817	0.150	114.10	15212.08	295.96	2.721E-01	1.49E-05	268.60	3.20	CO_2

Model Properties:

Component	Model ID	L (cm)	D (cm)	Mass (g)	%diff as drawn	x_{CG} from nose (cm)	st dev (cm)	%diff as drawn	I_{yy} (g-cm^2)	st dev	%diff as drawn	I_{xx} (g-cm^2)	st dev	%diff as drawn
Center Body	FS-03	0.538	0.766	1.9739	0.49%	0.331		1.48%	0.09	0.00	17.31%	0.09		-1.13%
Drag Skirt	DS-ADEPT-SS01	1.123	3.040	19.7424	-1.19%				13.68		-0.55%			

Center Body

Measured velocity

Station #	Time, t (s)	x (m)	y (m)	z (m)	θ (deg)	ψ (deg)	ϕ (deg)	total angle σ (deg)	V(x) from eqn. 1 (m/s)	M	Re_D	x_{av} (m)	V_{av} (m/s)
muzzle	0	0							3227.7	12.02	4.50E+05		
DT1	0.000362	1.0958		0.0039	−0.12				3217.9	11.98	4.49E+05		
DT2	0.000644	2.0058	-0.0034			−0.49			3209.7	11.95	4.48E+05	1.5508	3224.3
DT3	0.000947	2.9791		0.0030	−0.33				3201.1	11.92	4.47E+05	2.4925	3215.3
DT4	0.00124	3.9246		0.0017	−0.02				3192.7	11.89	4.45E+05	3.4519	3223.1
1	0.003176	10.1047	-0.0058	0.0055	0.39	−1.97	0.50	2.01	3138.3	11.68	4.38E+05		
2	0.003669	11.6533	-0.0059	0.0067	1.83	2.33	-7.50	2.96	3124.9	11.63	4.36E+05	10.8793	3138.9
3	0.004152	13.1620	-0.0070	0.0079	−1.75	2.07	-7.50	2.71	3111.8	11.59	4.34E+05	12.4079	3124.5
4	0.004634	14.6600	-0.0077	0.0109	−1.47	−2.06	-8.39	2.53	3098.9	11.54	4.32E+05	13.9112	3108.8
5	0.005128	16.1903	-0.0084	0.0113	2.49	−2.33	-8.63	3.41	3085.7	11.49	4.31E+05	15.4254	3094.0
6	0.005659	17.8256	-0.0090	0.0129	1.32	0.54	-8.63	1.43	3071.7	11.44	4.29E+05	17.0082	3078.7
7	0.006125	19.2515	-0.0102	0.0127	−1.56	2.52	-10.13	2.97	3059.6	11.39	4.27E+05	18.5388	3059.2
8	0.006622	20.7643	-0.0104	0.0149	−1.76	0.00	-7.38	1.76	3046.8	11.34	4.25E+05	20.0081	3047.1
9	0.007123	22.2831	-0.0111	0.0154	1.78	−2.06	-9.44	2.73	3033.9	11.30	4.23E+05	21.5239	3033.1
10	0.007629	23.8109	-0.0112	0.0162	3.02	2.19	-6.56	3.73	3021.1	11.25	4.21E+05	23.0473	3017.9
11	0.008134	25.3300		0.0165	4.52	−23.00	-13.56	23.44	3008.4	11.20	4.20E+05	24.5707	3006.1
13	0.009152	28.3810	-0.0111	0.0156	−1.30	114.15	-32.56	114.16	2983.0	11.11	4.16E+05	26.8565	2998.4
14	0.009661	29.8989	-0.0094	0.0167	180.86	−3.17	-57.56	180.89	2970.4	11.06	4.14E+05	29.1402	2980.6
15	0.010174	31.4207	-0.0075	0.0168	9.57	243.46	-71.77	243.65	2957.9	11.01	4.13E+05	30.6601	2969.3
16	0.010695	32.9645	-0.0059	0.0140	5.69	284.43	4.38	284.49	2945.2	10.96	4.11E+05	32.1929	2959.3

Drag Skirt

Measured velocity

Station #	Time, t (s)	x (m)	y (m)	z (m)	θ (deg)	ψ (deg)	ϕ (deg)	total angle σ (deg)	V(x) from eqn. 1 (m/s)	Drag Skirt Separation Δx, m	Source	x_{av} (m)	V_{av} (m/s)
muzzle	0	0							3250.0				
DT1	0.000362	1.0887		0.0034	2.44				3239.0	0.0071	image		
DT2	0.000644	1.9972	-0.0035			1.51			3229.9	0.0086	image	1.5429	3219.0
DT3	0.000947	2.9680		0.0033	−0.07				3220.1	0.0112	image	2.4826	3206.9
DT4	0.001240	3.9101		0.0024	1.40				3210.7	0.0145	image	3.4391	3211.6
1	0.003176	10.0564	-0.0058	0.0063	0.99	−5.97	-10.00	6.05	3150.0	0.0483	image		
2	0.003669	11.6005	-0.0060	0.0067	5.47	−3.70	-14.00	6.60	3134.9	0.0528	image	10.8288	3129.7
3	0.004152	13.1073	-0.0067	0.0080	1.72	6.39	-13.00	6.62	3120.3	0.0546	image	12.3542	3120.8
4	0.004634	14.6063	-0.0073	0.0101	−6.28	9.10	-12.80	11.06	3105.8	0.0537	image	13.8571	3110.7
5	0.005128	16.1395	-0.0078	0.0113	−3.89	−1.26	-17.20	4.09	3091.1	0.0507	image	15.3732	3100.1
6	0.005659	17.7802	-0.0083	0.0122	6.08	−4.42	-14.00	7.52	3075.3	0.0453	image	16.9602	3088.8
7	0.006125	19.2134	-0.0102	0.0129	1.55	8.18	-16.11	8.33	3061.7	0.0380	image	18.4971	3074.8
8	0.006622	20.7351	-0.0110	0.0147	−7.22	8.50	-14.06	11.16	3047.2	0.0292	image	19.9746	3064.9
9	0.007123	22.2626	-0.0116	0.0159	1.50	−17.25	-17.56	17.32	3032.8	0.0205	image	21.4991	3050.4
10	0.007629	23.7977	-0.0113	0.0168	8.02	−10.39	-17.28	13.13	3018.4	0.0132	image	23.0305	3032.3
11	0.008134	25.3201		0.0173	−2.04	14.00	-19.44	14.15	3004.2	0.0098	image	24.5592	3012.7
13	0.009152	28.3585	-0.0136	0.0182	−0.36	−11.75	-22.13	11.75	2975.9	0.0224	image	26.8405	2986.1
14	0.009661	29.8639	-0.0135	0.0191	19.03	−14.15	-22.50	23.71	2962.1	0.0350	image	29.1115	2955.8
15	0.010174	31.3760	-0.0115	0.0186	26.18	−29.39	-14.67	39.36	2948.2	0.0447	image	30.6202	2950.5
16	0.010695	32.9110	-0.0077	0.0172	12.14	−43.18	-55.36	44.86	2934.2	0.0535	image	32.1438	2942.2

Free Stream Conditions:

Shot #	P_∞ (atm)	P_∞ (Torr)	P_∞ (N/m^2)	T_∞ (K)	ρ_∞ (kg/m^3)	μ_∞ (kg/m-s)	Sound speed (m/s)	Relative humidity (%)	Test Gas
2818	0.150	114.00	15198.75	296.06	2.717E-01	1.49E-05	268.65	3.20	CO_2

Model Properties:

Component	Model ID	L (cm)	D (cm)	Mass (g)	%diff as drawn	x_{CG} from nose (cm)	st dev (cm)	%diff as drawn	I_{yy} (g-cm^2)	st dev	%diff as drawn	I_{xx} (g-cm^2)	st dev	%diff as drawn
Center Body	FS-04	0.536	0.766	2.0016	1.90%	0.326		0.02%	0.07	0.01	-10.68%	0.09	0.00	-1.33%
Drag Skirt	DS-SS02	1.118	3.033	21.3680	-3.27%				16.26	-2.69%				

Center Body

Measured velocity

Station #	Time, t (s)	x (m)	y (m)	z (m)	θ (deg)	ψ (deg)	ϕ (deg)	total angle σ (deg)	V(x) from eqn. 1 (m/s)	M	Re_D	x_{av} (m)	V_{av} (m/s)
muzzle	0	0							3210.1	11.95	4.47E+05		
DT1	0.000374	1.0960		0.0043	−0.22				3200.6	11.91	4.46E+05		
DT2	0.000656	1.9973	-0.0010			0.27			3192.7	11.88	4.45E+05	1.5386	3197.8
DT3	0.000971	3.0018		0.0060	2.03				3184.0	11.85	4.44E+05	2.4899	3175.6
DT4	0.001265	3.9388		-0.0010	0.62				3175.8	11.82	4.42E+05	3.4575	3181.5
1	0.003211	10.1475	-0.0034	0.0065	3.44	3.77	0.00	5.10	3122.5	11.62	4.35E+05		
2	0.003702	11.6795	-0.0030	0.0082	−0.43	−0.70	0.02	0.82	3109.5	11.57	4.33E+05	10.9138	3116.8
3	0.004188	13.1868	-0.0037	0.0092	−3.83	−4.83	0.88	6.17	3096.7	11.53	4.31E+05	12.4334	3103.8
4	0.00468	14.7067	-0.0039	0.0122	−0.23	0.67	0.00	0.71	3083.9	11.48	4.30E+05	13.9470	3089.5
5	0.005176	16.2338	-0.0042	0.0127	4.20	4.47	0.00	6.14	3071.1	11.43	4.28E+05	15.4705	3076.9
7	0.00618	19.3023	-0.0049	0.0144	−2.08	−3.26	-1.01	3.86	3045.5	11.34	4.24E+05	17.7691	3055.8
8	0.006676	20.8069	-0.0045	0.0166	6.40	10.33	-5.38	12.15	3033.1	11.29	4.23E+05	20.0548	3036.4
9	0.007179	22.3310	-0.0040	0.0174	19.38	33.11	0.00	38.36	3020.5	11.24	4.21E+05	21.5692	3028.1
10	0.007685	23.8579	-0.0028	0.0188	7.21	10.36	0.00	12.62	3007.9	11.20	4.19E+05	23.0947	3016.2
11	0.008194	25.3860	-0.0023	0.0198	−16.68	−22.73	-3.84	28.19	2995.4	11.15	4.17E+05	24.6222	3004.4
13	0.009211	28.4249	-0.0011	0.0225	6.53	8.05	-14.00	10.37	2970.7	11.06	4.14E+05	26.9065	2987.0
14	0.009724	29.9429	0.0001	0.0255	21.94	26.26	5.03	34.22	2958.4	11.01	4.12E+05	29.1841	2962.1
15	0.010239	31.4650	0.0010	0.0280	4.30	5.44	-12.97	6.93	2946.2	10.97	4.10E+05	30.7042	2951.7
16	0.010766	33.0136	0.0027	0.0273	−17.88	−26.69	-0.72	32.12	2933.8	10.92	4.09E+05	32.2396	2938.3

Drag Skirt

Measured velocity

Station #	Time, t (s)	x (m)	y (m)	z (m)	θ (deg)	ψ (deg)	ϕ (deg)	total angle σ (deg)	V(x) from eqn. 1 (m/s)	Drag Skirt Separation Δx, m	Source	x_{av} (m)	V_{av} (m/s)
muzzle	0	0							3233.1				
DT1	0.000374	1.0883		0.0050	−0.58				3222.3	0.0077	image		
DT2	0.000656	1.9888	-0.0008			1.05			3213.4	0.0085	image	1.5429	3219.0
DT3	0.000971	2.9907		0.0063	−0.60				3203.4	0.0111	image	2.4826	3206.9
DT4	0.001265	3.9242		-0.0007	0.70				3194.2	0.0146	image	3.4391	3211.6
1	0.003211	10.1015	-0.0037	0.0063	6.01	4.40		7.45	3134.0	0.0460	image		
2	0.003702	11.6334	-0.0034	0.0083	−5.20	8.93		10.34	3119.2	0.0462	image	10.8677	3116.4
3	0.004188	13.1452	-0.0031	0.0095	−7.63	−3.95		8.59	3104.7	0.0416	image	12.3896	3113.2
4	0.004680	14.6731	-0.0034	0.0111	1.68	−0.55		1.76	3090.1	0.0336	image	13.9095	3105.8
5	0.005176	16.2104	-0.0043	0.0127	−1.90	7.14		7.39	3075.5	0.0234	image	15.4421	3097.4
7	0.006180	19.2912	-0.0040	0.0148	1.27	−11.37		11.44	3046.4	0.0110	image	17.7520	3068.1
8	0.006676	20.7970	-0.0036	0.0172	−0.94	12.41		12.45	3032.3	0.0099	image	20.0444	3038.7
9	0.007179	22.3168	-0.0032	0.0177	−1.31	13.43		13.50	3018.1	0.0142	image	21.5572	3019.6
10	0.007685	23.8353	-0.0023	0.0187	−1.50	−8.79		8.92	3004.0	0.0227	image	23.0763	2999.6
11	0.008194	25.3521	-0.0035	0.0193	−1.40	−9.48		9.58	2990.0	0.0339	image	24.5940	2982.3
13	0.009211	28.3746	-0.0029	0.0235	−13.21	−19.10		23.23	2962.3	0.0503	image	26.8645	2970.9
14	0.009724	29.8889	-0.0009	0.0248	11.59	−13.28		17.63	2948.5	0.0539	image	29.1321	2955.0
15	0.010239	31.4095	0.0013	0.0264	18.03	10.52		20.87	2934.7	0.0555	image	30.6495	2948.6
16	0.010766	32.9578	0.0041	0.0275	−3.21	18.21		18.49	2920.7	0.0558	image	32.1839	2937.8

Free Stream Conditions:

Shot #	P_∞ (atm)	P_∞ (Torr)	P_∞ (N/m^2)	T_∞ (K)	ρ_∞ (kg/m^3)	μ_∞ (kg/m-s)	Sound speed (m/s)	Relative humidity (%)	Test Gas
2819	0.150	114.00	15198.75	295.26	2.725E-01	1.49E-05	268.29	4.10	CO_2

Model Properties:

Component	Model ID	L (cm)	D (cm)	Mass (g)	%diff as drawn	x_{CG} from nose (cm)	st dev (cm)	%diff as drawn	I_{yy} (g-cm^2)	st dev	%diff as drawn	I_{xx} (g-cm^2)	st dev	%diff as drawn
Center Body	FS-05	0.536	0.768	1.9678	0.18%	0.327	0.000	0.40%	0.07	0.02	2.78%	0.09	0.01	-5.76%
Drag Skirt	DS-Ti01	1.118	3.020	11.9841	-1.02%				9.37		0.50%			

Center Body

Station #	Time, t (s)	x (m)	y (m)	z (m)	θ (deg)	ψ (deg)	ϕ (deg)	total angle σ (deg)	V(x) from eqn. 1 (m/s)	M	Re_D	**Measured velocity** x_{av} (m)	V_{av} (m/s)
muzzle	0	0							3296.0	12.29	4.63E+05		
DT1	0.00034	1.0956		0.0024	−0.02				3284.1	12.24	4.61E+05		
DT2	0.000622	2.0166	-0.0009			0.51			3274.1	12.20	4.60E+05	1.5562	3267.0
DT3	0.000923	2.9988		0.0047	4.33				3263.4	12.16	4.58E+05	2.5078	3264.5
DT4	0.001217	3.9549		-0.0078	0.61				3253.1	12.13	4.57E+05	3.4769	3250.7
1	0.003118	10.1028	-0.0018	0.0021	4.92	2.20	3.00	5.39	3187.5	11.88	4.48E+05		
2	0.003597	11.6271	-0.0012	0.0027	−2.78	−3.36	6.25	4.36	3171.4	11.82	4.46E+05	10.8653	3178.3
3	0.004082	13.1596	-0.0018	0.0033	−3.38	−2.99	5.00	4.51	3155.4	11.76	4.43E+05	12.3936	3163.9
4	0.004558	14.6583	-0.0018	0.0059	2.80	1.64	5.00	3.25	3139.8	11.70	4.41E+05	13.9092	3147.5
5	0.005045	16.1851	-0.0019	0.0059	4.85	4.18	4.00	6.40	3123.9	11.64	4.39E+05	15.4220	3132.7
6	0.005568	17.8132	-0.0020	0.0071	−2.47	−1.37	4.94	2.83	3107.1	11.58	4.36E+05	16.9995	3115.8
7	0.006034	19.2577	-0.0029	0.0065	−4.55	−3.86	7.44	5.97	3092.3	11.53	4.34E+05	18.5358	3098.4
8	0.006531	20.7913	-0.0025	0.0086	1.11	0.15	1.98	1.12	3076.6	11.47	4.32E+05	20.0248	3084.4
9	0.007019	22.2875	-0.0028	0.0086	5.17	4.72	7.92	7.01	3061.4	11.41	4.30E+05	21.5397	3070.0
10	0.007525	23.8335	-0.0025	0.0089	1.28	−1.10	6.92	1.69	3045.7	11.35	4.28E+05	23.0608	3053.1
11	0.008018	25.3320	-0.0029	0.0089	−4.58	−4.14	2.92	6.18	3030.6	11.30	4.26E+05	24.5830	3038.4
12	0.008531	26.8810	-0.0042	0.0096	−0.50	1.85	3.92	1.92	3015.1	11.24	4.24E+05	26.1068	3022.6
13	0.009029	28.3813	-0.0045	0.0097	4.20	2.66	7.92	4.97	3000.2	11.18	4.21E+05	27.6314	3010.3
14	0.009538	29.9038	-0.0048	0.0114	2.18	1.58	2.92	2.69	2985.1	11.13	4.19E+05	29.1429	2990.5
15	0.010048	31.4224	-0.0051	0.0131	−3.57	−3.19	4.92	4.79	2970.1	11.07	4.17E+05	30.6634	2977.2

Drag Skirt

Station #	Time, t (s)	x (m)	y (m)	z (m)	θ (deg)	ψ (deg)	ϕ (deg)	total angle σ (deg)	V(x) from eqn. 1 (m/s)	Drag Skirt Separation Δx, m	Source	**Measured velocity** x_{av} (m)	V_{av} (m/s)
muzzle	0	0							3225.6				
DT1	0.000340	1.0880		0.0023	0.09				3218.5	0.0076	image		
DT2	0.000622	2.0061	-0.0011			0.32			3212.6	0.0106	image	1.5473	3256.6
DT3	0.000923	2.9809		0.0047	1.25				3206.2	0.0179	image	2.4937	3239.9
DT4	0.001217	3.9259		-0.0079	1.72				3200.1	0.0290	image	3.4536	3213.2
1	0.003118	9.9785	-0.0002	0.0035	10.43	17.45		20.33	3161.1	0.1243	image		
2	0.003597	11.4860	0.0000	0.0035	24.92	32.99		41.34	3151.4	0.1410	image	10.7325	3143.3
3	0.004082	13.0058	-0.0017	0.0039	31.28	39.14		50.11	3141.8	0.1537	image	12.2461	3137.7
5	0.005045	16.0214							3122.6	0.1637	photobeam	14.5180	3137.2
6	0.005568	17.6472		0.0035	−32.17	42.03		52.93	3112.3	0.1661	image	16.8381	3097.5
7	0.006034	19.0993		0.0103	45.74	88.81		99.90	3103.2	0.1585	image	18.3734	3114.6
8	0.006531	20.6448		0.0042	−42.62	−127.08		134.03	3093.5	0.1465	image	19.8722	3108.5
9	0.007019	22.1597	-0.0072	0.0050	220.54	34.75		223.27	3084.0	0.1278	image	21.4025	3108.5
10	0.007525	23.7270	-0.0094	0.0022	235.30	9.32		235.48	3074.2	0.1065	image	22.9436	3095.1
11	0.008018	25.2507	-0.0138	-0.0046	−45.91	79.77		92.04	3064.8	0.0814	image	24.4890	3089.3
12	0.008531	26.8219	-0.0205	-0.0100	34.01	−26.52		43.13	3055.0	0.0590	image	26.0365	3066.1
13	0.009029	28.3393	-0.0245	-0.0167	7.02	−109.24		109.47	3045.6	0.0420	image	27.5808	3044.6
14	0.009538	29.8793	-0.0311	-0.0243	−37.32	−86.21		93.94	3036.2	0.0245	image	29.1095	3024.9
15	0.010048	31.4154	-0.0367	-0.0296	2.43	22.34		22.47	3026.7	0.0070	image	30.6476	3011.4

Free Stream Conditions:

Shot #	P_∞ (atm)	P_∞ (Torr)	P_∞ (N/m^2)	T_∞ (K)	ρ_∞ (kg/m^3)	μ_∞ (kg/m-s)	Sound speed (m/s)	Relative humidity (%)	Test Gas
2820	0.250	190.00	25331.25	296.66	4.520E-01	1.50E-05	268.92	2.20	CO_2

Model Properties:

Component	Model ID	L (cm)	D (cm)	Mass (g)	%diff as drawn	x_{CG} from nose (cm)	st dev (cm)	%diff as drawn	I_{yy} (g-cm^2)	st dev	%diff as drawn	I_{xx} (g-cm^2)	st dev	%diff as drawn
Center Body	FS-06	0.535	0.769	2.0185	2.76%	0.323	0.002	-0.80%	0.10	0.01	31.59%	0.10	0.00	7.59%
Drag Skirt	DS-Ti02	1.120	3.018	11.9089	-1.64%	0.706	0.001	-1.91%	9.29		-0.33%			

Center Body

Station #	Time, t (s)	x (m)	y (m)	z (m)	θ (deg)	ψ (deg)	ϕ (deg)	total angle σ (deg)	V(x) from eqn. 1 (m/s)	M	Re_D	**Measured velocity** x_{av} (m)	V_{av} (m/s)
muzzle	0	0							3262.6	12.13	7.57E+05		
DT1	0.000352	1.1181		0.0034	1.68		0.00		3243.0	12.06	7.53E+05		
DT2	0.000633	2.0259	-0.0030			3.92	0.00		3227.1	12.00	7.49E+05	1.5722	3221.6
DT3	0.000931	2.9818		0.0065	0.38		8.00		3210.5	11.94	7.45E+05	2.5040	3215.7
DT4	0.001239	3.9689		0.0001	−0.34		11.00		3193.4	11.87	7.41E+05	3.4755	3198.0
1	0.003183	10.1021	-0.0060	0.0082	−4.00	−7.14	0.00	8.18	3089.3	11.49	7.17E+05		
2	0.003679	11.6272	-0.0057	0.0100	2.83	3.37	7.00	4.40	3064.0	11.39	7.11E+05	10.8652	3075.7
3	0.004183	13.1664	-0.0068	0.0119	−0.06	4.80	8.00	4.80	3038.6	11.30	7.05E+05	12.3973	3051.8
4	0.004676	14.6576	-0.0073	0.0157	−4.42	−4.48	11.00	6.29	3014.2	11.21	7.00E+05	13.9125	3026.1
5	0.005186	16.1875	-0.0080	0.0171	1.12	−0.93	16.00	1.46	2989.4	11.12	6.94E+05	15.4230	3002.6
6	0.005730	17.8087	-0.0084	0.0196	1.43	5.62	12.00	5.80	2963.4	11.02	6.88E+05	16.9987	2976.4
8	0.006750	20.8044	-0.0098	0.0243	−1.89	−2.69	21.00	3.29	2915.8	10.84	6.77E+05	19.3086	2938.9
9	0.007260	22.2854	-0.0104	0.0255	4.97	6.39	22.50	8.09	2892.5	10.76	6.71E+05	21.5454	2904.8
10	0.007795	23.8264	-0.0104	0.0274	−1.25	2.13	25.50	2.47	2868.6	10.67	6.66E+05	23.0564	2880.4
11	0.008338	25.3779	-0.0113	0.0290	−4.18	−4.82	28.00	6.38	2844.6	10.58	6.60E+05	24.6027	2856.9
13	0.009400	28.3767	-0.0136	0.0331	1.02	3.65	26.00	3.79	2798.9	10.41	6.50E+05	26.8793	2822.7
14	0.009945	29.8956	-0.0143	0.0372	−5.68	−3.78	23.00	6.82	2776.0	10.32	6.44E+05	29.1367	2785.1
15	0.010496	31.4173	-0.0150	0.0405	0.32	−0.08	28.00	0.33	2753.3	10.24	6.39E+05	30.6570	2764.7
16	0.011059	32.9628	-0.0148	0.0407	5.22	3.69	9.13	6.39	2730.4	10.15	6.34E+05	32.1906	2742.5

Drag Skirt

Station #	Time, t (s)	x (m)	y (m)	z (m)	θ (deg)	ψ (deg)	ϕ (deg)	total angle σ (deg)	V(x) from eqn. 1 (m/s)	Drag Skirt Separation Δx, m	Source	**Measured velocity** x_{av} (m)	V_{av} (m/s)
muzzle	0	0							3430.8				
DT1	0.000352	1.1105		0.0031	0.63				3396.9	0.0076	image		
DT2	0.000633	2.0113	-0.0033			0.73			3369.7	0.0106	image	1.5612	3196.7
DT3	0.000931	2.9549		0.0060	0.45				3341.4	0.0179	image	2.4835	3174.5
DT4	0.001239	3.9229		-0.0004	−2.52				3312.6	0.0290	image	3.4393	3136.1
1	0.003183	9.9451	-0.0050	0.0089	16.43	59.75		61.97	3139.0	0.1243	image		
3	0.004183	12.9965		0.0104	−9.29	−11.00		14.40	3054.5	0.1410	image	11.4743	3050.8
5	0.005186	16.0313		0.0149	0.18	−1.00		1.02	2972.7	0.1537	image	14.5173	3027.8
6	0.005730	17.6565	-0.0235	0.0200	−18.21	−17.73		25.41	2929.9	0.1637	image	16.8449	2983.5
8	0.006750	20.6383		0.0372	163.86	28.59		166.33	2852.8	0.1661	image	19.1507	2925.4
9	0.007260	22.0673							2816.4	0.1585	photobeam	21.3572	2817.0
11	0.008338	25.0586							2742.1	0.1465	photobeam	23.5735	2774.6
13	0.009400	27.9275							2672.6	0.1278	photobeam	26.5033	2700.4
16	0.011059	32.2658							2571.0	0.1065	photobeam	30.1109	2614.5

Free Stream Conditions:

Shot #	P_∞ (atm)	P_∞ (Torr)	P_∞ (N/m^2)	T_∞ (K)	ρ_∞ (kg/m^3)	μ_∞ (kg/m-s)	Sound speed (m/s)	Relative humidity (%)	Test Gas
2821	0.066	50.00	6666.12	296.26	1.191E-01	1.49E-05	268.74	2.90	CO_2

Model Properties:

Component	Model ID	L (cm)	D (cm)	Mass (g)	%diff as drawn	x_{CG} from nose (cm)	st dev (cm)	%diff as drawn	I_{yy} (g-cm^2)	st dev	%diff as drawn	I_{xx} (g-cm^2)	st dev	%diff as drawn
Center Body	FS-08	0.527	0.769	1.9688	0.23%	0.320	0.001	-1.84%	0.08	0.01	9.55%	0.11	0.00	17.00%
Drag Skirt	DS-AL02	1.127	3.032	7.6894	-0.90%	0.734	0.001	1.31%	5.83	0.01	-0.58%			

Center Body

Station #	Time, t (s)	x (m)	y (m)	z (m)	θ (deg)	ψ (deg)	ϕ (deg)	total angle σ (deg)	V(x) from eqn. 1 (m/s)	M	Re_D	**Measured velocity** x_{av} (m)	V_{av} (m/s)
muzzle	0	0							3389.8	12.61	2.08E+05		
DT1	0.000331	1.1024	0.0000	0.0026	−0.89	0.00	0.00	0.89	3384.5	12.59	2.07E+05		
DT2	0.000614	2.0527	-0.0006	0.0000	0.00	−0.70	0.00	0.70	3379.9	12.58	2.07E+05	1.5776	3367.8
DT3	0.000889	2.9838	0.0000	0.0031	−0.66	0.00	4.00	0.66	3375.4	12.56	2.07E+05	2.5183	3374.4
DT4	0.001169	3.9252	0.0000	0.0000	−0.59	0.00	4.00	0.59	3370.8	12.54	2.06E+05	3.4545	3370.9
1	0.003003	10.1057	0.0034	0.0029	0.81	−1.60	0.00	1.79	3341.1	12.43	2.05E+05		
2	0.003463	11.6374	0.0049	0.0036	1.06	−0.15	0.00	1.07	3333.8	12.41	2.04E+05	10.8717	3336.2
3	0.003923	13.1714	0.0051	0.0045	−1.25	−0.37	0.00	1.30	3326.5	12.38	2.04E+05	12.4045	3330.8
4	0.004371	14.6591	0.0059	0.0073	−1.84	0.04	0.00	1.84	3319.5	12.35	2.03E+05	13.9154	3322.7
5	0.004832	16.1887	0.0067	0.0075	−1.66	0.98	2.00	1.93	3312.2	12.32	2.03E+05	15.4240	3316.4
6	0.005327	17.8249	0.0075	0.0089	0.40	−0.45	4.00	0.60	3304.4	12.30	2.02E+05	17.0070	3309.3
8	0.00623	20.8026	0.0089	0.0111	0.77	−0.40	4.00	0.86	3290.4	12.24	2.01E+05	19.3143	3296.5
9	0.006681	22.2869	0.0097	0.0112	0.16	1.40	7.00	1.41	3283.4	12.22	2.01E+05	21.5449	3287.8
10	0.007152	23.8313	0.0109	0.0118	−1.62	1.07	5.00	1.94	3276.2	12.19	2.01E+05	23.0592	3279.7
11	0.007621	25.3646	0.0114	0.0122	−2.03	0.36	6.00	2.06	3269.0	12.16	2.00E+05	24.5981	3272.8
13	0.008545	28.3819	0.0118	0.0136	0.39	0.60	7.00	0.71	3254.9	12.11	1.99E+05	26.8738	3263.4
14	0.009012	29.8989	0.0126	0.0162	1.66	−0.89	3.00	1.88	3247.9	12.09	1.99E+05	29.1405	3248.5
15	0.009482	31.4233	0.0134	0.0181	0.64	−0.16	9.00	0.66	3240.8	12.06	1.98E+05	30.6613	3244.0
16	0.009959	32.9678	0.0150	0.0165	−0.95	−0.60	5.00	1.12	3233.6	12.03	1.98E+05	32.1957	3238.4

Drag Skirt

Station #	Time, t (s)	x (m)	y (m)	z (m)	θ (deg)	ψ (deg)	ϕ (deg)	total angle σ (deg)	V(x) from eqn. 1 (m/s)	Drag Skirt Separation Δx, m	Source	**Measured velocity** x_{av} (m)	V_{av} (m/s)
muzzle	0	0							3304.7				
DT1	0.000331	1.0948	0.0000	0.0026	0.48	0.00	0.00	0.48	3302.0	0.0076	image		
DT2	0.000614	2.0446	-0.0006	0.0000	0.00	−0.29	0.00	0.29	3299.7	0.0081	image	1.5699	3366.1
DT3	0.000889	2.9707	0.0000	0.0025	1.71	0.00	0.00	1.71	3297.4	0.0131	image	2.5078	3356.1
DT4	0.001169	3.9040	0.0000	-0.0008	2.13	0.00	0.00	2.13	3295.1	0.0212	image	3.4375	3342.1
1	0.003003	9.9847	0.0033	0.0039	19.36	0.33	-8.56	19.36	3280.1	0.1210	image		
2	0.003463	11.4907	0.0046	0.0039	29.19	3.18	-17.81	29.36	3276.4	0.1467	image	10.7378	3280.2
3	0.003923	12.9999	NaN	0.0048	30.01	4.00	-26.31	30.28	3272.6	0.1715	image	12.2454	3277.1
5	0.004832	15.9628	0.0000	0.0000	0.00	0.00	0.00	0.00	3265.4	0.2259	photobeam	14.4852	3267.6
6	0.005327	17.5822	NaN	0.0065	−21.62	−0.25	-42.69	21.62	3261.4	0.2427	image	16.7762	3260.5
9	0.006681	21.9856	0.0000	0.0000	0.00	0.00	0.00	0.00	3250.6	0.3013	photobeam	19.7881	3255.7
11	0.007621	25.0344	0.0000	0.0000	0.00	0.00	0.00	0.00	3243.2	0.3302	photobeam	23.5175	3245.5
12	0.008185	26.8625	0.0114	0.0159	15.25	3.25	-51.27	15.59	3238.8			25.9522	3227.6
13	0.008545	28.0282	0.0000	0.0000	0.00	0.00	0.00	0.00	3235.9	0.3537	photobeam	27.4490	3254.1
16	0.009959	32.5929	0.0000	0.0000	0.00	0.00	0.00	0.00	3224.9	0.3750	photobeam	30.3184	3228.5

Free Stream Conditions:

Shot #	P_∞ (atm)	P_∞ (Torr)	P_∞ (N/m^2)	T_∞ (K)	ρ_∞ (kg/m^3)	μ_∞ (kg/m-s)	Sound speed (m/s)	Relative humidity (%)	Test Gas
2822	0.150	114.10	15212.08	295.46	2.725E-01	1.49E-05	268.38	2.90	CO_2

Model Properties:

Component	Model ID	L (cm)	D (cm)	Mass (g)	%diff as drawn	x_{CG} from nose (cm)	st dev (cm)	%diff as drawn	I_{yy} (g-cm^2)	st dev	%diff as drawn	I_{xx} (g-cm^2)	st dev	%diff as drawn
Center Body	FS-09	0.534	0.767	1.9780	0.70%	0.325	0.000	-0.35%	0.08	0.00	10.23%	0.10	0.01	9.87%
Drag Skirt	DS-ADEPT-Al01	1.119	3.035	7.0847	-0.90%	0.719	0.001	-0.01%	4.94	0.01	2.24%			

Center Body

Station #	Time, t (s)	x (m)	y (m)	z (m)	θ (deg)	ψ (deg)	ϕ (deg)	total angle σ (deg)	V(x) from eqn. 1 (m/s)	M	Re_D
muzzle	0	0							3286.3	12.25	4.61E+05
DT1	0.000332	1.0674		0.0031	0.06	0.00	0.00	0.06	3274.8	12.20	4.59E+05
DT2	0.000646	2.0871	-0.0006		0.00	0.02	0.00	0.02	3263.8	12.16	4.58E+05
DT3	0.000924	2.9919		0.0047	−0.50	0.00	4.00	0.50	3254.1	12.13	4.56E+05
DT4	0.001217	3.9415		0.0118	0.13	0.00	4.00	0.13	3243.9	12.09	4.55E+05
1	0.003128	10.1045	0.0004	0.0040	0.54	−3.94	0.00	3.98	3178.8	11.84	4.46E+05
2	0.003609	11.6292	0.0014	0.0048	2.34	2.59	9.00	3.49	3162.9	11.79	4.43E+05
3	0.004097	13.1694	0.0011	0.0057	1.98	4.16	9.00	4.61	3146.8	11.73	4.41E+05
4	0.004572	14.6608	0.0015	0.0085	−0.28	0.06	12.00	0.29	3131.4	11.67	4.39E+05
5	0.005064	16.1979	0.0016	0.0085	−1.82	−4.13	11.00	4.51	3115.6	11.61	4.37E+05
6	0.005586	17.8199	0.0019	0.0099	1.09	−0.46	14.00	1.18	3099.0	11.55	4.35E+05
7	0.006051	19.2560	0.0017	0.0094	3.07	4.89	12.00	5.77	3084.4	11.49	4.32E+05
8	0.006551	20.7956	0.0023	0.0118	0.47	1.04	14.00	1.14	3068.8	11.43	4.30E+05
9	0.007037	22.2840	0.0027	0.0116	−2.01	−2.65	14.00	3.32	3053.8	11.38	4.28E+05
10	0.007539	23.8137	0.0033	0.0119	−0.05	−1.07	9.00	1.07	3038.4	11.32	4.26E+05
11	0.008050	25.3627	0.0034	0.0120	2.65	2.32	12.00	3.52	3023.0	11.26	4.24E+05
13	0.009053	28.3814	0.0030	0.0127	−1.32	−1.58	17.00	2.06	2993.1	11.15	4.20E+05
14	0.009562	29.8983	0.0032	0.0150	−1.34	−3.12	16.00	3.40	2978.2	11.10	4.18E+05
15	0.010075	31.4219	0.0036	0.0163	1.83	3.05	17.00	3.56	2963.3	11.04	4.15E+05
16	0.010598	32.9682	0.0048	0.0146	3.45	2.93	16.00	4.53	2948.2	10.99	4.13E+05

Measured velocity

x_{av} (m)	V_{av} (m/s)
1.5773	3254.0
2.5396	3248.8
3.4668	3241.5
10.8672	3169.4
12.3996	3155.5
13.9154	3139.0
15.4297	3124.4
17.0093	3107.9
18.5382	3090.4
20.0262	3076.8
21.5401	3062.1
23.0492	3046.1
24.5886	3031.1
26.8733	3009.5
29.1402	2982.7
30.6604	2971.0
32.1953	2956.2

Drag Skirt

Station #	Time, t (s)	x (m)	y (m)	z (m)	θ (deg)	ψ (deg)	ϕ (deg)	total angle σ (deg)	V(x) from eqn. 1 (m/s)	Drag Skirt Separation Δx, m	Source
muzzle	0	0							3204.0		
DT1	0.000332	1.0598		0.0032	−0.15	0.00	0.00	0.15	3195.3	0.0076	image
DT2	0.000646	2.0719	-0.0009		0.00	1.19	0.00	1.19	3187.1	0.0152	image
DT3	0.000924	2.9625		0.0047	−0.62	2.00	0.00	2.09	3179.8	0.0294	image
DT4	0.001217	3.8952		0.0113	−1.69	5.00	0.00	5.28	3172.3	0.0464	image
1	0.003128	9.9436							3123.5	0.1609	photobeam
3	0.004097	12.9601							3099.5	0.2093	photobeam
5	0.005064	15.9464							3076.0	0.2516	photobeam
7	0.006051	18.9691							3052.3	0.2869	photobeam
9	0.007037	21.9680							3029.0	0.3161	photobeam
11	0.008050	25.0243							3005.4	0.3384	photobeam
12	0.008664	26.8685	0.0026	0.0126	2.91	1.86	22.50	3.45	2991.3		
13	0.009053	28.0266							2982.4	0.3548	photobeam
16	0.010598	32.6054							2947.7	0.3628	photobeam

Measured velocity

x_{av} (m)	V_{av} (m/s)
1.5662	3229.5
2.5175	3197.9
3.4291	3183.6
11.4600	3112.4
14.4613	3087.9
17.4659	3063.8
20.4767	3040.0
23.5043	3016.4
25.9504	2993.6
27.4513	2992.6
30.3254	2964.7

Appendix D: Trajectory analysis results for the center body model for shots 2816, 2819 - 2822

Shot 2816, Center Body
CADRA trajectory values:

Station #	Time, t (s)	x (m)	y (m)	z (m)	θ (deg)	ψ (deg)	α (deg)	β (deg)	total angle σ (deg)	Mach
1	0	10.1013	-0.0010	0.0031	-5.07	-2.02	-5.04	-2.03	5.46	10.88
2	0.000529	11.6418	-0.0009	0.0039	8.19	2.92	8.02	3.52	8.69	10.82
3	0.001058	13.1733	-0.0009	0.0049	5.99	2.43	5.66	3.21	6.46	10.77
4	0.001573	14.6591	-0.0009	0.0058	-7.43	-1.53	-7.03	-2.83	7.59	10.71
5	0.002107	16.1913	-0.0010	0.0067	-7.73	-1.87	-7.16	-3.47	7.95	10.66
6	0.002676	17.8143	-0.0012	0.0076	6.83	1.78	6.27	3.33	7.05	10.60
7	0.003183	19.2545	-0.0014	0.0084	8.38	2.44	7.61	4.41	8.72	10.55
8	0.003728	20.7925	-0.0016	0.0093	-5.21	-0.75	-4.85	-1.98	5.26	10.50
9	0.004258	22.2846	-0.0019	0.0102	-9.41	-2.11	-8.72	-4.18	9.64	10.45
10	0.004812	23.8340	-0.0022	0.0110	3.42	1.08	3.17	1.73	3.59	10.39
11	0.005361	25.3609	-0.0026	0.0118	9.45	3.13	8.94	4.57	9.95	10.34
12	0.005908	26.8740	-0.0030	0.0126	-2.08	-0.24	-2.01	-0.46	2.09	10.29
13	0.006454	28.3796	-0.0035	0.0135	-9.86	-3.32	-9.76	-3.70	10.40	10.24
14	0.007011	29.9058	-0.0040	0.0143	0.02	0.29	0.06	0.27	0.29	10.18
15	0.007568	31.4235	-0.0046	0.0150	9.07	4.75	9.72	3.46	10.24	10.13
								RMS	**7.50**	

Shot 2816, Center Body
Residuals (calculated – measured):

Station #	Δx (mm)	Δy (mm)	Δz (mm)	Δθ (deg)	Δψ (deg)
1	-0.34	0.00	0.27	-0.15	0.26
2	0.33	-0.31	0.45	-0.51	-0.27
3	0.04	0.01	0.60	0.33	-0.07
4	0.15	0.00	-1.14	-0.41	0.05
5	-0.17	0.24	-0.31	-0.11	-0.03
6	-0.40	0.02	-0.84	0.44	0.29
7	0.36	0.58	0.47	-0.80	0.20
8	0.33	0.14	-0.84	1.04	-0.11
9	-0.01	-0.02	0.11	0.38	-0.63
10	0.07	-0.68	0.27	0.92	-0.13
11	0.04	-0.44	0.93	0.57	-0.06
12					
13	-1.12	0.32	1.53	-0.77	0.68
14	0.30	0.18	-0.40	-0.09	0.07
15	0.42	-0.05	-1.10	-0.72	0.22
RMS	**0.40**	**0.31**	**0.77**	**0.59**	**0.29**

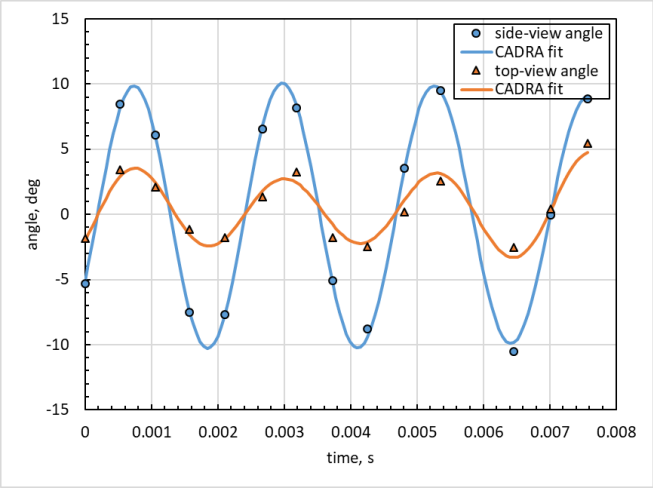

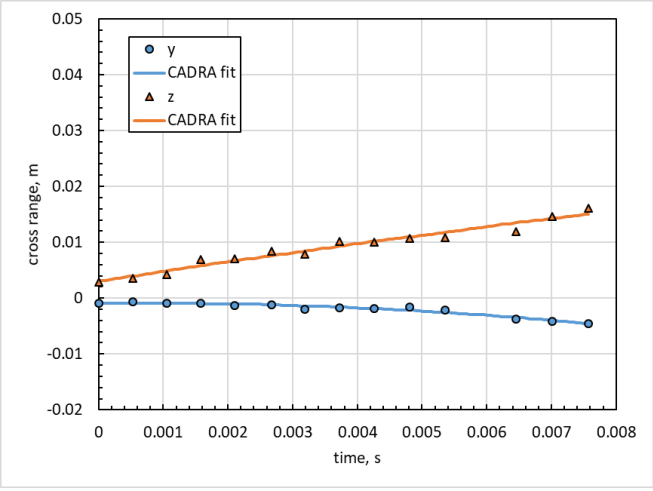

Shot 2819, Center Body

CADRA trajectory values:

Station #	Time, t (s)	x (m)	y (m)	z (m)	θ (deg)	ψ (deg)	α (deg)	β (deg)	total angle σ (deg)	Mach
1	0	10.1025	-0.0016	0.0023	4.58	2.53	4.61	2.54	5.23	11.88
2	0.000480	11.6274	-0.0016	0.0031	-2.96	-2.90	-3.02	-2.81	4.14	11.82
3	0.000964	13.1597	-0.0017	0.0040	-4.10	-3.08	-4.26	-2.83	5.13	11.76
4	0.001440	14.6584	-0.0017	0.0048	2.71	2.36	2.93	2.12	3.59	11.70
5	0.001928	16.1849	-0.0019	0.0056	5.10	3.62	5.49	3.08	6.26	11.65
6	0.002450	17.8128	-0.0021	0.0064	-1.51	-2.01	-1.72	-1.83	2.52	11.58
7	0.002916	19.2580	-0.0023	0.0070	-4.34	-3.75	-4.76	-3.18	5.73	11.53
8	0.003413	20.7916	-0.0025	0.0078	1.13	1.19	1.30	1.01	1.64	11.47
9	0.003901	22.2873	-0.0027	0.0084	5.08	3.96	5.60	3.24	6.44	11.41
10	0.004407	23.8336	-0.0031	0.0091	0.48	-0.34	0.46	-0.42	0.59	11.35
11	0.004900	25.3321	-0.0034	0.0096	-4.15	-3.75	-4.57	-3.24	5.59	11.30
12	0.005413	26.8812	-0.0038	0.0103	-0.46	-0.20	-0.45	-0.16	0.50	11.24
13	0.005911	28.3803	-0.0042	0.0108	4.71	3.59	5.05	3.14	5.93	11.18
14	0.006420	29.9039	-0.0047	0.0113	2.07	0.95	2.15	0.78	2.27	11.13
15	0.006930	31.4228	-0.0053	0.0118	-3.61	-3.12	-3.72	-2.99	4.77	11.07
								RMS	**4.48**	

Shot 2819, Center Body
Residuals (calculated – measured):

Station #	Δx (mm)	Δy (mm)	Δz (mm)	Δθ (deg)	Δψ (deg)
1	-0.31	0.20	0.22	0.33	-0.35
2	0.31	-0.47	0.47	0.46	-0.18
3	0.09	0.07	0.63	-0.08	-0.73
4	0.16	0.02	-1.09	0.72	-0.09
5	-0.24	0.07	-0.30	-0.55	0.25
6	-0.37	-0.09	-0.77	-0.64	0.96
7	0.27	0.61	0.53	0.11	0.21
8	0.31	0.07	-0.86	1.04	0.02
9	-0.16	0.03	-0.18	-0.76	-0.10
10	0.12	-0.61	0.17	0.75	-0.80
11	0.06	-0.50	0.73	0.39	0.43
12	0.27	0.38	0.66	-2.05	0.05
13	-1.01	0.25	1.16	0.93	0.52
14	0.12	0.10	-0.05	-0.63	-0.11
15	0.37	-0.15	-1.32	0.07	-0.03
RMS	**0.35**	**0.32**	**0.72**	**0.79**	**0.43**

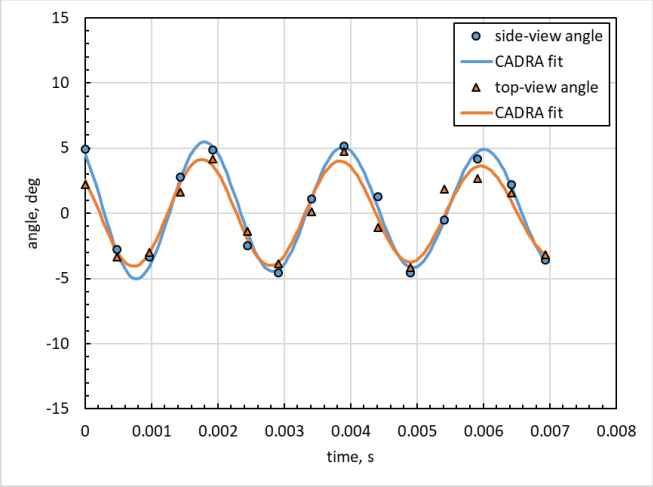

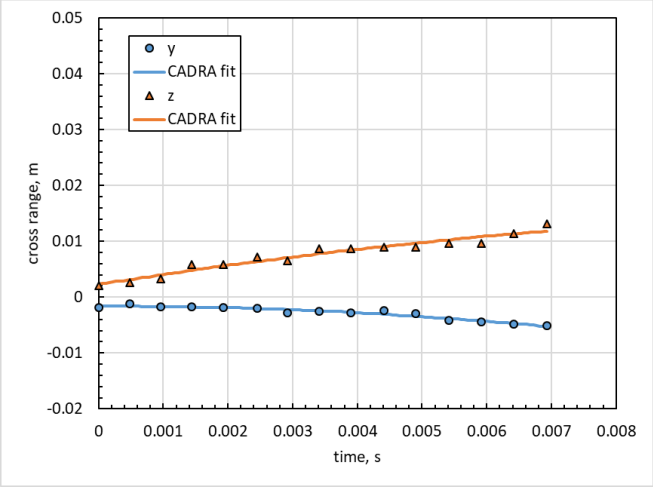

Shot 2820, Center Body
CADRA trajectory values:

Station #	Time, t (s)	x (m)	y (m)	z (m)	θ (deg)	ψ (deg)	α (deg)	β (deg)	total angle σ (deg)	Mach
1	0	10.1018	-0.0056	0.0083	-3.62	-6.39	-3.54	-6.44	7.35	11.49
2	0.000496	11.6275	-0.0062	0.0104	2.61	3.43	2.62	3.47	4.31	11.39
3	0.001000	13.1664	-0.0067	0.0126	0.33	4.84	0.18	4.84	4.85	11.30
4	0.001493	14.6577	-0.0072	0.0147	-4.55	-5.40	-4.06	-5.77	7.07	11.21
5	0.002003	16.1872	-0.0078	0.0168	0.76	-0.59	0.91	-0.51	0.96	11.12
6	0.002547	17.8085	-0.0085	0.0192	2.41	6.33	1.38	6.66	6.77	11.02
7	0.003057	19.3127	-0.0091	0.0213	-4.25	-2.83	-3.43	-3.72	5.10	10.93
8	0.003567	20.8048	-0.0097	0.0235	-1.66	-3.43	-0.52	-3.77	3.81	10.84
9	0.004076	22.2854	-0.0103	0.0256	4.04	5.50	1.94	6.59	6.83	10.76
10	0.004611	23.8266	-0.0110	0.0278	-1.91	1.30	-2.20	0.37	2.31	10.67
11	0.005155	25.3780	-0.0117	0.0301	-4.30	-4.51	-1.36	-6.06	6.23	10.58
12	0.005686	26.8829	-0.0124	0.0323	3.69	2.80	1.44	4.46	4.63	10.49
13	0.006217	28.3757	-0.0131	0.0345	1.63	4.05	-1.39	4.15	4.36	10.41
14	0.006762	29.8959	-0.0139	0.0367	-5.64	-3.01	-1.47	-6.17	6.39	10.32
15	0.007313	31.4177	-0.0146	0.0389	1.05	-0.42	1.02	0.66	1.13	10.24
16	0.007876	32.9628	-0.0155	0.0412	4.83	4.21	-1.43	6.31	6.41	10.15
								RMS	**5.29**	

Shot 2820, Center Body
Residuals (calculated – measured):

Station #	Δx (mm)	Δy (mm)	Δz (mm)	Δθ (deg)	Δψ (deg)
1	-0.23	0.39	0.06	0.75	0.38
2	0.26	-0.46	0.45	0.06	-0.22
3	0.00	0.08	0.68	0.04	0.38
4	0.16	0.05	-1.04	-0.93	-0.14
5	-0.22	0.13	-0.21	0.34	-0.36
6	-0.24	-0.08	-0.48	0.71	0.98
7	0.00	0.00	0.00	0.00	0.00
8	0.37	0.09	-0.89	-0.74	0.24
9	0.06	0.03	0.14	-0.88	-0.93
10	0.17	-0.59	0.48	-0.83	-0.66
11	0.04	-0.36	1.08	0.31	-0.12
12	0.00	0.00	0.00	0.00	0.00
13	-1.02	0.51	1.35	0.39	0.61
14	0.31	0.48	-0.49	0.77	0.04
15	0.33	0.40	-1.61	-0.35	0.73
16	-0.02	-0.66	0.49	0.52	-0.38
RMS	**0.32**	**0.35**	**0.76**	**0.58**	**0.49**

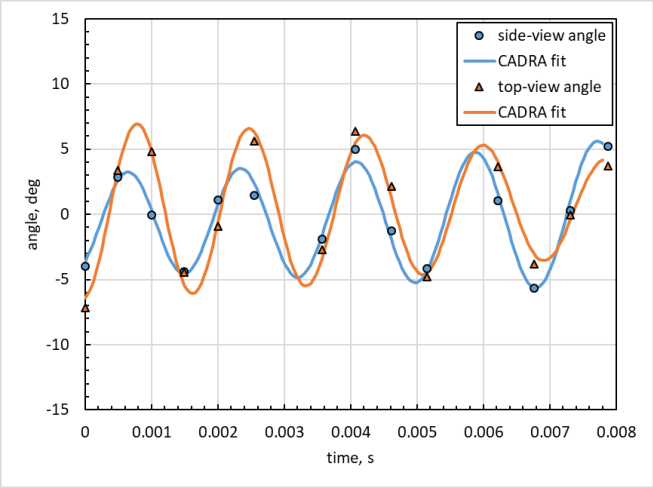

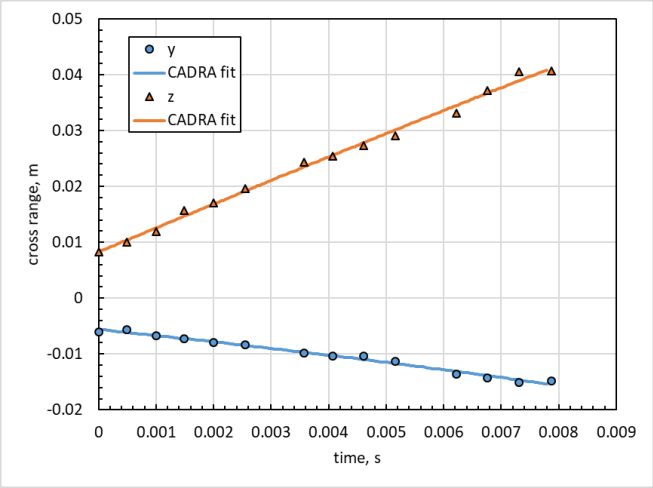

Shot 2821, Center Body
CADRA trajectory values:

Station #	Time, t (s)	x (m)	y (m)	z (m)	θ (deg)	ψ (deg)	α (deg)	β (deg)	total angle σ (deg)	Mach
1	0	10.1054	0.0035	0.0031	1.19	-0.66	1.24	-0.63	1.36	12.43
2	0.000459	11.6378	0.0044	0.0042	0.50	-0.29	0.54	-0.24	0.58	12.41
3	0.000920	13.1714	0.0053	0.0050	-0.93	0.38	-0.92	0.38	1.01	12.38
4	0.001367	14.6593	0.0061	0.0059	-1.86	0.77	-1.86	0.70	2.01	12.35
5	0.001829	16.1886	0.0068	0.0071	-1.52	0.54	-1.50	0.49	1.62	12.33
6	0.002323	17.8244	0.0075	0.0086	-0.05	-0.18	0.01	-0.16	0.19	12.30
7	0.002775	19.3153	0.0081	0.0098	1.10	-0.67	1.16	-0.61	1.28	12.27
8	0.003226	20.8031	0.0088	0.0108	1.07	-0.57	1.10	-0.54	1.21	12.25
9	0.003678	22.2870	0.0096	0.0114	-0.14	-0.03	-0.12	0.01	0.14	12.22
10	0.004149	23.8315	0.0105	0.0120	-1.61	0.50	-1.54	0.64	1.68	12.19
11	0.004617	25.3647	0.0112	0.0128	-2.00	0.52	-1.88	0.79	2.06	12.17
12	0.005080	26.8744	0.0118	0.0139	-0.96	0.10	-0.87	0.29	0.96	12.14
13	0.005542	28.3807	0.0124	0.0150	0.65	-0.32	0.60	-0.47	0.73	12.11
14	0.006009	29.8992	0.0130	0.0160	1.47	-0.41	1.29	-0.86	1.52	12.09
15	0.006479	31.4238	0.0137	0.0165	0.73	-0.23	0.60	-0.49	0.76	12.06
16	0.006956	32.9678	0.0144	0.0169	-0.98	-0.10	-0.87	0.41	0.98	12.03
									1.26	

Shot 2821, Center Body
Residuals (calculated – measured):

Station #	Δx (mm)	Δy (mm)	Δz (mm)	Δθ (deg)	Δψ (deg)
1	-0.31	0.17	0.21	0.94	0.38
2	0.32	-0.51	0.59	-0.14	-0.56
3	0.04	0.17	0.56	0.75	0.32
4	0.19	0.20	-1.36	0.73	-0.02
5	-0.07	0.17	-0.34	-0.44	0.14
6	-0.50	-0.05	-0.37	0.27	-0.46
7					
8	0.43	-0.06	-0.39	-0.17	0.30
9	0.08	-0.07	0.17	-1.43	-0.30
10	0.17	-0.44	0.23	-0.58	0.01
11	0.10	-0.14	0.68	0.16	0.03
12					
13	-1.13	0.57	1.46	-0.92	0.26
14	0.26	0.40	-0.28	0.48	-0.19
15	0.46	0.27	-1.55	-0.06	0.09
16	-0.05	-0.69	0.39	0.50	-0.03
RMS	**0.40**	**0.34**	**0.77**	**0.66**	**0.28**

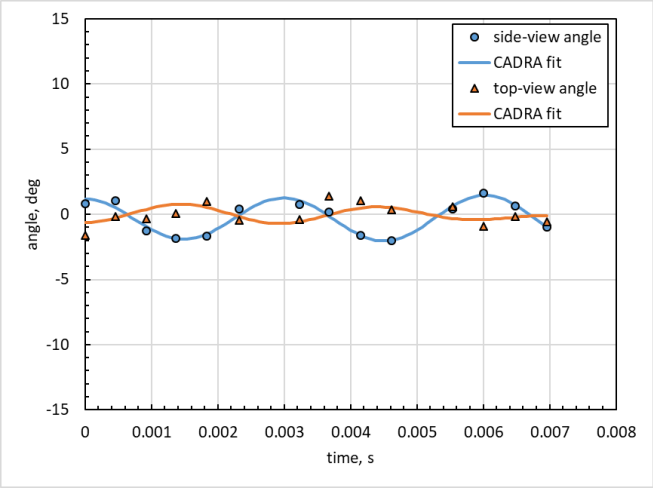

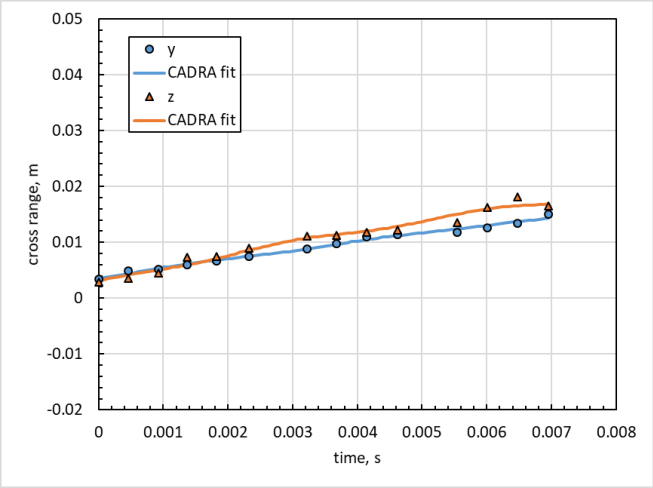

Shot 2822, Center Body
CADRA trajectory values:

Station #	Time, t (s)	x (m)	y (m)	z (m)	θ (deg)	ψ (deg)	α (deg)	β (deg)	total angle σ (deg)	Mach
1	0	10.1041	0.0007	0.0041	-0.13	-3.71	-0.09	-3.70	3.71	11.85
2	0.000481	11.6296	0.0009	0.0052	1.59	2.31	1.33	2.51	2.81	11.79
3	0.000969	13.1695	0.0012	0.0063	1.91	4.81	0.75	5.15	5.17	11.73
4	0.001444	14.6610	0.0015	0.0073	-0.37	-0.22	-0.24	-0.31	0.43	11.67
5	0.001936	16.1978	0.0017	0.0083	-1.54	-3.87	0.26	-4.14	4.17	11.61
6	0.002458	17.8195	0.0019	0.0093	1.30	0.31	1.00	0.93	1.33	11.55
7	0.002923	19.2564	0.0021	0.0101	3.18	4.04	0.48	5.15	5.14	11.49
8	0.003423	20.7960	0.0023	0.0109	0.77	1.27	-0.11	1.51	1.49	11.44
9	0.003909	22.2841	0.0026	0.0116	-1.99	-3.10	0.41	-3.65	3.69	11.38
10	0.004412	23.8139	0.0028	0.0123	-0.19	-1.69	0.97	-1.38	1.70	11.32
11	0.004923	25.3628	0.0030	0.0129	3.19	2.89	0.47	4.31	4.31	11.27
12	0.005424	26.8752	0.0032	0.0135	2.08	2.44	-0.09	3.23	3.21	11.21
13	0.005926	28.3801	0.0034	0.0140	-1.42	-1.99	0.28	-2.41	2.44	11.15
14	0.006434	29.8986	0.0037	0.0144	-1.17	-2.65	0.85	-2.75	2.90	11.10
15	0.006947	31.4222	0.0039	0.0148	2.24	1.66	0.69	2.72	2.79	11.04
16	0.007470	32.9683	0.0041	0.0152	2.66	3.30	0.17	4.25	4.23	10.99
									3.37	

Shot 2822, Center Body
Residuals (calculated – measured):

Station #	Δx (mm)	Δy (mm)	Δz (mm)	Δθ (deg)	Δψ (deg)
1	-0.41	0.32	0.13	0.24	-0.67
2	0.34	-0.45	0.44	-0.27	-0.75
3	0.07	0.05	0.64	0.65	-0.07
4	0.18	-0.06	-1.15	-0.29	-0.09
5	-0.16	0.13	-0.22	0.25	0.28
6	-0.36	0.00	-0.68	0.77	0.21
7	0.32	0.44	0.65	-0.85	0.11
8	0.31	-0.01	-0.90	0.23	0.30
9	0.02	-0.11	-0.01	-0.46	0.02
10	0.14	-0.58	0.33	-0.62	-0.14
11	0.05	-0.41	0.91	0.57	0.54
12					
13	-1.29	0.49	1.32	-0.41	-0.10
14	0.31	0.50	-0.53	0.47	0.17
15	0.30	0.33	-1.44	-1.39	0.40
16	0.18	-0.61	0.51	0.37	-0.80
RMS	**0.41**	**0.37**	**0.77**	**0.60**	**0.40**